

Thermal and transport properties of quasicrystals

Doctoral Thesis

Author(s):

Bianchi, Andrea Daniele

Publication date:

1999

Permanent link:

<https://doi.org/https://doi.org/10.3929/ethz-a-002092950>

Rights / license:

[In Copyright - Non-Commercial Use Permitted](#)

Diss. ETH No. 12915 **Ex. B**

Thermal and Transport Properties of Quasicrystals

*A dissertation submitted to the
SWISS FEDERAL INSTITUTE OF TECHNOLOGY
ZURICH*

*for the degree of
Doctor of Natural Sciences*

presented by

ANDREA DANIELE BIANCHI

Dipl. Phys. ETH

born on the 11th August 1968

Citizen of Olten (SO)



CatE

accepted on the recommendation of

Prof. Dr. H. R. Ott, examiner

Prof. Dr. T. M. Rice, co-examiner

1999

für Alexandra

Contents

Abstract	1
Kurzfassung	3
1 Introduction	7
2 Experimental	11
2.1 Sample preparation	11
2.1.1 Icosahedral Al-Mn-Pd	11
2.1.2 Icosahedral Al-Re-Pd	12
2.1.3 Decagonal Al-Cu-Co	12
2.1.4 Decagonal Al-Ni-Co	13
2.2 Experimental techniques	13
3 Thermal conductivity	17
3.1 Introduction	17
3.1.1 Excitations in quasiperiodic lattices	17
3.1.2 Umklapp scattering	21
3.2 Icosahedral Al-Mn-Pd	25
3.2.1 Thermal conductivity at low temperatures	27
3.2.2 Thermal conductivity at intermediate temperatures	35
3.2.3 Thermal conductivity at high temperatures–Einstein model	39
3.2.4 Thermal conductivity of icosahedral Al-Mn-Pd–Kinetic model	40
3.2.5 Summary	47
3.3 Icosahedral Al-Re-Pd	48
3.4 Decagonal quasicrystals	53

3.4.1	Decagonal Al-Cu-Co	54
3.4.2	Decagonal Al-Ni-Co	60
3.4.3	Conclusions	64
4	Specific heat	65
4.1	Icosahedral Al-Re-Pd	65
4.2	Decagonal Al-Cu-Co	73
4.3	Decagonal Al-Ni-Co	75
4.3.1	Electronic contribution	76
4.3.2	Lattice contribution	78
4.3.3	Summary and Conclusion	87
5	Electrical conductivity of icosahedral Al-Re-Pd quasicrystals	89
5.1	$Al_{70}Re_{10}Pd_{20}$	91
5.2	$Al_{70}Re_{8.6}Pd_{21.4}$	95
5.2.1	Summary	98
6	Summary and Conclusions	101
	Bibliography	107
	Dank	119
	Curriculum vitae	121

Abstract

In this work three topics related with the low-temperature transport and thermal properties of icosahedral and decagonal quasicrystals are described.

In the first part, the thermal conductivity $\lambda(T)$ investigations on icosahedral Al-Mn-Pd and Al-Re-Pd performed in temperature ranges between 0.065 and 310 K are reported. We found that below 1 K, the lattice thermal conductivity $\lambda_{\text{ph}}(T)$ in both systems is compatible with the scattering of phonons by tunneling states and grain boundaries. The most prominent feature of $\lambda_{\text{ph}}(T)$ is its approximate temperature independence between 20 and 80 K, for which the concept of quasiperiodic Umklapp scattering seems to offer the most plausible explanation. Above 80 K, the low values of $\lambda_{\text{ph}}(T)$ imply a phonon mean free path that is of the order of the phonon wavelength, suggesting that the lattice modes of an icosahedral quasiperiodic lattice in the THz frequency range propagate diffusively.

We also found that for decagonal quasicrystals in the Al-Cu-Co and in the Al-Ni-Co systems the lattice contribution $\lambda_{\text{ph}}^{\text{p}}(T)$ to the thermal conductivity along the periodic direction shows a maximum at ~ 25 K and a sizable negative slope $d\lambda_{\text{ph}}^{\text{p}}/dT$ above this temperature, characteristic of periodic crystals. The phonon thermal conductivity $\lambda_{\text{ph}}^{\text{q}}(T)$ along a direction in the quasiperiodic plane is, as in the case of icosahedral quasicrystals, only weakly temperature dependent between 30 and 70 K, thus indicating the dominance of quasiperiodic Umklapp processes.

In the second part, we report on the calorimetric investigation of icosahedral Al-Re-Pd and on decagonal Al-Cu-Co and Al-Ni-Co. For icosahedral $\text{Al}_{70}\text{Re}_{8.6}\text{Pd}_{21.4}$, the specific heat $C_p(T)$ below 0.4 K increases with decreasing T and, at the lowest temperatures it

varies as T^{-2} indicative of the interaction of the quadrupolar moments of ^{185}Re and ^{187}Re nuclei with the gradient of the electric field induced by their neighbours. The linear contribution γT to $C_p(T)$ is approximately 1/10 of the electronic contribution γ_{el} of Aluminum and has to be partially attributed to excitations of tunneling states, as suggested by the $\lambda_{\text{ph}}(T)$ results, indicating a very low density of electronic states at the Fermi energy E_F . The cubic-in- T term to $C_p(T)$ of icosahedral $\text{Al}_{70}\text{Re}_{8.6}\text{Pd}_{21.4}$ is distinctly higher than the calculated value of the acoustic phonon contribution, indicating a large excess specific heat $C_{\text{ex}}(T)$.

For decagonal Al-Cu-Co and Al-Ni-Co, the coefficient $\gamma \approx 0.6 \text{ mJ mol}^{-1} \text{ K}^{-2}$ of the linear term in $C_p(T)$ indicates a low density of electronic states at E_F for both systems. For Al-Ni-Co the magnitude of the cubic-in- T term in the low temperature specific heat is in fair agreement with the acoustic contribution to $C_p(T)$ calculated from the results of low-temperature measurements of the elastic stiffness constants c_{ij} . Above 4 K, C_{ph}/T^3 in decagonal Al-Ni-Co increases approximately as T^2 . While this variation may be ascribed to the dispersion of acoustic excitations, the magnitude of the T^5 term in $C_{\text{ph}}(T)$ is a few times larger than the value calculated from phonon dispersion curves measured using inelastic neutron scattering experiments, again suggesting the presence of a large excess specific heat.

In the third part of this work, temperature and magnetic field dependences of the electrical conductivity $\sigma(T, H)$ of two samples of icosahedral Al-Re-Pd with chemical composition of $\text{Al}_{70}\text{Re}_{10}\text{Pd}_{20}$ and $\text{Al}_{70}\text{Re}_{8.6}\text{Pd}_{21.4}$ are described. For temperatures below 0.2 K, the temperature and magnetic field dependence of $\sigma(T, H)$ in $\text{Al}_{70}\text{Re}_{10}\text{Pd}_{20}$ with a value of the residual conductivity of $\sigma_0 = 30 \text{ } \Omega^{-1} \text{ cm}^{-1}$, is compatible with quantum-interference effects including Coulomb interactions among itinerant electrons. The electrical conductivity of $\text{Al}_{70}\text{Re}_{8.6}\text{Pd}_{21.4}$, which has a residual conductivity value of $\sigma_0 = 1.7 \text{ } \Omega^{-1} \text{ cm}^{-1}$, saturates below 0.1 K in all applied magnetic fields up to 40 kOe, suggesting that for this material an approach different from quantum interference effects needs to be considered to describe the electronic transport at the lowest temperatures.

Kurzfassung

In dieser Doktorarbeit werden drei Aspekte im Zusammenhang mit den thermischen sowie den Transporteigenschaften von ikosahedrischen und dekadagonalen Quasikristallen bei tiefen Temperaturen beleuchtet.

Im ersten Teil werden Wärmeleitfähigkeitsmessungen $\lambda(T)$ an ikosahedrischen Al-Mn-Pd und Al-Re-Pd Quasikristallen in verschiedenen Temperaturbereichen zwischen 0.065 und 310 K beschrieben. Unterhalb von 1 K ist der Wärmeleitfähigkeit der Phononen $\lambda_{\text{ph}}(T)$ in beiden Systemen begrenzt durch die Streuung der Phononen an Zwei-Niveau Systemen sowie an Korngrenzen. Das auffälligste Merkmal von $\lambda_{\text{ph}}(T)$ ist die schwache Temperaturabhängigkeit im Bereich von 20 bis 80 K welche wir quasiperiodische Umklapp Prozesse zuschreiben. Die tiefen Werte von $\lambda_{\text{ph}}(T)$ oberhalb von 80 K bedingen eine mittlere freie Weglänge der Phononen in der Größenordnung der Wellenlänge der Phononen. Dies weist darauf hin, dass der Wärmetransport von Gitterschwingungen im THz Bereich überwiegend diffusiv erfolgt.

Im weitem wurde beobachtet, dass der Gitteranteil die Wärmeleitfähigkeit $\lambda_{\text{ph}}^{\text{p}}(T)$ von dekadagonalem Al-Cu-Co und Al-Ni-Co entlang der periodischen Achse in beiden Systemen ein Maximum bei ~ 25 K besitzt. Oberhalb dieser Temperatur beobachtet man eine negative Steigung $d\lambda_{\text{ph}}^{\text{p}}/dT$; ein Verhalten wie man es typischerweise von den periodischen Kristallen her kennt. Die Wärmeleitfähigkeit entlang einer Richtung in der quasiperiodischen Ebene $\lambda_{\text{ph}}^{\text{q}}(T)$ zeigt zwischen 30 und 70 K nur eine schwache Temperaturabhängigkeit. Solch ein Verhalten hat man auch in ikosahedrischen Quasikristallen beobachtet und es deutet auf eine bestimmende Rolle der quasiperiodischen Umklapp Prozesse hin.

Im zweiten Teil wird die kalorimetrische Untersuchung von ikosahedrischem Al-Re-Pd sowie von dekadagonalem Al-Cu-Co und Al-Ni-Co beschrieben. Unterhalb von 0.4 K wird in $\text{Al}_{70}\text{Re}_{8,6}\text{Pd}_{21,4}$ mit sinkender Temperatur ein zu T^{-2} proportionaler Anstieg von $C_p(T)$ beobachtet, welcher auf eine Wechselwirkung zwischen dem nuklearen Quadrupolmoment der ^{185}Re und ^{187}Re Kerne und dem elektrischen Feldgradienten der Gitternachbarn hindeutet. Der lineare Beitrag γT zu $C_p(T)$ ist klein und ein Teil dieses Beitrages ist auf Zwei-Niveau Systeme zurückzuführen, deren Vorhandensein durch die $\lambda_{\text{ph}}(T)$ Daten angezeigt ist, was auf eine sehr kleine Zustandsdichte am Fermi-niveau schliessen lässt. Der zu T^3 proportionale Beitrag zu $C_p(T)$ von ikosahedrischem $\text{Al}_{70}\text{Re}_{8,6}\text{Pd}_{21,4}$ ist deutlich grösser als der Beitrag den man auf Grund der akustischen Phononen erwarten würde und deutet somit auf einen zusätzlichen Beitrag $C_{\text{ex}}(T)$ unbekanntem Ursprungs zur spezifischen Wärme.

In dekadagonalem Al-Cu-Co und Al-Ni-Co deutet der kleine Koeffizient des linearen Beitrages γT von $\approx 0.6T \text{ mJ mol}^{-1} \text{ K}^{-1}$ zur spezifischen Wärme $C_p(T)$ auf eine kleine elektronische Zustandsdichte bei der Fermienergie E_F . Der zu T^3 proportionale Beitrag zu $C_p(T)$ in Al-Ni-Co ist in guter Übereinstimmung mit dem akustischen Beitrag, der aus den Tieftemperaturwerten der elastischen Konstanten c_{ij} berechnet werden kann. In dekadagonalem Al-Ni-Co steigt oberhalb von 4 K das Verhältnis C_{ph}/T^3 proportional zu T^2 an. Obwohl man einen Beitrag zu $C_p(T)$ mit einer zu T^5 proportionalen Temperaturabhängigkeit auf Grund der Dispersion der akustischen Anregungen erwartet, so ist der aus den mittels inelastischer Neutronenstreuung gemessenen Dispersionskurven berechnete Wert um fast eine Grössenordnung kleiner, was wieder auf einen zusätzlichen Beitrag zur spezifischen Wärme hindeutend.

Im dritten Teil wird die Temperatur- und Magnetfeldabhängigkeit der elektrischen Leitfähigkeit $\sigma(T, H)$ von zwei Proben von ikosahedrischem Al-Re-Pd mit der chemischen Zusammensetzung $\text{Al}_{70}\text{Re}_{10}\text{Pd}_{20}$ und $\text{Al}_{70}\text{Re}_{8,6}\text{Pd}_{21,4}$ beschrieben. Für Temperaturen unterhalb von 0.2 K kann die Temperatur- und Magnetfeldabhängigkeit der Leitfähigkeit von $\text{Al}_{70}\text{Re}_{10}\text{Pd}_{20}$, welches eine Restleitfähigkeit von $\sigma_0 = 30 \text{ } \Omega^{-1} \text{ cm}^{-1}$ besitzt, mit Quanteninterferenzeffekten der beweglichen Ladungsträger unter Berücksichtigung der Coulomb Wechselwirkung erklärt werden. Im Fall von $\text{Al}_{70}\text{Re}_{8,6}\text{Pd}_{21,4}$, welches eine Restleitfähigkeit von $\sigma_0 = 1.7 \text{ } \Omega^{-1} \text{ cm}^{-1}$ besitzt, zeigt die elektrische Leitfähigkeit unterhalb von 1 K die Tendenz zur Saturierung. Diese Tendenz wird auch bei angelegten Magnetfeldern bis zu 40 kOe noch beobachtet, was darauf hindeutet, dass die elektrische

Leitfähigkeit bei den tiefsten Temperaturen in diesem Material durch andere Mechanismen als Quanteninterferenzeffekte bestimmt wird.

Leer - Vide - Empty

1 Introduction

Quasicrystals were discovered by Shechtman *et al.* in rapidly quenched Al-Mn alloys [1]. They reported electron diffraction patterns with fairly sharp diffraction spots showing the crystallographically forbidden tenfold rotational symmetry [1]. Additionally to the tenfold diffraction patterns, three- and twofold patterns were observed forming a set of angular displacements between the different axes with the crystallographically forbidden icosahedral point-group symmetry. For three dimensional periodic crystals only two-, three-, four-, and sixfold rotations around appropriately chosen axes are allowed. Instead of translational symmetry, the diffraction patterns of icosahedral quasicrystals show an inflation symmetry and can be scaled by some power of the golden mean τ . The higher dimensional crystallographic approach applied previously to index incommensurate structures [2,3] was adapted to describe the intrinsic incommensurability of icosahedral quasicrystals [4–6]. For example, the diffraction pattern of icosahedral quasicrystals can successfully be indexed using six reciprocal lattice vectors, that point from the center to the vertices of an icosahedron [4–6].

The three dimensional aperiodic structure of icosahedral quasicrystals in the real three dimensional space (physical space) X^{\parallel} can be obtained as a cut under an irrational angle of a cubic structure in six dimensions $X = (X^{\parallel}, X^{\perp})$ with a basis extending into the three dimensional space (perpendicular space) X^{\perp} orthogonal to X^{\parallel} [4–8]. Displacements of the six dimensional structure along the physical space correspond simply to acoustic modes, whereas displacements of the structure in the orthogonal space lead to so called phason modes which are commonly manifest in the physical space as non-acoustic modes depending on the structure [6,9–11].

Two different types of icosahedral quasilattices have been observed. The first discovered Al-Mn [1] and also Al-Li-Cu [12] are of the simple icosahedral type for which the six indices of the diffraction pattern are unrestricted. The discovery of quasicrystals led to a considerable experimental and theoretical activities to study the influence of the quasiperiodic order on the physical properties. It was, however, soon realized that Al-Mn and other quasicrystals of the simple icosahedral type possess a high degree of intrinsic disorder [13] that inhibited unambiguous investigations and evaluations of anticipated unusual physical properties of this novel type of condensed matter.

New opportunities for experimental studies of physical properties of quasiperiodic crystals were provided by the discovery of the thermodynamically stable quasicrystals in the Al-Cu-(Fe,Ru,Os) system [14, 15] which have a face-centered icosahedral structure. For this structure, the indices of the diffraction pattern have all the same parity, analogous to face-centered cubic crystals in three dimensions. In face-centered icosahedral quasicrystals structural coherence lengths up to 10^4 Å are observed in dynamical X-ray diffraction experiments, comparable to those of well-ordered periodic crystals [16]. Three years later, stable icosahedral phases were reported in the Al-(Mn,Re)-Pd systems [17–20] without phason broadening of the Bragg peaks even in the non-annealed state. Structural analysis indicates that icosahedral Al-Mn-Pd forms a chemically ordered state [21–24]. Recently a new group of rare earth containing icosahedral quasicrystals crystals was found in the RE-Mg-Zn system, where RE is either yttrium or a rare earth out of the (Tb,Dy,Ho,Er) series [25–27]. Besides the fact that large single grains of RE-Mg-Zn of high structural quality can be obtained using, for example, the self-flux technique their discovery generated special interest as some of them contain localized 4f magnetic moments [28].

In addition to icosahedral quasicrystals that are quasiperiodic in three dimensions, there exists a second class of materials which are periodic along one direction and quasiperiodic in the plane perpendicular to it. Almost at the same time as icosahedral quasicrystals were discovered, dodecagonal Ni-Cr with a twelvefold rotational symmetry was found, the first member of the group of the so-called axial quasicrystals [29]. Later examples of all other symmetries possible for axial quasiperiodic structures have been reported, having decagonal [30], octagonal [31] and pentagonal [32] symmetries. The advent of measurements of physical properties was the discovery of thermodynamically stable decagonal quasicrystals in the Al-Cu-Co and Al-Ni-Co systems [33, 34]. In these systems

millimetre sized single quasicrystals with decaprismatic growth morphology can be obtained by slow solidification of the melt, crucial for a reliable study of the anisotropy of the physical properties along the periodic direction and the quasiperiodic plane.

Leer - Vide - Empty

2 Experimental

2.1 Sample preparation

The polygrained sample of icosahedral Al-Mn-Pd was synthesized and characterized by electron microscopy by Dr. K. Beeli. The other samples listed below were prepared by Dr. M. Chernikov. On these, the selected area electron diffraction patterns and the back-scattered electron images were taken by Dr. S. Ritsch and P. Wägli. A brief description of the synthesis and structural characterization of the samples is given for the benefit of the reader.

2.1.1 Icosahedral Al-Mn-Pd

The sample of icosahedral $\text{Al}_{70}\text{Mn}_9\text{Pd}_{21}$ was synthesized from 99.997 % pure aluminium, 99.9 % pure palladium and 99.94 % pure manganese by arc melting suitable amounts of the constituents to a single piece and remelting it several times to provide homogeneity. The resulting button was annealed for 2 days at 800 °C, and subsequently quenched into water directly from 800 °C. The initial sample composition is chosen to be optimal for the formation of the thermodynamically stable icosahedral phase in the Al-Mn-Pd system. The absence of any inclusions of other phases was confirmed by surface analysis from back-scattered electron images. Also, selected-area electron-diffraction patterns show a high degree of order and a low density of phason-defects [35]. For the thermal conductivity measurements, a specimen in the form of a prism with dimensions $1.07 \times 1.22 \times 5.80 \text{ mm}^3$ was cut from the ingot by electro-erosion.

2.1.2 Icosahedral Al-Re-Pd

Icosahedral Al-Re-Pd samples with nominal compositions $\text{Al}_{70}\text{Re}_{10}\text{Pd}_{20}$ and $\text{Al}_{70}\text{Re}_{8.6}\text{Pd}_{21.4}$ from 99.999 % pure Aluminum, 99.9975 % Palladium and 99.94 % pure Rhenium were synthesized by arc-melting suitable amounts of the constituent elements to a single piece in an argon atmosphere and remelting it several times. The resulting ingots were annealed in vacuum for 2 days and subsequently rapidly cooled to room temperature. Powder X-ray diffraction and surface analysis with back-scattered electron images confirmed the absence of inclusion of other phases. Selected-area electron-diffraction patterns revealed a high degree of structural order. For the measurements of the electrical conductivity and the specific heat, specimens in the form of prisms with approximate dimensions $0.8 \times 1.4 \times 6 \text{ mm}^3$ were cut from the ingots using spark-erosion. For the thermal conductivity measurements a sample with dimensions $1.1 \times 1.6 \times 6.5 \text{ mm}^3$ was cut from a part of the $\text{Al}_{70}\text{Re}_{8.6}\text{Pd}_{21.4}$ ingot adjacent to the one used in the investigation of the electrical conductivity and specific heat.

2.1.3 Decagonal Al-Cu-Co

The ingot with a nominal composition $\text{Al}_{65}\text{Cu}_{20}\text{Co}_{15}$ was synthesized from 99.999 % pure Aluminum, 99.9985 % pure Copper, and 99.997 % pure Cobalt by arc-melting suitable amounts of the constituents to a single piece and remelting it several times. The resulting ingot was remelted again at $1100 \text{ }^\circ\text{C}$ in an alumina crucible sealed under vacuum inside a silica ampoule, cooled to $920 \text{ }^\circ\text{C}$ at the rate $2 \text{ }^\circ\text{C}$ per hour, annealed at $920 \text{ }^\circ\text{C}$ for 24 hours, and subsequently cooled to room temperature. Faceted decaprisms up to 1.5 mm in diameter and up to 6 mm in length were cut from the ingot using spark-erosion. Two decaprisms with approximate dimensions $2.9 \times 1.5 \times 0.4 \text{ mm}^3$ and $2.0 \times 0.6 \times 0.4 \text{ mm}^3$ have been selected for our experiments. Their naturally formed facets were polished to remove possible surface contaminations. A high degree of quasicrystalline order was confirmed by electron diffraction experiments. Laue photographs taken on both samples have confirmed that they are single grains. The smaller sample has been used for measurements of the thermal conductivity $\lambda^p(T)$ along the ten-fold symmetry axis, while the larger grain has been used for measuring $\lambda^q(T)$ along a direction in the quasiperiodic plane and also for the specific heat $C_p(T)$ measurements.

2.1.4 Decagonal Al-Ni-Co

Al-Ni-Co quasicrystals were grown using the self-flux technique. An $\text{Al}_{70}\text{Co}_{15}\text{Ni}_{15}$ alloy was prepared by arc-melting using high purity elemental metals (99.999 % pure Aluminium, 99.9985 % pure Nickel, and 99.997 % pure Cobalt). The resulting button was loaded in an alumina crucible and sealed under vacuum in a silica ampoule. The ingot was remelted at 1250 °C, cooled to 1030 °C at the rate 2 °C per hour, annealed at 1030 °C for 5 days, and subsequently rapidly cooled to room temperature. The resulting ingot contained several large grains with decaprismatic morphology, partly embedded in the bulk of the material. Samples were cut from the decaprisms using a spark-cutter. Two samples cut perpendicular and parallel to the decagonal (periodic) axis A_{10} with approximate dimensions $4 \times 2.2 \times 1.7 \text{ mm}^3$ and $2.4 \times 2.1 \times 1.5 \text{ mm}^3$ were selected for our experiments. No grain boundaries were observed in a scanning electron microscope analysis. An electron-diffraction experiment has revealed that these samples are highly ordered quasicrystals with a very small phason strain and with the S1 superstructure type of decagonal order, indicating that the most probable chemical composition of the samples is $\text{Al}_{71}\text{Ni}_{16}\text{Co}_{13}$ [36]. Laue photographs taken on both samples have confirmed that they are single quasicrystals.

2.2 Experimental techniques

In all the different types of experiments temperatures in the range between 0.06 and 1 K were reached by a dilution refrigerator. Conventional pumped ^3He and ^4He cryostats were used for temperatures between 0.35 and 3 K, and above 1.5 K, respectively.

The thermal conductivity was measured by a standard steady-state heat-flow technique monitoring the temperature gradient along the sample in the temperature range between 0.065 and 320 K. The heating power was applied by a non-inductively wound heater with approximately 300 Ω resistance, made from manganin wire glued to a small copper cylinder. For bar shaped samples the heater was glued directly on a flat surface of the sample using a thin layer of electrically conducting epoxy bond (EpoTek H20E) in order to obtain both a good thermal and mechanical contact. Subsequently, the sample with the heater was glued to a copper sample holder for mounting to the cryostat. In the

case of the decagonal Al-Cu-Co samples, a 300 μm thick copper wire was first bonded at both ends of the sample. These copper wires were then crimped to the heater body and the sample holder, respectively. For measuring the temperature gradient, two thermometers fabricated from commercially available resistors were calibrated against the temperature standard of the respective cryostat. For temperatures below 3 K, split 100 Ω Matsushita carbon resistors were employed. Between 2 and 80 K those were replaced by a pair of 480 Ω Allen-Bradley carbon resistors and for temperatures above 40 K thin film 100 Ω platinum chip resistors were used. The carbon resistors were ground on sandpaper to the appropriate room temperature resistance values of 330 Ω for the Matsushita's and 950 Ω for the Allen-Bradley's. After the grinding a thin layer of an epoxy resin (Stycast 2850) was applied as electrical insulation. A flattened 100 μm gold wire was then wrapped tightly around the resistor and covered with an additional layer of epoxy. In the case of the platinum chip resistors a silver foil was glued on the back of the Al_2O_3 isolation with GE-7031 varnish before a gold wire was spot-welded to it. The thermometers were then thermally connected by bonding the gold wire to the sample with silver epoxy. For measurements in different temperature ranges the thermometers were exchanged by spot-welding a suitable thermometer by the gold wire, thus retaining the geometrical factor. The stray heat conductance of the electrical connections to the sample thermometers was minimized by using 30 cm of 30 μm manganin wire [37]. Electrical leads of 11 μm NbTi filaments were used to provide sufficient thermal isolation of the heater for temperatures below 7 K. At higher temperatures 100 μm manganin wire was used for the heater current. The gold wires attached to the sample served subsequently as voltage terminals for the electrical conductivity measurements, thus reducing the error due to the geometrical factor in the estimate of the electronic contribution to the thermal conductivity via the Wiedemann-Franz law.

The electrical conductivity $\sigma(T)$ and the magnetoconductivity $\Delta\sigma(H)$ were measured using a standard four probe a.c. technique at low frequency. The measurements of the electrical conductivity $\sigma(T)$ covered the temperature range between 0.04 K and 295 K. The magnetoconductivity $\Delta\sigma(H)$ was measured at temperatures between 0.04 K and 1.2 K and in magnetic fields up to 56 kOe.

E. Felder measured the specific heat using a conventional relaxation type method [38] between 0.065 and 36 K. The samples were fixed on a sapphire disk with a diameter of 5 mm and a thickness of 0.25 mm by Apiezon N grease. On the back of the sapphire

disk a 200 Ω heater and electrical contacts for the thermometers were produced by vapor deposition of a layer of 120 \AA of chromium and 70 \AA of gold. Below 1 K, a split 100 Ω Matsushita resistor served as thermometer and for temperatures above 1 K, a 2000 \AA thick layer of $\text{Au}_{1-x}\text{Ge}_x$ with $x \approx 0.01$ was vapor deposited as thermometer [39]. The 10 μm $\text{Cu}_{0.98}\text{Be}_{0.02}$ leads to the heater and the thermometer gave a weak thermal link between the sapphire disk with the sample and the heat reservoir of the cryostat. The specific heat of the addenda is subtracted from the measured specific heat data in all experiments.

Leer - Vide - Empty

3 Thermal conductivity

3.1 Introduction

3.1.1 Excitations in quasiperiodic lattices

Theoretical models

For a one-dimensional model of a quasicrystal, the Fibonacci chain, the exact solution of the acoustic eigenmode problem has been found [41–43] using the transfer matrix method [44,45]. The results can be summarized as follows: The excitation spectrum $\omega(q)$ of a Fibonacci chain is singular, however, in the zero frequency limit $\omega \rightarrow 0$ the spectrum appears continuous, as the widths of the gaps become smaller than the separation of eigenmodes of a chain of finite length [41, 42]. A series of major gaps in the spectrum is observed, which are located at the strongest harmonics in the Fourier image of the density, and the width of these gaps $\delta\omega$ behave as $\delta\omega \propto \omega^2$ in the case considered [45–47]. In Fig. 3.1, the spectrum of the eigenmodes of a Fibonacci chain consisting of 233 atoms with 2 different masses are plotted as a function of the pseudo wave vector q [40]. Instead of a wave vector, which strictly is an undefined quantity here because of the instability of the eigenstates, the density of nodes of the eigenmode is used [40]. In the $\omega(q)$ plot of Figure 3.1 only major gaps are visible. The eigenfunctions $\Psi(x)$ are neither extended nor localized as a function of the distance x , but critical e.g., decaying as some power-law of the distance $\Psi \propto x^\alpha$ [41, 42, 44, 45], and the degree of localization of phonons increases with increasing frequency [41, 42].

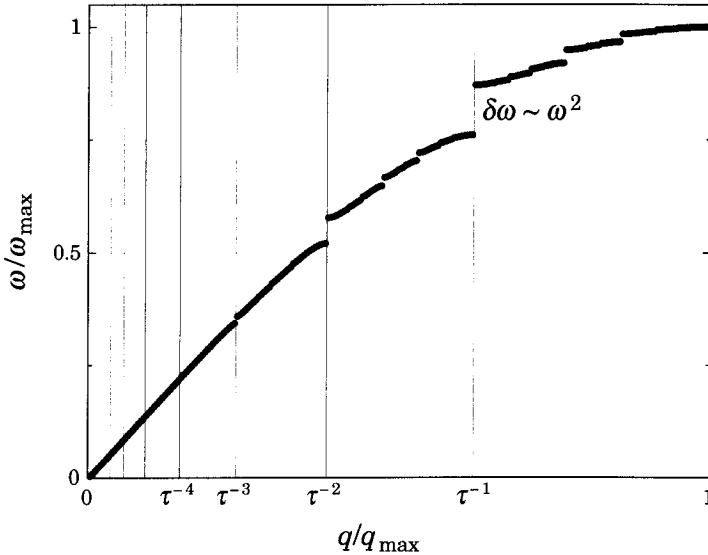


Figure 3.1: Frequencies of phonon eigenmodes of a Fibonacci chain composed of 233 atoms with two different masses. The mass ratio is 1.5 (see Ref. 40).

In the three-dimensional case it has solely been possible to show that the eigenstates in quasicrystals are not localized in momentum space and are consequently always affected by an intrinsic decay rate [45]. This decay rate varies exponentially with the strength of the quasiperiodic potential [48]. For the case of phonons in the long wave length limit it is therefore possible that a phonon scattering mechanism different from the intrinsic decay, like phonon-phonon scattering due to the lattice anharmonicity, may overcome the intrinsic decay rate and become the leading mechanism in limiting the phonon lifetime [40, 43]. Thus thermal conductivity measurements are the ideal spectroscopic tool to investigate phonon interactions in quasicrystals.

For icosahedral quasicrystals in the Al-Mg-Zn [49], Al-Li-Cu [50] and Al-Mn [51] systems theoretical investigations of the lattice dynamics of rational approximants containing a large number of atoms per unit cell were undertaken. The dynamical structure factor $S(\vec{q}, \omega)$ in these systems shows pronounced peaks emerging at zero frequency from strong Bragg reflections. Along high symmetry directions, the maxima of $S(\vec{q}, \omega)$ follow

a linear dispersion law at low frequencies. With increasing frequency the width of the peaks increases, and dispersion is observed, e.g. $d\omega/dq$ decreases. At the Brillouin zone boundary the dispersion curve becomes flat, and at the intersection of branches of the same symmetry originating from different zone centers a gap opens up. Around high symmetry points at the Brillouin-zone boundary a hierarchy of non-dispersive stationary modes is noted. Analyzing a series of consecutive approximants, it was noted that the dispersion curves scale with a constant factor for consecutive approximants [52]. Therefore, in the quasiperiodic limit it is expected that optical branches, as well as gaps in the density of states, can be found at arbitrarily low frequency values [52]. The width of the gaps vanishes in the low frequency limit, and the density of states $g(\omega)$ varies as $g(\omega) \sim \omega^2$.

Neutron scattering experiments

A number of inelastic neutron scattering experiments were undertaken to study lattice excitations in quasicrystals [53]. For icosahedral quasicrystals in the Al-Cu-Fe [54], Al-Li-Cu [55] and Al-Mn-Pd [56] systems phonon modes with no apparent intrinsic width showing a linear dispersion for small wave vectors $|\vec{q}|$ were observed close to strong Bragg reflections in inelastic neutron scattering experiments using triple axis spectrometers. As an example the dispersion relation of the lowest transversal acoustic branch of icosahedral Al-Mn-Pd measured at 300 K is shown in Fig. 3.2 [57]. For small wave vectors $|\mathbf{q}|$, $\omega = v_t/|\mathbf{q}|$ and the transverse sound velocity v_t is in good agreement with the values obtained from acoustic experiments [57,58]. For $|\vec{q}| < 0.35 \text{ \AA}^{-1}$ the width of the transverse mode is limited by the resolution of the spectrometer only. For $|\vec{q}| > 0.35 \text{ \AA}^{-1}$ the mode broadens rapidly with increasing wave vector.

For icosahedral Al-Li-Cu (see Fig. 3.3) it was reported that the integrated phonon intensity I_{Phonon} is proportional to the integrated intensity of the Bragg peak F_{stat}^2 from which the phonon branch is emerging [55]

$$\frac{d^2\sigma}{d\omega d\Omega} \sim F_{\text{stat}}^2 q_{\parallel}^2, \quad (3.1)$$

where q_{\parallel} denotes the component of \mathbf{q} parallel to the polarization of the phonon branch. Scaling of the integrated phonon intensity was also observed in icosahedral Al-Mn-Pd [60].

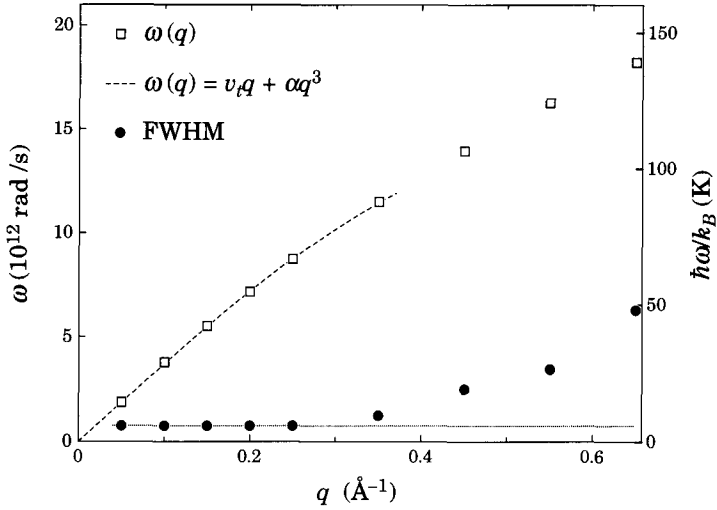


Figure 3.2: The open squares show the dispersion relation of the transverse acoustic excitations of icosahedral Al-Mn-Pd measured at 300 K, and the full circles show the full width at half maximum of the excitation [57]. The broken line is a fit of the phonon dispersion to Eq. 4.15, and the dotted line is a guide to the eye.

These findings are in agreement with theoretical calculations of the dynamical structure factor $S(\vec{q}, \omega)$, suggesting that the integrated phonon intensity close to strong Bragg reflections in quasicrystals has the same scaling behavior as in periodic crystals [50, 61, 62].

A series of broad dispersionless modes were observed for icosahedral Al-Mn-Pd at various energies up to 23 meV in a triple axis experiment [63, 63]. In the same energy range the presence of dispersionless modes was inferred from the generalized vibrational density of states measured with a time-of-flight technique [64]. A stationary mode was also noted for quasicrystals in the Al-Li-Cu system [55].

To summarize, inelastic neutron scattering experiments in quasicrystals indicate well defined lattice modes in the vicinity of strong Bragg reflections showing linear dispersion in the long wave length limit.

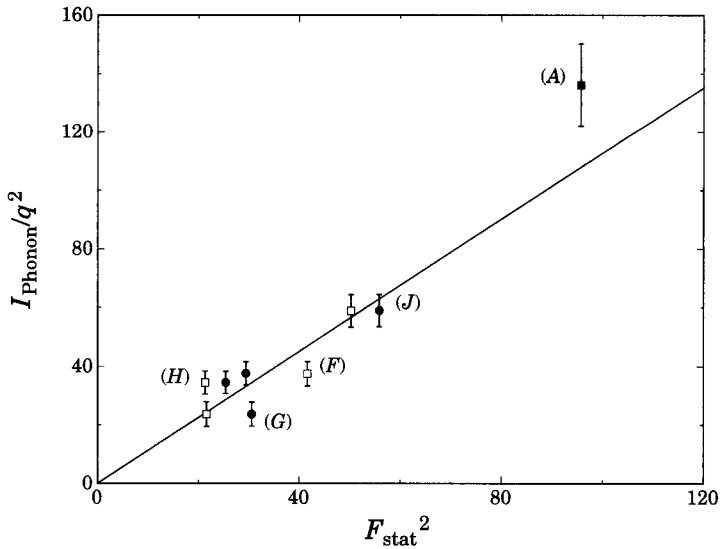


Figure 3.3: The integrated phonon intensity I_{Phonon} of icosahedral Al-Li-Cu is shown as a function of the integrated intensity of the Bragg peak (open squares), or the static structure factor F_{stat}^2 obtained by Gayle [59] (full circles), respectively. Letters denote the different Bragg peaks of the measurements, and the solid line is a guide to the eye. Figure taken from Goldman *et al.*, Ref. 55.

3.1.2 Umklapp scattering

Periodic crystals

A perfectly harmonic periodic crystal has an infinite thermal conductivity [65]. To restore thermodynamic equilibrium in the presence of a thermal gradient, anharmonic processes are required [65]. The anharmonic correction can be considered as perturbation of the harmonic Hamiltonian causing transitions from one harmonic eigenstate to another. In the next order corrections, processes where a phonon of wavevector \mathbf{q} collides with a second one \mathbf{q}' , and both are destroyed in the creation of a third \mathbf{q}'' (or vice versa) have to be considered. Conservation of crystal momentum and conservation of energy require

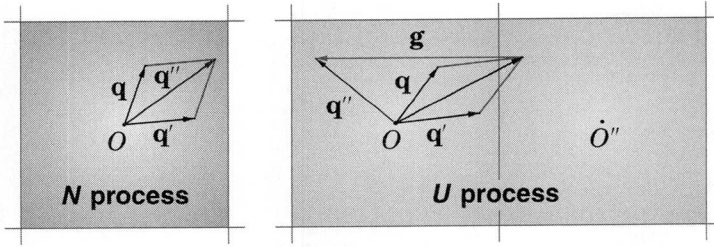


Figure 3.4: Normal process, the crystal momentum is conserved in the collision of \mathbf{q} , and \mathbf{q}' to \mathbf{q}'' – Umklapp process, crystal momentum is not conserved in the collision due to the addition of a reciprocal lattice vector \mathbf{g} .

$$\begin{aligned} \mathbf{q} + \mathbf{q}' &= \mathbf{q}'' + \mathbf{g} \\ \hbar\omega + \hbar\omega' &= \hbar\omega'' \end{aligned} \quad (3.2)$$

where \mathbf{g} is some reciprocal lattice vector. The Crystal momentum is only defined modulo the addition of a reciprocal lattice vector. Therefore two different processes can distinguished as shown in Fig. 3.4; normal processes with $\mathbf{g} = 0$, and Umklapp processes with $\mathbf{g} \neq 0$. However, normal processes lead only to a redistribution of crystal momentum, and are ineffective in restoring the thermodynamic equilibrium [65]. Thus solely the Umklapp processes are limiting the thermal conductivity. Energy conservation requires, that the resulting phonon \mathbf{q}'' must be large enough for its energy to equal the sum of the energies of \mathbf{q} and \mathbf{q}' . Either \mathbf{q} or \mathbf{q}' has to be of the order of $\frac{1}{2}|\mathbf{g}|$ and as a consequence also \mathbf{q}'' . The resulting phonon in an Umklapp process \mathbf{q}'' must thus have an energy $\hbar\omega''$ of the order half of the maximum lattice frequency ω_{\max} , e.g., of the Debye frequency ω_D [66]:

$$\omega'' > \frac{\omega_D}{b}, \quad b \approx 2 \quad (3.3)$$

The rate at which Umklapp processes occur is proportional to the occupational number of initial phonons n_q , and $n_{q'}$:

$$n_q n_{q'} = \frac{1}{e^{\hbar\omega/k_B T} - 1} \frac{1}{e^{\hbar\omega'/k_B T} - 1} \approx e^{-\hbar\omega''/k_B T} < e^{-\Theta_D/bT} \quad (3.4)$$

For temperatures below the Debye temperature Θ_D the lattice thermal conductivity λ_{ph} is expected to vary as [65]

$$\lambda_{\text{ph}} \sim T^\xi e^{\Theta_D/bT} \quad , \quad (3.5)$$

where ξ is of the order of unity. For an observation of this exponential relation the crystal needs to be of high structural quality and isotopically pure. The relevant temperature range of Umklapp scattering is limited to approximately $0.03\Theta_D < T < 0.1\Theta_D$ [67]. A crossover to the Casimir regime of boundary-limited thermal conductivity at the lowest temperatures leads to a maximum in the $\lambda_{\text{ph}}(T)$ dependence. Defects and isotope inhomogeneities suppress this maximum and they alter the exponential relation for $\lambda_{\text{ph}}(T)$. However, even in polycrystalline and impure samples a distinct maximum of $\lambda_{\text{ph}}(T)$ is still observed. An example for the rapid increase of the λ_{ph} with decreasing temperature is shown in Fig. 3.6 for isotopically pure ${}^4\text{LiF}$.

Quasicrystals

In this section an outline will be given how the concept of Umklapp scattering can be generalized to quasicrystals. The process termed Umklapp scattering is due to the interplay of two subsequent scattering events, as pointed out in Ref. 40. In one of these processes, e.g., in multi-phonon scattering, the momentum of lattice excitations, often called crystal momentum, is conserved. The other process, i.e., a Bragg reflection or structural scattering violates the law of conservation of crystal momentum. For periodic crystals, and also for quasicrystals, the important point is that neither of the two scattering processes, if considered separately, will give rise to the same physical consequences as the Umklapp process as whole does, i.e., finite thermal conductivity [40]. In periodic crystals the natural scale for Umklapp scattering is set by the reciprocal lattice. In quasicrystals there is no such scale and the momentum of phonons can be transferred to the lattice in inelastic scattering events by arbitrarily small portions not limited from below in magnitude. This leads to a power-law temperature dependence of the phonon mean free path l , contrary to the exponential temperature dependence of l of periodic crystals at intermediate temperatures [40].

The lattice excitation spectrum of one dimensional quasicrystals is self similar and contains an infinite number of gaps, as can be seen in Fig 3.1 [42]. However, a series of major gaps is observed associated with reciprocal lattice vectors corresponding to the strongest harmonics of the Fourier image of the mass density. These wave vectors form a geometrical series $q_n \propto C^n$, where C is a constant depending on the specific type of quasilattice under consideration [68]. For small wavevectors q , the width of these gaps $\delta\omega$ scales as $\delta\omega \propto \omega^2$ [40]. This scaling of the gaps is also expected and assumed to hold in the case of three dimensional quasicrystals [40]. The contribution of the small gaps to the Umklapp scattering rate is expected to be small as the amplitude of the associated harmonic is small and only the gaps belonging to the major series have to be considered [40]. Let now q_0 denote a reciprocal lattice vector associated with one of the major gaps. Then only those phonons which are newly created in a multi-phonon process and whose wave vectors are in the resonance region $|q - q_0| < \delta\omega/v$ are efficiently scattered by the wave vector q_0 , where v is the sound velocity. For a three dimensional quasicrystal the probability of a newly created phonon to be scattered by the structure can be estimated as follows: In the spherical layer between Cq_{ph} and q_{ph}

$$Cq_{\text{ph}} < q < q_{\text{ph}} \quad , \quad (3.6)$$

there is always a constant number of these harmonics as expected from self-similarity arguments [68]. Using the ω^2 scaling of the major series gap widths it follows that the probability P is proportional to ω , more precisely, $P = A\omega/\omega_{\text{max}}$, where A is a dimensionless constant depending on the structure of the quasicrystal [40]. The scattering probability of three phonon processes itself is proportional to ωT^4 [40]. Here it was supposed that only one phonon in the three-phonon process has a low frequency and that the two others are merely thermal ones with their frequency proportional to the temperature. All in all, the average transport cross-section for the anharmonic and quasiperiodic structural scattering, together denoted as quasiperiodic Umklapp process, is proportional to $\omega^2 T^4$, i.e., not exponential in frequency or temperature as is valid for Umklapp processes in common crystals. In the limit of low temperatures and assuming that quasiperiodic Umklapp processes are the main source for the quasilattice thermal resistance $\lambda_{\text{ph}}^{-1}(T)$, a Debye-type approximation then leads to the expectation that $\lambda_{\text{ph}} \propto T^{-3}$. However, as noted for periodic crystals, it will be difficult to observe the temperature dependence of $\lambda_{\text{ph}} \propto T^{-3}$

expected for generalized Umklapp scattering in quasicrystals, as there is always an additional contribution to the thermal resistance due to Rayleigh scattering on mass density fluctuations that will alter the overall temperature characteristic of $\lambda_{\text{ph}}(T)$.

3.2 Icosahedral Al-Mn-Pd

Among thermodynamically stable quasicrystals, icosahedral Al-Mn-Pd is considered as the quasiperiodically ordered material possessing the highest structural quality as revealed by X-ray structure analysis or electron microscopy investigations [16, 22–24]. For example, high resolution X-ray diffraction experiments performed on Al-Mn-Pd quasicrystals revealed a mosaic full width at half maximum of less than 0.001° and resolution limited widths of the diffraction peaks [16]. At the same time, a high degree of structural perfection of icosahedral Al-Mn-Pd has been confirmed by anomalous transmission of X-rays through this material [16]. Therefore icosahedral Al-Mn-Pd is a suitable material for the investigation of the influence of quasiperiodicity on thermal transport, as proposed in Sec. 3.1.2.

In Fig. 3.5 the thermal conductivity λ of the polygrained sample of icosahedral $\text{Al}_{70}\text{Mn}_9\text{Pd}_{21}$ is shown between 0.065 and 320 K on logarithmic scales. An estimate of the electronic contribution λ_{el} to λ can be obtained using the Wiedemann-Franz law from electrical conductivity data reported previously for a sample cut from the same ingot [69]. The result of this calculation is shown as the solid line in Fig. 3.5. It may be seen that over most of the covered temperature range λ_{el} is at least an order of magnitude lower than λ , and therefore the phonon contribution λ_{ph} may be evaluated quite accurately there by subtracting off λ_{el} from λ .

The result of this subtraction is shown Fig. 3.6 on logarithmic scales. From 0.065 up to 25 K $\lambda_{\text{ph}}(T)$ of icosahedral Al-Mn-Pd increases monotonically with increasing T . For temperatures above 10 K $\lambda_{\text{ph}}(T)$ shows a trend to saturation. Between 25 and 55 K $\lambda_{\text{ph}}(T)$ is almost temperature independent, and $\lambda_{\text{ph}}(T)$ increases slowly with T above 55 K.

This overall temperature dependence of λ_{ph} is reminiscent of that of an insulating or metallic glass, where λ_{ph} in general varies as T^2 at low temperatures, and a plateau in $\lambda_{\text{ph}}(T)$ is observed between approximately 2 and 10 K. Nevertheless, we note

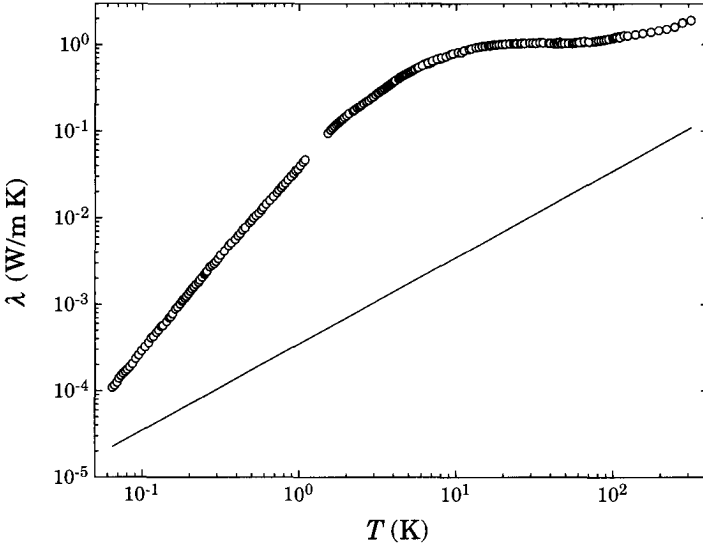


Figure 3.5: Measured thermal conductivity λ of icosahedral $\text{Al}_{70}\text{Mn}_9\text{Pd}_{21}$ between 0.065 and 320 K. The solid line is an estimate of the electronic contribution λ_{ei} to λ .

some important differences in the region of the λ plateau. The λ plateau of icosahedral $\text{Al}_{70}\text{Mn}_9\text{Pd}_{21}$ is developed at higher temperatures, and it extends over a wider temperature range than in amorphous solids. Moreover, the lattice thermal conductivity of $\text{Al}_{70}\text{Mn}_9\text{Pd}_{21}$ in the plateau range is higher than that of amorphous solids [72]. This can be seen in Fig. 3.6 where λ_{ph} of vitreous silica [70] is shown for comparison. In the plateau range λ_{ph} of icosahedral Al-Mn-Pd rather shows a behaviour intermediate between that of an amorphous and a crystalline insulator. To illustrate this point λ_{ph} of a periodic crystal, isotopically pure ${}^7\text{LiF}$ [71], is shown in Fig. 3.6.

The phonon mean free path in periodic crystals at low temperatures is determined by either the sample dimensions or the spatial distribution of imperfections, and λ_{ph} varies as T^3 [73]. With increasing temperature the number of high frequency phonons available for Umklapp scattering increases leading to an exponential decrease of λ_{ph} . A maximum is reached when the phonon mean free path due to phonon-phonon scattering is comparable

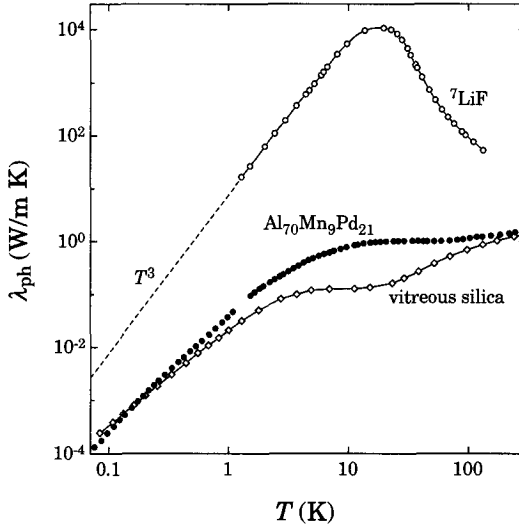


Figure 3.6: Phonon thermal conductivity λ_{ph} of the polygrained sample of $\text{Al}_{70}\text{Mn}_9\text{Pd}_{21}$ is shown on the same scales as that of the amorphous solid vitreous silica [70], and a periodic crystal of isotopically pure ${}^7\text{LiF}$ [71]. The broken line is an extrapolation of λ_{ph} in the Casimir limit to lower temperatures.

to that due to boundary scattering. In the following analysis, the differences and similarities of $\lambda_{\text{ph}}(T)$ of icosahedral Al-Mn-Pd to that of amorphous and periodic solids will be discussed.

3.2.1 Thermal conductivity at low temperatures

Tunneling states

The analysis of $\lambda_{\text{ph}}(T)$ of icosahedral $\text{Al}_{70}\text{Mn}_9\text{Pd}_{21}$ will be first focussed on the temperature range between 0.35 and 1.6 K. For these temperatures, the $\lambda_{\text{ph}}(T)$ -curve can be well described by a power-law $\lambda_{\text{ph}} = AT^n$, with $n = 2.06 \pm 0.01$. A power-law behaviour of λ_{ph} with an exponent n close to 2 in this temperature range is similar to what is observed in amorphous solids and compatible with scattering of phonons by tunneling states [74, 75].

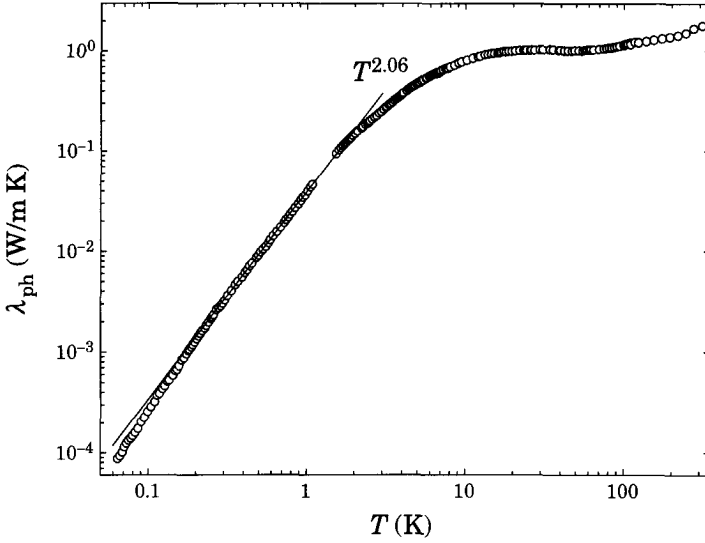


Figure 3.7: Phonon contribution $\lambda_{\text{ph}}(T)$ to the thermal conductivity of $\text{Al}_{70}\text{Mn}_9\text{Pd}_{21}$. The solid line is a power-law approximation to the data between 0.35 and 1.6 K.

In the tunneling states model the presence of asymmetric double well potentials is assumed [74, 75]. Phonons can couple to these two-level systems via a deformation of the double-well potentials. At low temperatures resonant absorption and emission of phonons becomes the dominant scattering mechanism. The phonon mean free path l_{TS} can be calculated under the assumption that the density of tunneling states is constant over a wide range of parameters of both the asymmetry and the intrinsic relaxation time. In this case l_{TS} is expected to vary as $l_{\text{TS}} \propto \omega^{-1}$ [74, 75]. Employing the Debye approximation, i.e. assuming an isotropic linear phonon dispersion, the thermal conductivity is then given by

$$\lambda_{\text{TS}} = \frac{\rho k_B^3 \bar{v}}{6\pi\hbar^2 \bar{P}\gamma^2} T^2, \quad (3.7)$$

where ρ is the mass density, \bar{v} is the weighted average of the sound velocities v_i , and v_l for transverse and longitudinal waves, respectively, \bar{P} is the density of tunneling states and γ^2 describes the average coupling between them and the phonons. We note that in glasses the actual exponent in the power-law description of $\lambda_{\text{ph}}(T)$ is almost never exactly 2. This is

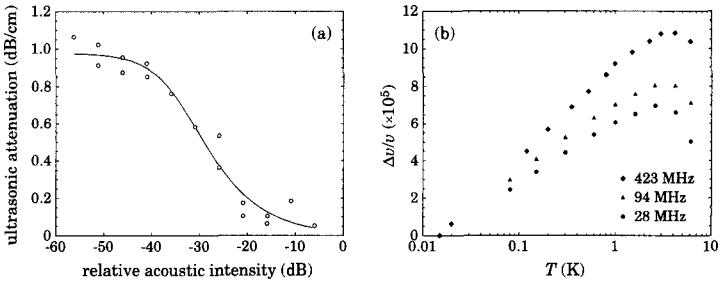


Figure 3.8: (a)–Non-linear attenuation of shear waves with a frequency of 423 MHz as function of the relative incident power at a temperature of 0.015 K [77]. (b)–Relative variation of the sound velocity of shear waves with temperature for different frequencies [77]. In both measurements a magnetic field of 50 kOe was applied to fully orient the magnetic moments and to suppress spin-glass ordering.

thought to arise from a weak energy dependence of the density of tunneling states acting as scattering centers.

A fit of the data to Eq. 3.7 in the temperature range between 0.35 and 1.6 K yields a value of $\bar{P}\gamma^2 = 6.5 \times 10^7 \text{ erg cm}^{-3}$ for the coupling parameter, fairly close to the values previously deduced from the thermal-conductivity data of typical insulating and metallic glasses [76]. Here values of $v_t = 3.8 \times 10^5 \text{ cm s}^{-1}$ and $\rho = 5.1 \text{ g cm}^{-3}$ from Ref. 77 were used and it was assumed that v_t is close to \bar{v} [58] calculated as

$$\frac{3}{\bar{v}^3} = \frac{1}{v_l^3} + \frac{2}{v_t^3} \quad (3.8)$$

Evidence for the presence of tunneling states in Al-Mn-Pd quasicrystals was claimed by Vernier and coworkers by analyzing the results of ultrasound experiments on an Al-Mn-Pd quasicrystal with a slightly different chemical composition than the sample used here [77]. They revealed a non-linear attenuation of acoustic shear waves at low-temperatures and a small logarithmic deviation in the sound-velocity variation with temperature.

Measurements of the attenuation Γ of shear waves with a frequency of 423 MHz as function of the incident power J at 0.015 K showed a decrease of the attenuation with

increasing incident power. For the highest values of the incident power used in the experiment a trend to saturation of the attenuation is noticed, as can be seen in Fig. 3.8(a). Such a behaviour of $\Gamma(J)$ is typically observed in glasses and thought to be a characteristic signature of tunneling states. With increasing acoustic intensity the upper level of a two-level system becomes more and more populated and is no longer effective in absorption processes [78]. This leads to a variation of $\Gamma(J)$ as [79]

$$\Gamma = \pi \frac{\bar{P}\gamma^2}{\rho v_i^2} \frac{\omega}{\sqrt{1 + J/J_c}} \tanh\left(\frac{\hbar\omega}{2k_B T}\right) \quad , \quad (3.9)$$

where J_c is the critical power, and v_i the sound velocity for longitudinal and transverse waves, respectively.

The interaction between tunneling states and phonons gives rise to dispersion of the phonons. The strength of this interaction is proportional to the population of the levels and consequently the sound velocity $d\omega/dq$ is temperature dependent [78]. For $\hbar\omega/k_B T \ll 1$ the sound velocity v_i is expected to vary as [80]

$$\frac{v_i(T) - v_i(T_0)}{v_i} = \frac{\bar{P}\gamma^2}{\rho v_i^2} \ln\left(\frac{T}{T_0}\right) \quad , \quad (3.10)$$

here T_0 denotes some reference temperature. Below 1 K, the data taken for different frequencies show a linear behavior in the representation as $\Delta v/v$ vs. $\ln T$ in Fig. 3.9(b), albeit with a frequency dependent slope. A fit of the sound attenuation data obtained at 423 MHz using Eq. 3.9 gives $\bar{P}\gamma^2 = 1.3 \times 10^7$ erg cm⁻³ and a fit of the sound velocity variation measured at the same frequency using Eq. 3.10 yields $\bar{P}\gamma^2 = 1.6 \times 10^7$ erg cm⁻³.

These values are obviously very close to $\bar{P}\gamma^2 = 1.9 \times 10^7$ erg cm⁻³ obtained from sound-velocity measurements on the metallic glass Pd-Si [81]. The fact that the coupling constant obtained from sound-velocity experiments is several times lower than the value compatible with the measured thermal conductivity is well known in metallic glasses [76]. It was argued that the presence of conduction electrons in glassy metals may dramatically decrease the relaxation times of tunneling states and, therefore, change the average coupling parameter [82].

Tunneling states in quasicrystals have been associated with phasons [83]. Even in structurally perfect Al-Mn-Pd, phason-type disorder of the chemical occupation of

specific atomic surfaces was revealed by anomalous X-ray diffraction close to the Pd edge [24]. The atomic surfaces in quasicrystals are mostly discontinuous and the phason motion has presumably to be associated with atomic jumps [84, 85]. In icosahedral Al-Mn-Pd and Al-Cu-Fe the presence of atomic jumps with an activation energy of the order of several 100 meV for temperatures above 450 °C was claimed from an inelastic neutron scattering investigation with a time-of-flight spectrometer [84, 86, 87]. However, the different energy scales render a connection between the excitations observed in inelastic neutron scattering at high temperatures and the tunneling states manifest in the thermal conductivity at very low temperatures rather improbable. Recent ^{27}Al 2D exchange NMR experiments in icosahedral $\text{Al}_{70}\text{Re}_{8.6}\text{Pd}_{21.4}$ indicated slow atomic motions in the sub-kHz range at temperatures between 0.16 and 130 K which are limited in space to several interatomic distances [85]. For temperatures below 1 K, the average jump rate τ_{exch}^{-1} of these motions is only weakly temperature dependent. Between 5 and 30 K, the temperature dependence of τ_{exch}^{-1} is compatible with an activation energy ϵ of 1.5 meV. This value is considerably lower than the value of the activation energy of $2k_B\theta_D$ corresponding to $\epsilon = 70$ meV [88] assumed to be characteristic of fast phason diffusion processes in quasicrystals [89]. An estimate of the diffusion constant \mathcal{D} may be calculated from the $\tau_{\text{exch}}(T)$ assuming the typical jump length to be $l \approx 0.1$ nm yielding $\mathcal{D} \approx 3 \times 10^{-15}$ cm²/s at 130 K, much faster than the bulk diffusion rate $D = 10^{-22}$ cm²/s obtained with radiotracer methods in icosahedral Al-Mn-Pd [90]. At present, the relation between the atomic motion observed in ^{27}Al 2D exchange NMR and the tunneling states indicated by the thermal conductivity results is not fully understood. The microscopic origin of tunneling states in amorphous solids is not known either, although the existence of these states is unambiguously established by various independent experiments. They are assumed to be related to a tunneling motion of a group of atoms and it is generally accepted that a continuous density of tunneling states results from some kind of randomness of their structure. We note that a continuous density of tunneling states has been observed even in periodic crystals. An example is a crystalline $\text{Ti}_{0.67}\text{V}_{0.33}$ alloy with b.c.c. structure [91]. The low-temperature phonon thermal conductivity of this solid-solution alloy varies as T^2 and the values of λ_{ph} are of the same order of magnitude as those reported for insulating and metallic amorphous solids. This was ascribed to the high degeneracy in this material of energetically similar configurations of positional disorder [91].

Boundary scattering

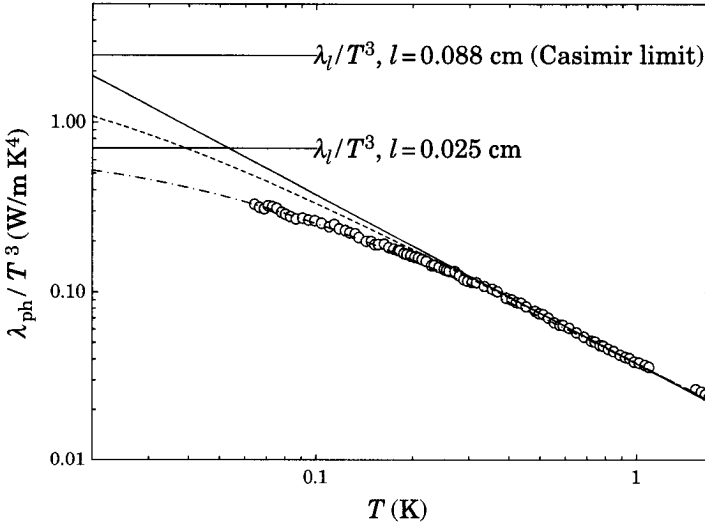


Figure 3.9: λ_{ph}/T^3 vs. T of icosahedral $\text{Al}_{70}\text{Mn}_9\text{Pd}_{21}$ below 1.6 K. The solid line is a fit of the thermal conductivity due to scattering on tunneling states $\lambda_{\text{TS}} \propto T^2$ between 0.35 and 1.6 K. The broken line is calculated from Eq. 3.11 assuming phonon scattering on tunneling states and on the sample boundary. The dash-dotted line is a fit of Eq. 3.11 using the phonon mean free path l as fit parameter (see text).

For temperatures below 0.35 K, λ_{ph} decreases distinctly faster with decreasing temperature than T^2 , as can be seen in Fig. 3.7. In order to obtain a better understanding of the data below 0.35 K, λ_{ph} is plotted as λ_{ph}/T^3 vs. T in Fig. 3.9. The solid straight line in Fig. 3.9 depicts the fit to the data of Eq. 3.7 between 0.35 and 1.6 K. The diagram reveals that below 0.35 K, λ_{ph}/T^3 falls under the T^{-1} -variation with decreasing T , indicative of a stronger than T^2 variation of $\lambda_{\text{ph}}(T)$. It should be noted that the distinct deviation from an approximate T^2 behaviour cannot be ascribed to a systematic error since even at 0.06 K the calculated electronic contribution λ_{el} to the measured thermal conductivity λ amounts to only 20 per cent of λ .

This trend suggests that an additional mechanism of phonon scattering becomes effective at low temperatures which limits the phonon mean free path to below that imposed by scattering involving tunneling states. The resulting total mean free path becomes less frequency-dependent, and it varies approximately as $T^{-0.5}$ at the lowest temperatures of our experiment. Similar λ_{ph} vs. T behaviour as shown in Fig. 3.9 for icosahedral $\text{Al}_{70}\text{Mn}_9\text{Pd}_{21}$, i.e., that the T -dependence of λ_{ph} is stronger than T^2 at very low temperatures, is particularly pronounced in composite glassy systems with an additional source of phonon scattering. Examples are fused capillary arrays of boro-silicate glass or polycarbonate [92] and boro-alumino-silicate glass containing mica crystallites [93]. There are some other differences in the behaviour of the above mentioned materials that are not important at this point. Introduction of holes or crystallites in a glassy matrix produces a frequency-independent phonon mean free path. This results in a strong suppression of the phonon mean free path below the value determined by the phonon scattering on tunneling states alone. Therefore the thermal conductivity of composite glassy systems also shows a gradual increase of the slope in $\lambda_{\text{ph}}(T)$ with decreasing temperature. At the lowest temperatures the $\lambda_{\text{ph}}(T)$ variation is reported to be close to T^3 [94].

The above mentioned composite glassy systems represent cases of extremely strong additional phonon scattering corresponding to mean free paths of the order of 10^{-4} – 10^{-3} cm. If the mean free path l due to excessive scattering is long enough the T^3 -regime will not be reached down to the lowest temperatures of the order of 0.05 K readily accessible to thermal-conductivity measurements.

Below it will be argued that the λ_{ph} behaviour of icosahedral $\text{Al}_{70}\text{Mn}_9\text{Pd}_{21}$ between 0.06 and 0.35 K most likely manifests a crossover between a regime, where the phonon mean free path is limited by scattering on tunneling states with a mean free path $l \propto T^{-1}$ and a regime of excessive phonon scattering with a temperature-independent mean free path. These two phonon scattering mechanisms can be combined by adapting Matthiessen's rule to phonons

$$\lambda_{\text{ph}} = (\lambda_l^{-1} + \lambda_{\text{TS}}^{-1})^{-1} \quad (3.11)$$

where λ_{T}^{-1} is the thermal resistance due to phonon scattering involving tunneling states and given by Eq. 3.7, and λ_l is the thermal conductivity limited by the temperature-independent mean free path l_c [73]

$$\lambda_l = \frac{2\pi^2 k_B^4 l}{15h^3 v^2} T^3 \quad . \quad (3.12)$$

The first explanation at hand for the deviation from an approximate T^2 -behaviour of $\lambda_{\text{ph}}(T)$ postulates the growing importance of a boundary-limited conductivity in the Casimir limit, presuming nonspecular scattering of phonons at the sample surface.

Size-limited thermal conductivities are well documented for pure periodic crystals [95,96]. Apparently different is the situation in glassy materials, where nonspecular boundary scattering at the surfaces is usually absent. It was argued that the defects responsible for diffusive scattering of phonons at the surfaces of periodic crystals are not present in amorphous solids [94]. It is not known whether the necessary kind of defects exists at surfaces of quasicrystals.

The calculated λ_{ph}/T^3 vs. T variation given by Eq. 3.11 with the sample-boundary limited mean free path $l_c = \alpha(4A/\pi)^{1/2} = 0.088$ cm, where A is the area of the sample cross-section and the factor α accounts for the finite sample length [97] is plotted as the dashed line in Fig. 3.9. The ratio of length and width of this sample leads to a coefficient α of 0.68 [97].

A slightly reduced value of $\bar{P}\gamma^2 = 6.1 \times 10^7$ erg cm⁻³ is needed to fit the data above 0.35 K. Below 0.35 K, this line strongly deviates from the experimentally measured λ_{ph}/T^3 values. This indicates that the effective mean free path for phonons at very low temperatures is substantially shorter than 0.088 cm and, therefore, we cannot attribute the observed deviation of $\lambda_{\text{ph}}(T)$ from the T^2 -variation below 0.35 K to the proximity of the Casimir limit, shown as the upper horizontal solid line in Fig. 3.9. The possibility of a boundary-limited conductivity with specular scattering can also be discarded because it would imply an even higher thermal conductivity.

In the following the mean free path l_c is considered as a fitting parameter to obtain an estimate of its value from a fit of Eq. 3.11 to the data in the temperature range between

0.06 and 1.6 K. The result of this fit, displayed as the dash-dotted line in Fig. 3.9, yields a length of $l_c = 0.025$ cm. It is not clear which mechanism of phonon scattering is responsible for this length scale. Scattering of phonons on microholes or grain boundaries may limit the phonon mean free path to the above mentioned length of 0.025 cm. It should be noted that different types of faceted microholes with an average diameter between 20 and 25 μm have been observed in $\text{Al}_{70}\text{Mn}_9\text{Pd}_{21}$ quasicrystals [21]. The limiting value compatible with this mean free path is shown as the lower horizontal solid line in Fig. 3.9.

3.2.2 Thermal conductivity at intermediate temperatures

Rayleigh scattering

The most prominent property of icosahedral $\text{Al}_{70}\text{Mn}_9\text{Pd}_{21}$ at higher temperatures is that $\lambda_{\text{ph}}(T)$ is only weakly temperature dependent in the temperature range between 25 and 55 K. This behaviour is similar to the plateau-type λ_{ph} typically observed in amorphous solids. However, one should note important differences regarding the thermal-conductivity behaviour of icosahedral $\text{Al}_{70}\text{Mn}_9\text{Pd}_{21}$ and that of amorphous solids in the λ -plateau regions. The λ -plateau of icosahedral $\text{Al}_{70}\text{Mn}_9\text{Pd}_{21}$ is developed at substantially higher temperatures than in amorphous solids, where generally a λ -plateau occurs in a temperature range between approximately 2 and 10 K [72]. Moreover, the thermal conductivity of icosahedral in the temperature range where the plateau is observed is *substantially* higher than that of insulating and metallic glasses in their respective plateau regions [72]. To illustrate this point the scaled λ_{ph}/K vs. T/Θ_D of icosahedral $\text{Al}_{70}\text{Mn}_9\text{Pd}_{21}$ is shown in Fig. 3.10 together with a number of different insulating and metallic glasses. In insulating and metallic glasses the phonon mean free path l at low temperatures as deduced from thermal conductivity data is of the order of $l = 150\lambda$, where λ is the wavelength of the phonons [98]. Thus, the coupling constant $\bar{P}\gamma^2$ between the phonons and the tunneling states as calculated from Eq. 3.7 is almost the same for a large variety of amorphous systems. It was this finding that led to assertion that tunneling states are intrinsic in glasses. The correlation $l = 150\lambda$ was used by Freeman and Anderson [98] to show that the thermal conductivity data for different amorphous systems can be brought into a

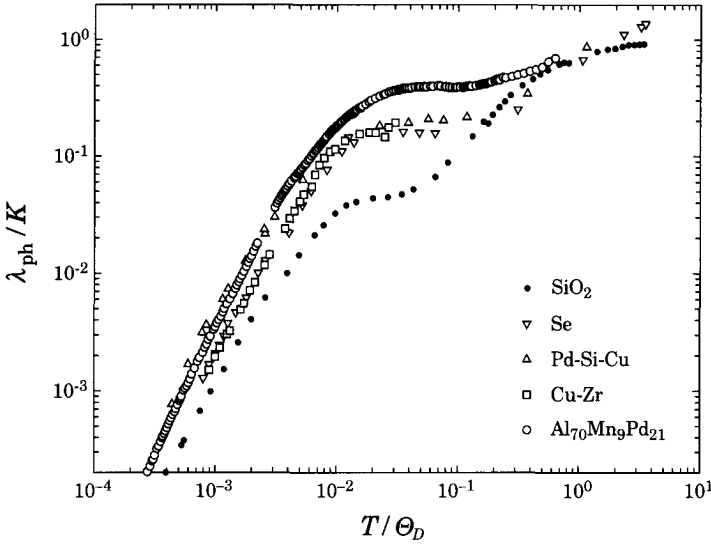


Figure 3.10: Scaled phonon thermal conductivity λ_{ph}/K versus T/Θ_D of icosahedral $\text{Al}_{70}\text{Mn}_9\text{Pd}_{21}$ in comparison with four insulating and metallic glasses (from Ref. 98).

common register at low, and at high temperatures, when the ratio of λ_{ph}/K with

$$K = \frac{k_B^3}{\pi \hbar^2} \frac{\Theta_D^2}{\bar{v}} \quad (3.13)$$

is plotted as λ_{ph}/K vs. T/Θ_D . Here \bar{v} denotes the weighted average to the sound velocity, and Θ_D the Debye temperature. For the scaling of the quasicrystal data the Θ_D value of 493 K, as deduced from the low-temperature values of the sound velocities was used [99]. In the range $T/\Theta_D < 10^{-2}$ the λ_{ph}/K values are fairly close to those of most amorphous solids (Fig. 3.10). In the intermediate temperature range $10^{-1} < T/\Theta_D < 10^{-2}$ the thus scaled thermal conductivity exceeds the λ_{ph}/K values typical for amorphous solids. At higher temperatures $T/\Theta_D > 10^{-2}$, of quasicrystalline $\text{Al}_{70}\text{Mn}_9\text{Pd}_{21}$ again a tends to approach the values typical for amorphous solids.

The plateau of λ_{ph} in amorphous solids is thought to be the consequence of a rapidly decreasing phonons mean free path $l(\omega)$ with increasing frequency [92]. The available

experimental evidence indicates that the phonon mean free path in amorphous solids has a frequency dependence $l \propto \omega^{-n}$, with $n \approx 3 - 4$ [98]. The explicit relation $l \propto \omega^{-4}$ does account for the λ plateau in many amorphous solids. Rayleigh scattering on mass density fluctuations with a correlation length shorter than the phonon mean free path leads to a frequency dependence of the mean free path $l \propto \omega^{-4}$ [66]. In some periodic crystals, the mass difference of the different chemical isotopes is known to be an equally strong source of scattering as the phonon-phonon interaction [66]. However, in the case of amorphous solids it was questioned whether sufficiently strong sources of Rayleigh scattering are present to explain the magnitude of the observed λ -plateau [92]. On the other hand, evidence in favor of Rayleigh scattering and $l \propto \omega^{-4}$ was put forward from direct numerical calculations of the diffusion constant and thermal conductivity on a disordered percolating network [100,101]. Completely different is the situation in icosahedral $\text{Al}_{70}\text{Mn}_9\text{Pd}_{21}$: As the λ plateau is developed at a much higher temperature and extends over a wider temperature range than in amorphous solids a variation of $l \propto \omega^{-4}$ is by far not adequate for fitting the data of icosahedral $\text{Al}_{70}\text{Mn}_9\text{Pd}_{21}$. The characteristically different behaviour of λ_{ph} of quasicrystals and amorphous solids in the plateau region may readily be seen for single grained Al-Mn-Pd in Fig. 3.11.

Quasiperiodic Umklapp scattering

In Fig. 3.11 the lattice thermal conductivity $\lambda_{\text{ph}}(T)$ of a single grain sample of $\text{Al}_{70.5}\text{Mn}_{8.5}\text{Pd}_{21}$ synthesized by Tamura *et al.* [103] is shown on linear scales up to 100 K together with literature values for a single grain $\text{Al}_{70}\text{Mn}_{10}\text{Pd}_{20}$ quasicrystal [102] and the previously discussed data of the polygrained $\text{Al}_{70}\text{Mn}_9\text{Pd}_{21}$ sample. For the single grain Al-Mn-Pd quasicrystals a distinct maximum of λ_{ph} is observed around 20 K. Above the maximum follows a region with a negative slope $d\lambda_{\text{ph}}/dT$ extending up to 85 K. The appearance of the maximum in the $\lambda_{\text{ph}}(T)$ curve implies that the mean free path of phonons with a given frequency decreases with increasing temperature. Thus, the phonon mean free path $l(\omega, T)$ in icosahedral $\text{Al}_{70}\text{Mn}_9\text{Pd}_{21}$ quasicrystals is *temperature- and frequency dependent*, whereas in amorphous solids an explicit temperature dependence of l is not required to explain the λ_{ph} variation.

As argued in Sec. 3.1.2, in the regime where quasiperiodic Umklapp scattering is the dominant scattering process, the thermal conductivity is expected to vary as $\lambda_{\text{ph}} \propto T^{-3}$.

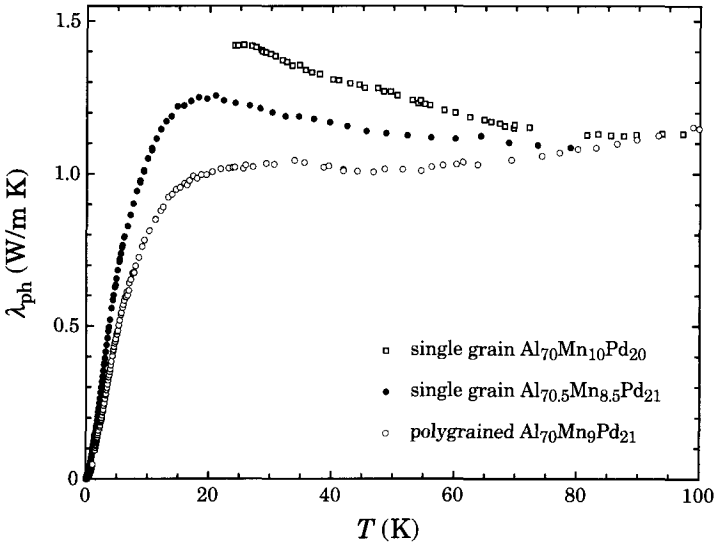


Figure 3.11: Lattice thermal conductivity $\lambda_{\text{ph}}(T)$ of icosahedral $\text{Al}_{70}\text{Mn}_9\text{Pd}_{21}$. Data of the single grain $\text{Al}_{70}\text{Mn}_{10}\text{Pd}_{20}$ quasicrystal is taken from Ref. 102.

Although this T^{-3} temperature dependence of λ_{ph} is not really observed probably due to an additional thermal resistance from Rayleigh scattering, it is reasonable to believe that the decrease of λ_{ph} with increasing T from 20 to 85 K above the maximum is due to quasiperiodic Umklapp processes. The maximum in the $\lambda_{\text{ph}}(T)$ curve has to be interpreted as a crossover from the regime of a dominant scattering of phonons by tunneling states to the regime where quasiperiodic Umklapp processes are important. The lower rate of phonon scattering on tunneling states in the single grain samples leads to an enhancement of the height of the $\lambda_{\text{ph}}(T)$ maximum and to an extension of the temperature range where the slope of $\lambda_{\text{ph}}(T)$ is negative. As can be seen in Fig. 3.12, all three samples show an approximate T^2 behaviour of $\lambda_{\text{ph}}(T)$ at low temperatures that is characteristic of phonon scattering on tunneling states. The absolute values of $\lambda_{\text{ph}}(T)$ of the single grain $\text{Al}_{70}\text{Mn}_{10}\text{Pd}_{20}$ quasicrystal are about a factor of 4 higher than for the polygrained $\text{Al}_{70}\text{Mn}_9\text{Pd}_{21}$, suggesting a lower concentration of tunneling states.

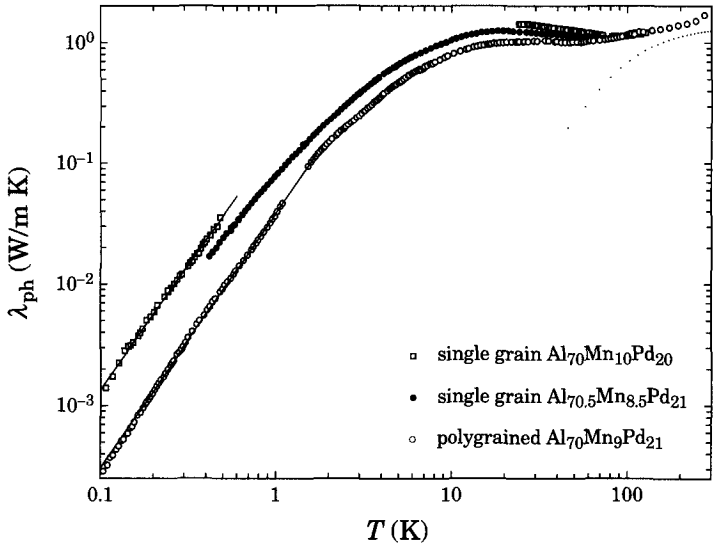


Figure 3.12: Lattice thermal conductivity $\lambda_{\text{ph}}(T)$ of icosahedral Al-Mn-Pd. Data of the single grain $\text{Al}_{70}\text{Mn}_{10}\text{Pd}_{20}$ quasicrystal is taken from Ref. 102. The solid line is a power-law approximation to the data between 0.35 and 1.6 K. The dotted line is an estimate of the thermal conductivity diffusive phonon propagation using Eq. 3.14.

3.2.3 Thermal conductivity at high temperatures—Einstein model

Above 85 K the $\lambda_{\text{ph}}(T)$ of icosahedral Al-Mn-Pd increases slowly and almost the same values of $\lambda_{\text{ph}}(T)$ are measured for the three different samples. Magnitude and temperature dependence of $\lambda_{\text{ph}}(T)$ of icosahedral Al-Mn-Pd are similar to those reported in amorphous solids (see Fig. 3.10). In amorphous solids two models are in use to explain the increase of $\lambda_{\text{ph}}(T)$ above the plateau: Kittel [104] has suggested that in this regime l is a constant of the order of an average interatomic distance. Alternatively, Einstein [105] assumed that the heat is transported via energy transfer between coupled neighbouring atoms vibrating with random phases. A modification of the original result by Cahill and Pohl [106] that removes the uncertainty of choosing the Einstein temperature is compatible with l of the order of $\pi\bar{v}\omega^{-1}$, i.e., half of the wavelength of the excitation. Above a few tens of degrees Kelvin this model adequately describes the lower limit of the thermal conductivity of

amorphous solids which is often referred to as the minimum thermal conductivity [106]. The modification of Einstein's original result leads to a thermal conductivity λ_{\min} [106]:

$$\lambda_{\min} = (6\pi^2 n)^{1/3} \frac{k_B^2 T^2}{h\Theta_D} \int_0^{\Theta_D/T} \frac{x^3 e^x}{(e^x - 1)^2} dx \quad , \quad (3.14)$$

where n is the number of atoms per unit volume and Θ_D is the Debye temperature. The resulting minimal thermal conductivity of icosahedral Al₇₀Mn₉Pd₂₁ calculated from Eq. 3.14 and $\Theta_D = 493$ K is shown as the dotted line in Fig. 3.12. The calculated value of λ_{\min} suggests that in icosahedral Al-Mn-Pd heat transport at high temperatures occurs predominantly via phonon diffusion and the assumption of propagating phonons is no longer valid at high temperatures, i.e., high frequencies. In the case of amorphous solids, a direct numerical study of a disordered model system consisting of a cubic lattice with a site occupation probability p of 0.65 leads to a similar conclusion [100, 101]. In this study it was shown that although phonon localization may occur at high frequencies, thermal transport persists due to diffusion, which can be described within the concept of the minimal thermal conductivity [100, 101].

3.2.4 Thermal conductivity of icosahedral Al-Mn-Pd–Kinetic model

The thermal conductivity in the relaxation time approximation can be calculated as [67]

$$\lambda_{ph}(T) = \frac{1}{3} \int_0^\infty \rho_{\text{mol}} g(\omega) \bar{v} l(\omega, T) \frac{\partial}{\partial T} \left(\frac{1}{\exp(\hbar\omega/k_b T) - 1} \right) d\omega \quad , \quad (3.15)$$

where \bar{v} is the sound velocity, $l(\omega, T)$ the *temperature- and frequency-dependent* mean free path, $g(\omega)$ is the phonon density of states and ρ_{mol} is the molar density. An estimate of the density of vibrational states (DOVS) $g(\omega)$ can be obtained from the lattice specific heat $C_{\text{ph}}(T)$, as the characteristic temperature dependence of $C_{\text{ph}}(T)$ is governed mostly by the low-frequency part of the DOVS (see Sec. 4.3.2).

The lattice specific heat $C_{\text{ph}}(T)$ of a single grain sample of icosahedral Al-Mn-Pd after subtracting off the linear contribution γT and the magnetic contribution $C_m(T)$ from $C_p(T)$ as reported by Wälti *et al.* [57] is shown as a plot of C_{ph}/T^3 vs. T in Fig. 3.13.

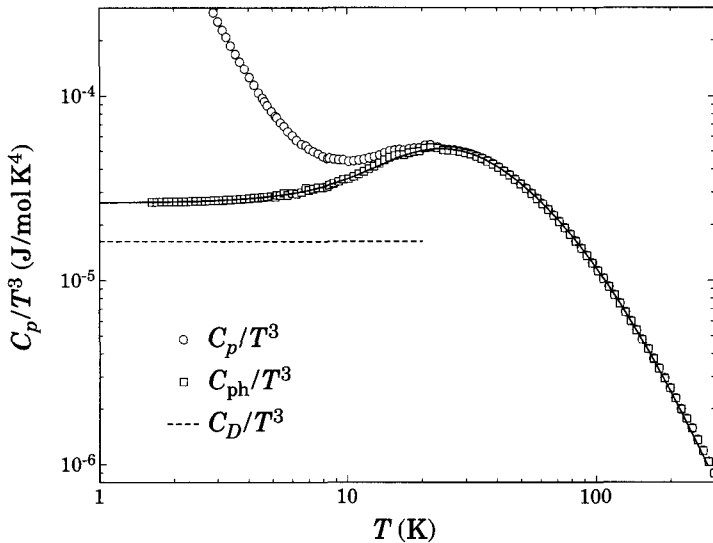


Figure 3.13: Specific heat of $\text{Al}_{68.2}\text{Mn}_9\text{Pd}_{22.8}$ plotted as C_p/T^3 vs. T (circles). The squares represent the lattice contribution C_{ph}/T^3 . The horizontal broken line indicates the Debye specific heat C_D/T^3 , calculated from measured sound-velocities using Eq. 4.5. The solid line is calculation of the lattice specific heat using the model DOVS given in Eq. 3.17. The experimental data is taken from Ref. 57.

The $C_p(T)$ -data obtained on this single grain sample with a chemical composition of $\text{Al}_{68.2}\text{Mn}_9\text{Pd}_{22.8}$ was found to be in very good agreement with $C_p(T)$ -data obtained on a sample cut from the same ingot as the polygrained $\text{Al}_{70}\text{Mn}_9\text{Pd}_{21}$ sample used in the thermal conductivity measurements [57]. Thus it can be assumed with some confidence that the specific heat data of the $\text{Al}_{68.2}\text{Mn}_9\text{Pd}_{22.8}$ represents the specific heat of the samples used in the thermal conductivity measurements. Below 3 K, a temperature independent ratio of C_{ph}/T^3 is observed. However, the value of C_{ph}/T^3 is distinctly larger than the estimate of the Debye contribution C_D/T^3 calculated using Eq. 4.5 and the measured low-temperature values of the sound velocities v_l and v_t , indicating a large excess specific heat C_{ex} [57]. This excess specific heat has most likely to be attributed to non-propagating lattice excitations [57]. With increasing temperature, C_{ph}/T^3 increases rapidly, and reaches a maximum at 22 K, indicating that at low frequencies the $g(\omega)$ varies more strongly than the Debye DOVS, i.e. $n \propto \omega^2$. In Fig. 3.14, C_{ph}/T^3 vs. T^2 is shown in the temperature

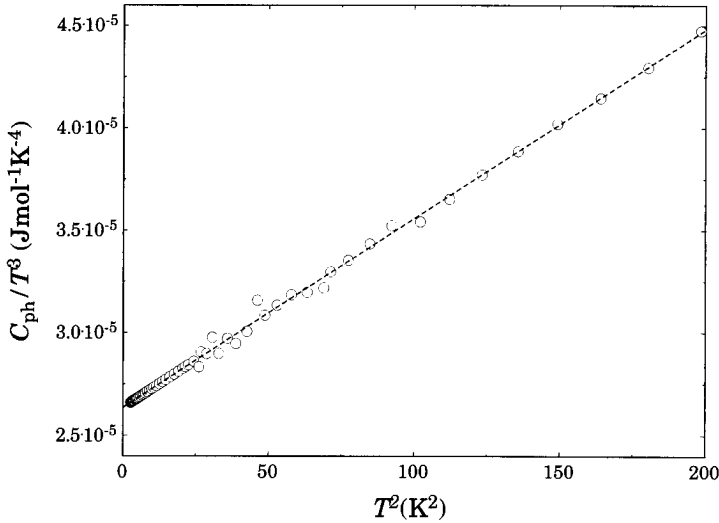


Figure 3.14: Lattice contribution to the specific heat of icosahedral $\text{Al}_{68.2}\text{Mn}_9\text{Pd}_{22.8}$ plotted as $C_{\text{ph}}(T)/T^3$ versus T^2 at low temperatures. The broken line is a fit of Eq. (3.16), as explained in text.

range between 1.6 and 14 K. The data are well represented by [57]

$$C_{\text{ph}} = \beta T^3 + \delta T^5 \quad , \quad (3.16)$$

with the parameters $\beta = 2.63 \times 10^{-5} \text{ J mol}^{-1} \text{ K}^{-4}$ and $\delta = 9.21 \times 10^{-8} \text{ J mol}^{-1} \text{ K}^{-6}$ shown as the broken line in Fig. 3.14. This temperature dependence of $C_{\text{ph}}(T)$ is compatible with a DOVS, which varies at low frequencies as $g(\omega) = a\omega^2 + b\omega^4$. A possible origin of a contribution to $C_{\text{ph}}(T)$ varying as T^5 is the dispersion of the acoustic phonons (see Sec. 4.3.2). However, a calculation of the T^5 -term to $C_{\text{ph}}(T)$ deduced from neutron scattering experiments gives $\delta = 2.5 \times 10^{-8} \text{ J mol}^{-1} \text{ K}^{-6}$, a value that is distinctly smaller than the corresponding value $\delta = 9.21 \times 10^{-8} \text{ J mol}^{-1} \text{ K}^{-6}$ obtained from the fit of Eq. 3.16, again suggesting the presence of an excess specific heat C_{ex} [57].

The analysis of the lattice specific heat $C_{\text{ph}}(T)$ presented above adverts to the following model DOVS [107]:

$$g(\omega) = \begin{cases} a\omega^2 + b\omega^4 & \text{for } \omega < \omega_c, \\ a\omega_c^2 + b\omega_c^4 & \text{for } \omega_c < \omega < \omega_{\max}, \\ 0 & \text{for } \omega > \omega_{\max}, \end{cases} \quad (3.17)$$

This simple model accounts for both the increase of C_{ph}/T^3 with increasing T at low temperatures, and for the maximum in the C_{ph}/T^3 vs. T curve. The maximum lattice frequency ω_{\max} is chosen such that the C_{ph} approaches the constant Dulong-Petit value $C_{\text{ph}} = 3N_A k_B$ in the limit of high temperatures, i.e.,

$$3N_A = \frac{a}{3}\omega_c^3 + \frac{b}{5}\omega_c^5 + (a\omega_c^2 + b\omega_c^4)(\omega_{\max} - \omega_c) \quad . \quad (3.18)$$

The substitution of Eq. 3.17 into Eq. 4.14, leads to a specific heat $C_{\text{ph}}(T)$ of the same form as given in Eq. 3.16. The parameters β , and δ obtained from the fit of Eq. 3.16 to the data correspond to $a = 3.27 \times 10^{-17} \text{ s}^3 \text{ rad}^{-3} \text{ mol}^{-1}$ and $b = 2.37 \times 10^{-43} \text{ s}^5 \text{ rad}^5 \text{ mol}^{-1}$. Using Eq. 4.14, $g(\omega)$ was fitted to the $C_{\text{ph}}(T)$ data in order to determine $\omega_c = 1.72 \times 10^{13} \text{ rad/s}$ and consequently $\omega_{\max} = 7.29 \times 10^{13} \text{ rad/s}$. The resulting DOVS is shown as the solid line in Fig. 3.15, and is meant to illustrate the *trend* for the DOVS. For comparison we also show in Fig. 3.15 the experimentally determined generalized vibrational density of states (GDOVS) of icosahedral Al-Mn-Pd measured between $1.22 \times 10^{13} \text{ rad/s}$, and $7.9 \times 10^{13} \text{ rad/s}$ in an inelastic neutron scattering experiment with a time-of-flight spectrometer [64]. Below $1.22 \times 10^{13} \text{ rad/s}$, the data was extrapolated as $g(\omega) = a\omega^2$, with $a = 7.7 \times 10^{-17} \text{ s}^3 \text{ rad}^{-3} \text{ mol}^{-1}$.

The discrepancy manifests itself below $1.7 \times 10^{13} \text{ rad/s}$ between $g(\omega)$ inferred from the analysis of $C_{\text{ph}}(T)$, and the GDVOS reported in Ref. 64 has most likely to be ascribed to the limited frequency resolution of the energy-loss technique at low frequencies [57]. Using Eq. 4.14, the lattice specific heat $C_{\text{ph}}(T)$ corresponding to GDVOS given in Ref. 64 can be calculated. The result of this calculation is shown as the solid line in the inset of Fig. 3.15, and it is much higher than the measured value of $C_{\text{ph}}(T)$ [57]. The lattice specific heat $C_{\text{ph}}(T)$ is an integral measure of $g(\omega)$ and is fairly insensitive to the exact details of the DOVS, especially at high frequencies, i.e., of the order of the Debye frequency $\omega \approx k_B \Theta_D / \hbar$. For this reason the model DOVS given by Eq. 3.17 that is compatible with the experimentally determined lattice specific heat will be used in the calculation of lattice thermal conductivity via Eq. 3.15.

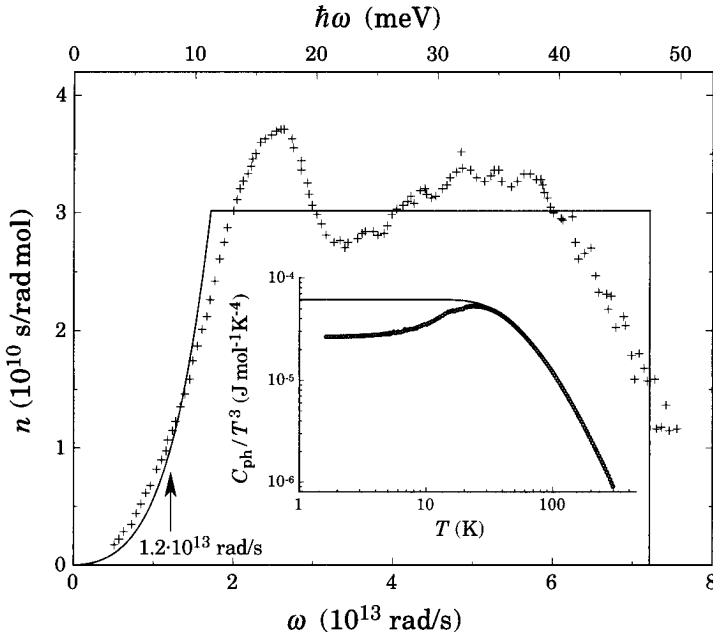


Figure 3.15: Generalized density of vibrational states (GDOVS) of icosahedral $Al_{71}Mn_{10}Pd_{19}$ (from Ref. 64). The solid line indicates the model DOVS given by Eq. 3.17 which corresponds to low-temperature lattice specific heat $C_{ph}(T)$ of icosahedral $Al_{68.2}Mn_9Pd_{22.8}$. The inset shows C_{ph}/T^3 vs. T of $Al_{68.2}Mn_9Pd_{22.8}$. The solid line indicates C_{ph} as calculated from the GDOVS derived from neutron scattering experiments using Eq. 4.14.

At low temperatures, i.e. low frequencies, $\lambda_{ph}(T)$ in icosahedral quasicrystals is due to propagating lattice excitations. The dominant contributions to thermal resistance $\lambda_{ph}(T)^{-1}$ are resonant scattering of phonons on tunneling states (c.f. Sec. 3.2.1), Umklapp scattering (c.f. Sec. 3.1.2 and 3.2.2), and scattering of phonons on mass density fluctuations (c.f. Sec. 3.2.2). Applying the phonon equivalent of Matthiessen's rule we obtain

$$l_{LT} = \left(\frac{\omega}{a} + \frac{\omega^2 T^4}{b} + \frac{\omega^4}{c} \right)^{-1} \quad (3.19)$$

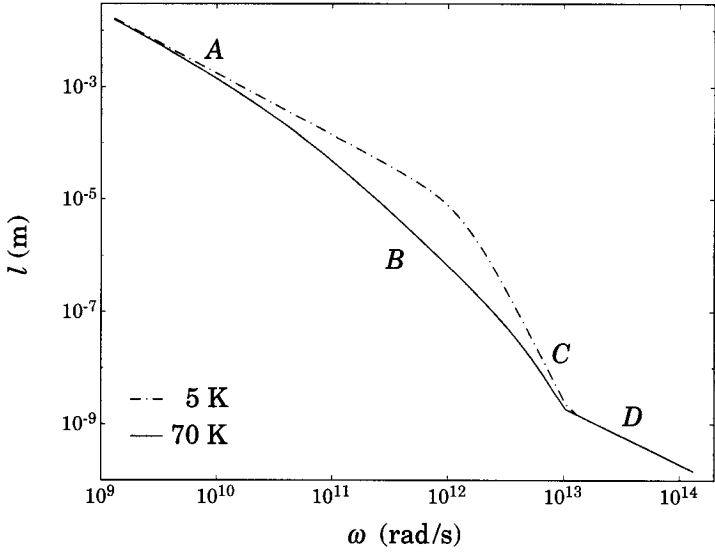


Figure 3.16: Frequency dependence of the phonon mean free path $l(\omega, T)$ of single grain $\text{Al}_{70.5}\text{Mn}_{8.5}\text{Pd}_{21}$ quasicrystal at two different temperatures. The letters denote the dominant mechanism: Tunneling states (A), quasiperiodic Umklapp processes (B), Rayleigh scattering (C), and diffusive phonon propagation.

At high temperatures, $\lambda_{\text{ph}}(T)$ is presumably due to the energy exchange between strongly coupled localized oscillators, implying a mean free path

$$l_{\text{HT}} = d \frac{\pi \bar{v}}{\omega}, \quad d \approx 1 \quad (3.20)$$

of the order of half the wavelength of the excitation (c.f. Sec. 3.2.3). Thus, the mean free path in the whole frequency range can be described

$$l(\omega, T) = \max \{l_{\text{LT}}(\omega, T), l_{\text{HT}}(\omega)\} \quad (3.21)$$

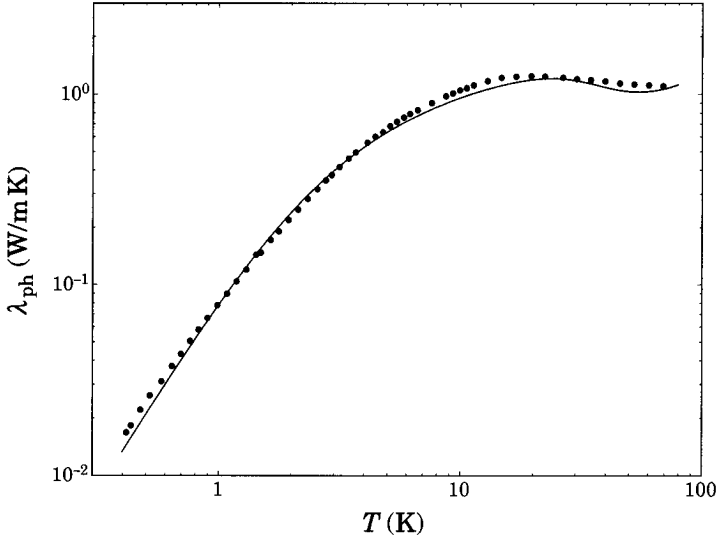


Figure 3.17: Lattice thermal conductivity $\lambda_{ph}(T)$ of single grain $\text{Al}_{70.5}\text{Mn}_{8.5}\text{Pd}_{21}$ quasicrystal. The solid line is the fit using Eq. 3.15 and Eq. 3.21.

as Eq. 3.19 underestimates the phonon mean free path at high frequencies. The thermal conductivity data was then fitted to the data of the single grain $\text{Al}_{70.5}\text{Mn}_{8.5}\text{Pd}_{21}$ quasicrystal using Eq. 3.15, and Eq. 3.21, and the DOVS as determined above. The following parameters $a/\omega^{1+\delta} = 1.7 \times 10^8 \omega^{-1.1} \text{ m}$, $b = 1.7 \times 10^{25} \text{ m rad}^2 / \text{s}^2 \text{ K}^4$, $c = 2.7 \times 10^{43} \text{ m rad}^4 / \text{s}^4$, and $d = 0.9$ were obtained in the fit. The result of the fit is presented in Fig. 3.17 as the solid line, reproducing fairly well the overall temperature characteristics of $\lambda_{ph}(T)$. The corresponding mean free path for two different temperatures is shown in Fig. 3.16. The crossover from the regime where thermal conduction is due to propagating lattice excitations to the regime of diffusive thermal transport occurs at $\omega_l \approx 1 \times 10^{13} \text{ rad/s}$. Measurements of the phonon dispersion in icosahedral Al-Mn-Pd by inelastic neutron scattering show that the width of the lowest transverse acoustic phonon branch starts to broaden considerably for frequencies above $1 \times 10^{13} \text{ rad/s}$ [56, 57], as can be seen in Fig. 3.2. Theoretical calculations of the dynamical properties of quasicrystals indicated that the reason for the broadening of the acoustic modes is twofold [53, 56]—The dense set of dispersionless modes located at high frequencies [50, 62, 108, 109], and the increasing degree

of localization of the modes with increasing frequency [42, 50, 62, 108]. The results on the phonon dispersion thus corroborate the conjecture of diffusive heat transport at high frequencies, e.g., high temperatures.

3.2.5 Summary

The thermal conductivity of a polygrained $\text{Al}_{70}\text{Mn}_9\text{Pd}_{21}$ sample and of a single crystalline $\text{Al}_{70.5}\text{Mn}_{8.5}\text{Pd}_{21}$ sample was measured in varying temperature ranges between 0.06 and 310 K. The results indicate important differences in the dynamic properties of low-energy lattice excitations in icosahedral Al-Mn-Pd compared to those of either periodic or amorphous solids.

For temperatures between 0.35 and 1.6 K, the phonon contribution $\lambda_{\text{ph}}(T)$ to the thermal conductivity of icosahedral Al-Mn-Pd varies approximately as $\lambda_{\text{ph}} \propto T^2$. This variation suggests that phonons are scattered predominantly by tunneling states and the values of λ_{ph} are of the same order of magnitude as those reported for insulating and metallic amorphous solids. However, the coefficient of the quadratic temperature variation of $\lambda_{\text{ph}}(T)$ is larger for the single grain $\text{Al}_{70.5}\text{Mn}_{8.5}\text{Pd}_{21}$ sample than for the polygrained Al-Mn-Pd sample, suggesting a lower density of tunneling states in the single grain sample.

With decreasing temperature, distinct deviations from the approximately quadratic temperature dependence of λ_{ph} of the polygrained $\text{Al}_{70}\text{Mn}_9\text{Pd}_{21}$ become apparent below 0.35 K. They are compatible with a crossover between a regime in which the phonon mean free path is predominantly limited by scattering on the tunneling states and a regime which is characterized by a temperature-independent mean free path. This mean free path is substantially shorter than the Casimir length of this sample of $\text{Al}_{70}\text{Mn}_9\text{Pd}_{21}$ and is determined by a phonon scattering in the bulk of the sample, presumably by microholes.

The most prominent feature in the temperature dependence of λ_{ph} of icosahedral Al-Mn-Pd is the shallow maximum at 20 K, followed by a temperature region extending up to 85 K with a slightly negative slope $d\lambda_{\text{ph}}/dT$ as observed for the single crystalline $\text{Al}_{70.5}\text{Mn}_{8.5}\text{Pd}_{21}$ implying a frequency and temperature dependent phonon mean free path.

We attribute the maximum to a crossover from the regime of phonon scattering by tunneling states to the regime of quasiperiodic phonon Umklapp scattering. A higher density of tunneling states is expected to lead to a suppression of the maximum in the $\lambda_{\text{ph}}(T)$ curve and to a shift of the maximum to higher temperatures, very much as what is observed in $\lambda_{\text{ph}}(T)$ data of the polygrained $\text{Al}_{70}\text{Mn}_9\text{Pd}_{21}$ sample.

Above 100 K, the value of $\lambda_{\text{ph}}(T)$ of icosahedral Al-Mn-Pd is close to the prediction of Einstein's model, suggesting that the lattice vibrations in the THz frequency range are predominantly localized, and the energy transfer between them occurs via a strong coupling mechanism.

The overall temperature dependence of λ_{ph} of icosahedral Al-Mn-Pd can adequately be described by a kinetic model of the thermal conductivity employing a frequency and temperature dependent phonon mean free path.

3.3 Icosahedral Al-Re-Pd

Thermodynamically stable face centered icosahedral quasicrystals in the Al-Re-Pd system [14, 15] with a high structural quality can be obtained over a fairly narrow range of chemical compositions [110, 111]. Quasicrystals in this system show very low values of the electrical conductivity comparable to those observed for heavily doped semiconductors [110–113]. Correspondingly, the electronic contribution λ_{el} to the thermal conductivity λ is expected to be negligible as compared to the lattice contribution λ_{ph} .

In Fig. 3.18 the measured thermal conductivity λ of icosahedral $\text{Al}_{70}\text{Re}_{8.6}\text{Pd}_{21.4}$ is shown on double logarithmic scales for the whole temperature range between 0.35 and 90 K covered in this experiment. The phonon contribution λ_{ph} to the thermal conductivity was obtained by subtracting off an estimate of the electronic contribution λ_{el} [114] shown as the solid line in Fig. 3.18. One should note that over the whole covered temperature range λ exceeds λ_{el} by at least an order of magnitude due to the very low values of the electrical conductivity of $\text{Al}_{70}\text{Re}_{8.6}\text{Pd}_{21.4}$ (see Sec. 5). Therefore, the evaluation of λ_{ph} is expected to be quite reliable. Fig. 3.19 shows the phonon thermal conductivity $\lambda_{\text{ph}}(T)$ of icosahedral $\text{Al}_{70}\text{Re}_{8.6}\text{Pd}_{21.4}$ as established in the way described above. In the

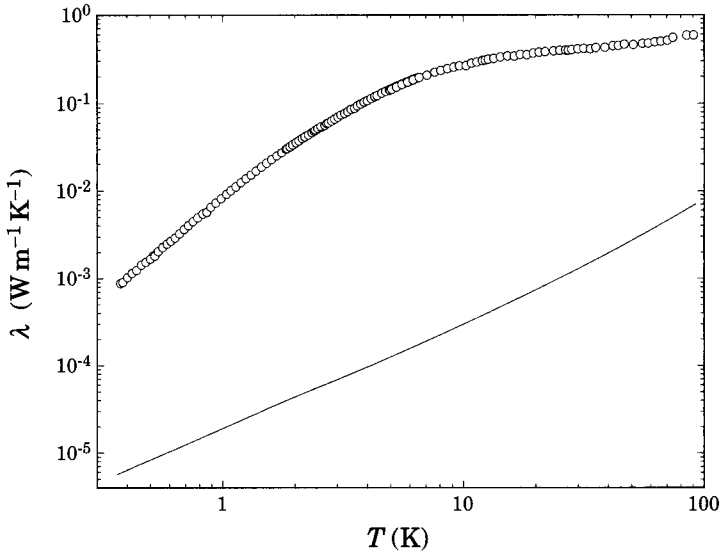


Figure 3.18: Thermal conductivity $\lambda(T)$ of a polygrained sample of icosahedral $\text{Al}_{70}\text{Re}_{8.6}\text{Pd}_{21.4}$ quasicrystal between 0.35 and 90 K. The solid line is an estimate of the electronic contribution λ_{el} .

whole covered temperature range λ_{ph} increases monotonically with increasing T . Above approximately 5 K, a tendency to saturation of $\lambda_{ph}(T)$ becomes evident. Between 15 and 70 K, $\lambda_{ph}(T)$ changes only little with temperature.

The analysis will concentrate first on the low-temperature behaviour of $\lambda_{ph}(T)$. Between 0.35 and 1 K the variation of λ_{ph} with temperature is compatible with a crossover from a regime of a temperature independent phonon mean free path l and $\lambda_{ph} \propto T^3$ at the lowest temperatures to a regime where l is limited by scattering on tunneling states and l varies as $l \propto \omega^{-1}$. Here, $\lambda_{ph} \propto T^2$ is expected. In both regimes the respective limiting temperature dependence of λ_{ph} is indicated in Fig. 3.19 as solid line.

The separation of the two contributions to λ_{ph} may be best achieved in a representation of the data as λ_{ph}/T^3 vs. T as in the inset of Fig. 3.19. In this representation the Casimir regime of a thermal conductivity limited by boundary scattering can be identified by a constant ratio of λ_{ph}/T^3 at the lowest temperatures. Assuming the validity of a

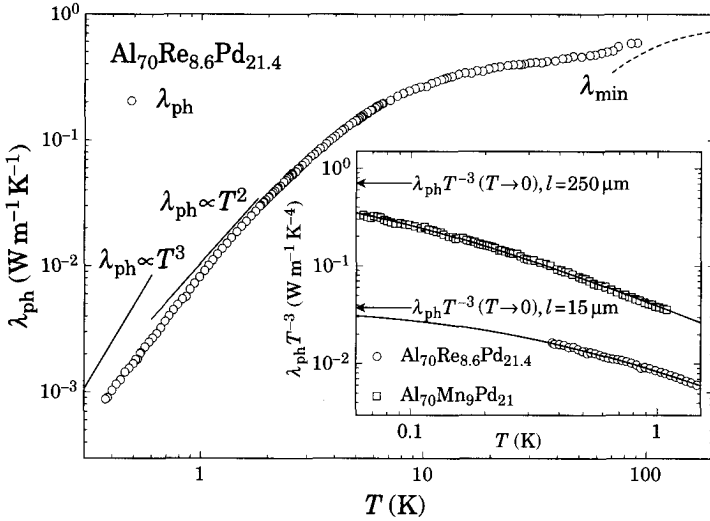


Figure 3.19: Lattice contribution $\lambda_{\text{ph}}(T)$ to the thermal conductivity of icosahedral $\text{Al}_{70}\text{Re}_{8.6}\text{Pd}_{21.4}$. The regimes where $\lambda_{\text{ph}}(T)$ is dominated by resonant boundary scattering $\lambda_{\text{ph}} \propto T^3$, and scattering on tunneling states $\lambda_{\text{ph}} \propto T^2$ are indicated as solid lines. The dashed line is the minimal thermal thermal conductivity calculated from Eq. 3.14. Inset: λ_{ph}/T^3 of icosahedral $\text{Al}_{70}\text{Re}_{8.6}\text{Pd}_{21.4}$ (open circles) as a function of T below 1.5 K in comparison with analogous data for icosahedral $\text{Al}_{70}\text{Mn}_9\text{Pd}_{21}$ (open squares). The solid lines are a fit to Eq. 3.11 for both quasicrystals.

phonon equivalent of Matthiessen's rule and that the main contributions to the thermal resistance λ_{ph}^{-1} are due to scattering processes of acoustic phonons leads to a thermal conductivity as given in Eq. 3.11. Fitting Eq. 3.11 to the λ_{ph} data in the temperature range between 0.35 and 1 K yields $\bar{P}\gamma^2/\rho\bar{v} = (1.4 \pm 0.2) \times 10^2 \text{ cm s}^{-1}$ and $l_c = (1.5 \pm 0.3) \times 10^{-3} \text{ cm}$. The result of this fit is displayed as the solid line in the inset of Fig. 3.19. For comparison an analogous fit to the data obtained on icosahedral $\text{Al}_{70}\text{Mn}_9\text{Pd}_{21}$ is shown as well.

The large error bars of the mean free path l_c reflect the fact that the T^3 regime is not yet reached at the lowest temperatures of this experiment. Nevertheless, the fitted value of l_c is in good agreement with the average grain size determined from scanning electron microscope investigation of this sample. The comparison of the fitted values of $\bar{P}\gamma^2/\rho\bar{v}$ as

	Ref.	$\bar{P}\gamma^2$ [erg cm ⁻³]
polygrained Al ₇₀ Re _{8.6} Pd _{21.4}	117	22×10^7
polygrained Al ₇₀ Mn ₉ Pd ₂₁	72	6.5×10^7
single grained Al _{70.5} Mn _{8.5} Pd ₂₁	107	2.4×10^7
single grained Al ₇₀ Mn ₁₀ Pd ₂₀	102	1.6×10^7

Table 3.1: Comparison of the product of the density of tunneling states \bar{P} and the average coupling between them and the phonons γ^2 for a number of icosahedral quasicrystals. (See text.)

obtained from thermal conductivity results below 1 K in Al₇₀Re_{8.6}Pd_{21.4} with those in icosahedral Al-Mn-Pd indicates a remarkable sample dependence, as listed in Tab. 3.1. For example, the value determined for the Al_{70.5}Mn_{8.5}Pd₂₁ is a factor of 2.5 larger than the one for Al₇₀Mn₉Pd₂₁ (see also Refs. 115 and 102). This strongly suggests that tunneling states are not necessarily intrinsic in quasicrystals. Nevertheless, their occurrence, depending on sample quality, seems inevitable because defects are always present in quasicrystals. Owing to the fact of a general lack of “growth rules” for quasicrystals [116] it is impossible to grow a quasicrystal with a density of defects lower than some intrinsic value. On the contrary, $\bar{P}\gamma^2/\rho\bar{v}$ is almost the same for all kinds of amorphous materials [98], as can be seen in Fig. 3.10. This observation led to the assertion that tunneling states are intrinsic in glasses.

In the temperature range between 15 and 70 K, the temperature dependence of λ_{ph} is weak and it may be approximated as $\lambda \propto T^{0.2}$. This overall $\lambda_{\text{ph}}(T)$ behaviour is reminiscent of that of icosahedral Al₇₀Mn₉Pd₂₁ [72], which shows a well developed λ plateau between 25 and 55 K. The occurrence of a λ plateau in the phonon thermal conductivity of quasicrystals is compatible with the concept of Umklapp processes in condensed matter with quasiperiodic order [40]. In quasicrystals a maximum in the $\lambda_{\text{ph}}(T)$ curve is expected at intermediate temperatures followed by a region with a negative slope $d\lambda/dT$ is negative [40]. However, as argued in Sec. 3.2.2 the $\lambda_{\text{ph}}(T)$ variation in this region may be substantially weaker than $\lambda_{\text{ph}} \propto T^{-3}$ or it may even be reduced to an extended plateau, depending on the strength of phonon scattering by tunneling states at lower temperatures, very much as what is observed here for $\lambda_{\text{ph}}(T)$ of Al₇₀Re_{8.6}Pd_{21.4}.

Above 70 K, the magnitude of λ_{ph} is fairly small, indicating that the mean free path of vibrational excitations l is of the order $\pi\bar{v}\omega^{-1}$, i.e., half of the wavelength of the excitation. This result suggests that the quasilattice vibrations in icosahedral $\text{Al}_{70}\text{Re}_{8.6}\text{Pd}_{21.4}$ in the THz frequency range are predominately localized and that the energy transfer between them occurs via a strong coupling mechanism [106], in qualitative agreement with Einstein's model of the heat transport via energy transfer between coupled neighbouring atoms vibrating with random phases [105]. The minimal thermal conductivity λ_{min} for $\text{Al}_{70}\text{Re}_{8.6}\text{Pd}_{21.4}$ was calculated using Θ_D calculated from the renormalized values of the sound velocities (see Sec. 4.1). The result of this calculation is shown in Fig. 3.19 as the dashed line.

In summary, the thermal conductivity of icosahedral $\text{Al}_{70}\text{Re}_{8.6}\text{Pd}_{21.4}$ was measured between 0.35 and 90 K. Below 1 K, the temperature variation of the phonon thermal conductivity $\lambda_{\text{ph}}(T)$ of icosahedral $\text{Al}_{70}\text{Re}_{8.6}\text{Pd}_{21.4}$ is compatible with a cross-over between a regime, which is characterized by a constant phonon mean free path l_{ph} at the lowest temperatures, and a regime, in which l_{ph} is limited by scattering on tunneling states. The coefficient $\bar{P}\gamma^2/\rho\bar{v}$ of the density of tunneling states \bar{P} and the effective coupling to the phonons γ^2 as obtained from a fit of the tunneling state contribution to phonon thermal resistance λ_{ph}^{-1} below 1 K shows a remarkable sample dependence in icosahedral quasicrystals, and a comparison of the value obtained for $\text{Al}_{70}\text{Re}_{8.6}\text{Pd}_{21.4}$ with the respective values of icosahedral Al-Mn-Pd strongly suggests that tunneling states are not necessarily intrinsic in quasicrystals. Between 15 and 70 K is λ_{ph} of icosahedral $\text{Al}_{70}\text{Re}_{10}\text{Pd}_{20}$ only weakly temperature-dependent, in agreement with the concept of quasiperiodic Umklapp processes. A plateau type feature of λ_{ph} was also observed for icosahedral Al-Mn-Pd system and seems to be a general observation for quasicrystals.

3.4 Decagonal quasicrystals

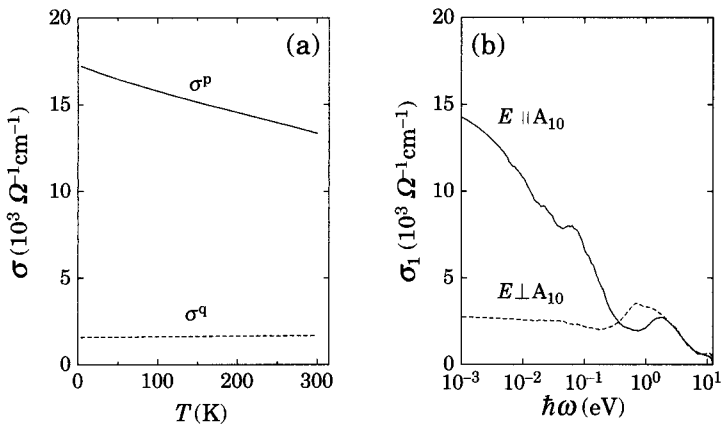


Figure 3.20: (a)–Electrical conductivity of single grained decagonal Al-Ni-Co measured along the periodic direction σ^p (solid line) and along a direction in the quasiperiodic plane σ^q (broken line) [118]. (b)–Real part $\sigma_1(\omega)$ of the optical conductivity at 300 K along both polarization directions for single crystalline decagonal Al-Ni-Co [119].

The atomic arrangement in decagonal quasicrystals is periodic along the tenfold symmetry axis and quasiperiodic in the plane perpendicular to it. Thus, these materials share structural properties of periodically and quasiperiodically ordered matter. Since the recent discovery of thermodynamically stable decagonal quasicrystals in the Al-Cu-Co and Al-Ni-Co systems [33, 34], it has become possible to study properties of both periodically and quasiperiodically structured matter along different directions of one single sample. In the Al-Cu-Co alloy system [120], millimetre sized grains with decaprismatic growth morphology can be obtained by slow solidification from the melt [34, 121]. A detailed investigation of the phase equilibria in the Al-Ni-Co alloy system revealed a large stability region of the decagonal phase and large single-grained decagonal quasicrystals can be obtained by solidification of an off-stoichiometric melt [122–125], which is of prime importance for reliable investigations of anisotropic physical properties.

For decagonal quasicrystals in the Al-Cu-Co and Al-Ni-Co systems, strong anisotropies of electrical [126, 127] and thermal transport [119, 128–132] as well as the optical conductivity [119, 133] have been established experimentally. The values of the residual

electrical conductivity σ observed in decagonal quasicrystals along the periodic σ_0^p and along the quasiperiodic direction σ_0^q show an anisotropy σ_0^p/σ_0^q of the order of 10. However, $\sigma^p(T)$ as well as $\sigma^q(T)$ change only little with temperature. This can be seen in Fig. 3.20a, where electrical conductivity data of single grain Al-Ni-Co are shown for both directions [118]. A distinct anisotropy is also observed for the optical conductivity spectra $\sigma_1(\omega)$ [119, 133]. In Fig. 3.20b the optical conductivity of single grain $\text{Al}_{71}\text{Ni}_{16}\text{Co}_{13}$ is presented as a function of frequency with the electrical field vector \mathbf{E} of the linearly polarized light parallel and perpendicular to the tenfold axis [119]. The difference between $\sigma_1(\omega)$ for the periodic direction and for a direction in the quasiperiodic plane is most prominent in the frequency range below 2 eV. For the periodic direction, $\sigma_1(\omega)$ shows a typical Drude-like component, indicating rather conventional metallic behaviour, whereas $\sigma_1(\omega)$ in the quasiperiodic plane displays a frequency-independent behaviour [119].

3.4.1 Decagonal Al-Cu-Co

Periodic direction

In Fig. 3.21 the thermal conductivity $\lambda^p(T)$ of decagonal $\text{Al}_{65}\text{Cu}_{20}\text{Co}_{15}$ measured along the periodic direction between 0.45 and 105 K is plotted on logarithmic scales. An estimate of the phonon contribution λ_{ph}^p to the thermal conductivity may be obtained by subtracting off an estimate of the electronic contribution λ_{el}^p . The latter was calculated by assuming the validity of the Wiedemann-Franz law and using the electrical conductivity data obtained from this same sample. Special care was taken in the experimental setup to eliminate the error resulting from the limited precision of the measurement of the geometrical factor. As explained in Sec. 2.2, this was achieved by using the voltage leads of the electrical conductivity measurement subsequently in the thermal conductivity measurement to anchor the thermometers thermally to the sample. In Fig. 3.21 the calculated electronic contribution λ_{el}^p is shown as the solid line.

In simple metals the Wiedemann and Franz law is expected to be valid in the temperature regions in which the temperature variation of the electrical resistivity is governed by an elastic phonon scattering mechanism, e.g., at low temperatures where scattering on point imperfections is dominant and at temperatures high enough for which the electron-phonon scattering can be considered as elastic [134, 135]. In alloys elastic scattering of

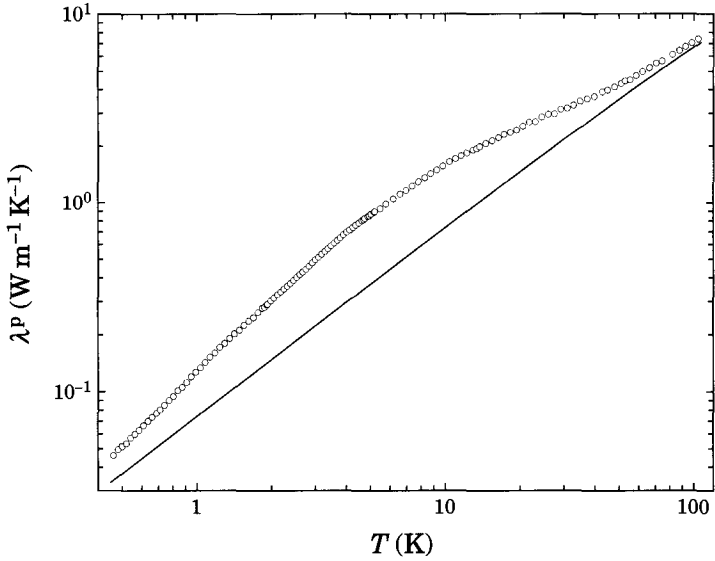


Figure 3.21: Temperature dependence of the total thermal conductivity $\lambda^P(T)$ along the periodic direction of decagonal $\text{Al}_{65}\text{Cu}_{20}\text{Co}_{15}$ between 0.45 and 105 K. The solid line is an estimate of the electronic contribution λ_{e1}^P , as explained in the text.

electrons on point defects prevails and the electrical conductivity σ is almost temperature independent; in these systems λ_{e1} can be determined fairly reliably using the Wiedemann and Franz law [135]. The value of the electrical conductivity along the periodic direction σ^P in decagonal $\text{Al}_{65}\text{Cu}_{20}\text{Co}_{15}$ is comparable to values observed in d-transition metals and alloys and σ^P varies only little with temperature [118, 126, 127]. At the lowest and at the highest temperatures of this experiment, i.e., where the phonon contribution λ_{ph}^P is expected to be small, λ_{e1}^P is close in magnitude to λ^P . This observation corroborates the conjecture, that the law of Wiedemann and Franz is approximately valid for the periodic direction of decagonal $\text{Al}_{65}\text{Cu}_{20}\text{Co}_{15}$.

The phonon contribution $\lambda_{\text{ph}}^P(T)$ obtained as explained in the previous section is shown on a double logarithmic plot in Fig. 3.22. The overall λ_{ph}^P variation of decagonal

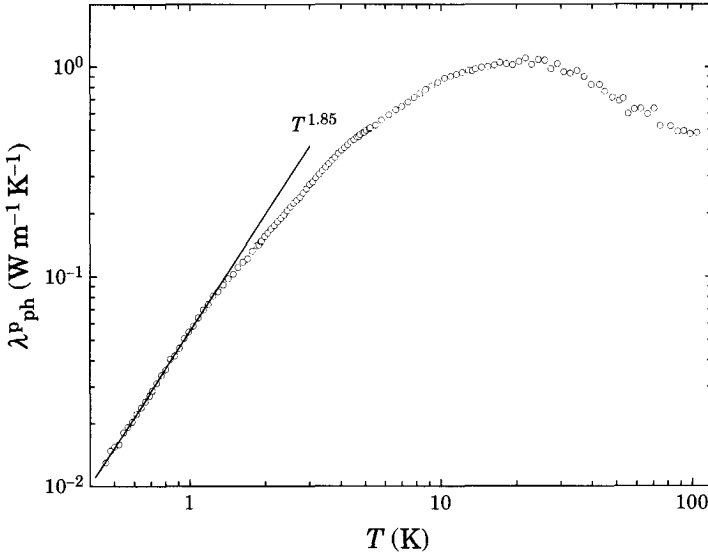


Figure 3.22: Phonon contribution $\lambda_{\text{ph}}^{\text{p}}$ along the periodic direction of decagonal $\text{Al}_{65}\text{Cu}_{20}\text{Co}_{15}$ as a function of temperature. The solid line indicates a power-law approximation to the $\lambda_{\text{ph}}^{\text{p}}$ data between 0.45 and 1.2 K.

$\text{Al}_{65}\text{Cu}_{20}\text{Co}_{15}$ resembles that of periodic crystals; there is a distinct maximum at an intermediate temperature. In periodic crystals, in the temperature region just above that maximum, the phonon thermal conductivity is dominated by the onset of Umklapp processes and hence the phonon thermal conductivity is expected to decrease exponentially with increasing temperature due to an exponential increase in the number of occupied high-frequency phonon states that allow the occurrence of Umklapp processes [65]. Above the maximum, a rapid decrease of $\lambda_{\text{ph}}^{\text{p}}(T)$ with increasing temperature may be seen in Fig. 3.22, although we cannot claim that the exponential dependence is actually verified. In general, this exponential dependence is most often masked by isotope or impurity scattering effects [67]. Results on $\lambda_{\text{ph}}(T)$ similar to what is observed here were reported in an investigation of the thermal conductivity of a series of dilute metallic alloys [136, 137]. Even though the height of the maximum of λ_{ph} in those systems is reduced with increasing impurity content due to the scattering of phonons by point imperfections, the maximum in the $\lambda_{\text{ph}}(T)$ curve is still clearly perceived [136, 137].

Between 0.45 and 1.2 K, the slope of $\lambda_{\text{ph}}^{\text{p}}(T)$ of this sample is almost constant and it may be seen that $\lambda_{\text{ph}}^{\text{p}}(T)$ can adequately be approximated as $\lambda_{\text{ph}}^{\text{p}} = AT^n$ with $n = 1.85 \pm 0.01$ (see solid line in Fig. 3.22). There are two mechanisms of phonon scattering that give rise to an approximately quadratic temperature dependence of the phonon thermal conductivity, i.e., scattering of phonons by either conduction electrons [135] or tunneling states [74,75].

As discussed in Secs. 3.2.1 and 3.3 the presence of tunneling states in icosahedral Al-Mn-Pd and Al-Re-Pd is indicated by measurements of the low temperature thermal conductivity [72,102,115,117] and by the results of a low temperature ultrasound experiment which revealed a logarithmic deviation in the sound-velocity variation with temperature and a non-linear attenuation of acoustic shear waves [77].

The relaxation rate of phonons due to scattering on electrons τ_{pe}^{-1} is proportional to the phonon frequency, i.e. $\tau_{\text{pe}}^{-1} \propto \omega$ and hence the corresponding lattice thermal conductivity $\lambda_{\text{ph}}(T)$ is expected to be proportional to T^2 [135]. Such a $\lambda_{\text{ph}}(T)$ variation has been verified for metallic alloys, for which the lattice contribution λ_{ph} is comparable to the measured thermal conductivity [136,137]. One example is the lattice conduction in the normal state of single crystals of Cadmium doped Tin where a fair agreement between the measured values of λ_{ph} and theoretical calculations was observed [137].

To conclude this discussion of the mechanism responsible for the thermal resistance of decagonal $\text{Al}_{65}\text{Cu}_{20}\text{Co}_{15}$ at low temperatures, we note that the relatively low electrical resistivity $\rho^{\text{p}}(T)$ of decagonal $\text{Al}_{65}\text{Cu}_{20}\text{Co}_{15}$ along the periodic direction is of the order of those of d-transition metals and alloys [118], suggesting that a substantial part of the phonon thermal resistance $(\lambda_{\text{ph}}^{\text{p}})^{-1}$ is due to phonon-electron scattering.

Quasiperiodic direction

The thermal conductivity λ^{q} along a direction in the quasiperiodic plane of decagonal $\text{Al}_{65}\text{Cu}_{20}\text{Co}_{15}$ is shown in Fig. 3.23 between 0.06 and 100 K, together with the electronic contribution $\lambda_{\text{el}}^{\text{q}}$ to the thermal conductivity calculated assuming the validity of the Wiedemann-Franz law.

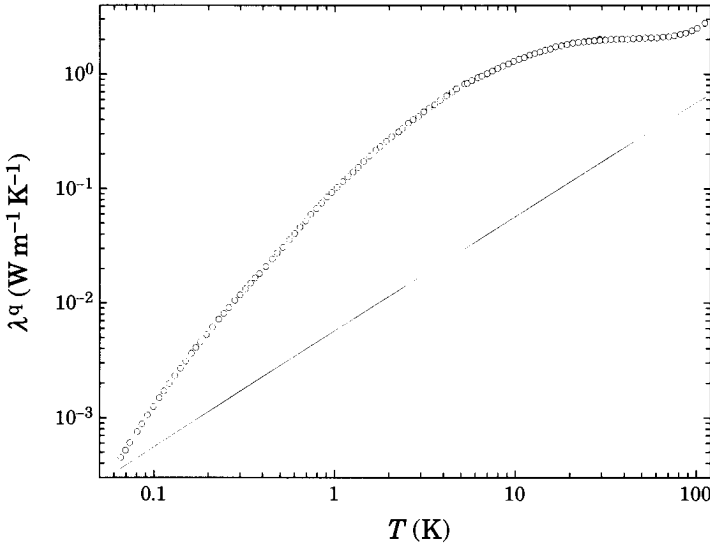


Figure 3.23: The total thermal conductivity $\lambda^q(T)$ of decagonal $\text{Al}_{65}\text{Cu}_{20}\text{Co}_{15}$ along direction in the quasiperiodic plane between 0.06 and 110 K. The solid line is an estimate of the electronic contribution λ_{el}^q (see text).

The phonon thermal conductivity λ_{ph}^q , obtained by subtracting λ_{el}^q from λ^q , is shown in Fig. 3.24. From 0.06 to 0.1 K, λ_{ph}^q increases rapidly with increasing temperature. From 0.2 to 0.8 K, the slope of $\log(\lambda_{\text{ph}}^q)$ vs. $\log(T)$ is almost constant and $\lambda_{\text{ph}}^q(T)$ can be well fitted by $\lambda_{\text{ph}}^q = AT^n$ with $n = 1.90 \pm 0.01$. As for the periodic direction such a temperature dependence of λ_{ph}^q is compatible with the scattering of phonons by either itinerant electrons or tunneling states. The result of this fit is displayed in Fig. 3.24 as a solid line. At higher temperatures, the slope $d\lambda_{\text{ph}}^q/dT$ decreases gradually and $\lambda_{\text{ph}}^q(T)$ shows a trend to saturation at about 25 K. From 30 to 70 K, λ_{ph}^q is almost temperature-independent and slowly increases again above 70 K. A closer inspection of $\lambda_{\text{ph}}^q(T)$ reveals a shallow maximum at the lower end of the plateau region, as may be seen in the inset of Fig. 3.24.

The overall $\lambda_{\text{ph}}^q(T)$ variation for decagonal $\text{Al}_{65}\text{Cu}_{20}\text{Co}_{15}$ described above is reminiscent of $\lambda_{\text{ph}}(T)$ of icosahedral $\text{Al}_{70}\text{Mn}_9\text{Pd}_{21}$ [72], except for the rapid increase in the lowest temperature range between 0.06 and 0.1 K. A detailed analysis of λ_{ph}^q in this temperature

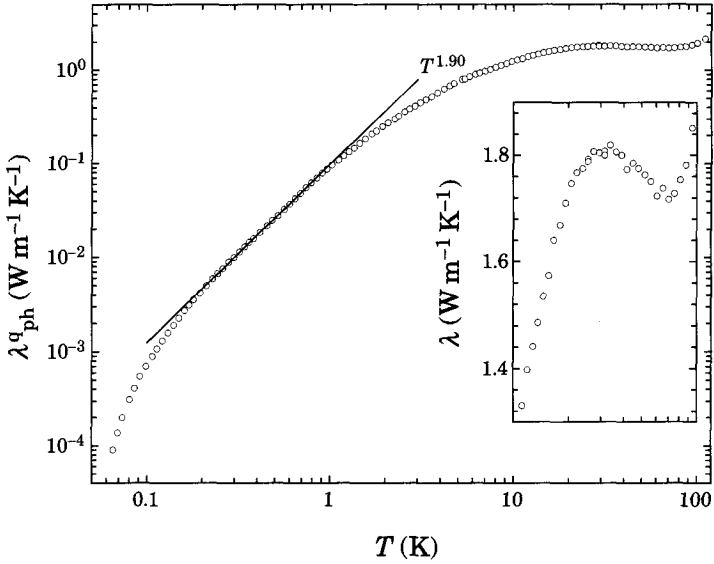


Figure 3.24: Phonon thermal conductivity $\lambda_{\text{ph}}^q(T)$ of decagonal Al-Cu-Co along a direction in the quasiperiodic plane. The solid line is a power-law approximation to the data between 0.2 and 0.8 K. The inset shows λ_{ph}^q between 10 and 100 K on an expanded vertical scale.

range meets difficulties because of the large electronic contribution to the total thermal conductivity, as may be seen in Fig. 3.23. This problem is much less severe at higher temperatures [129]. A power-law with an exponent close to 2 was also observed for λ_{ph} of icosahedral $\text{Al}_{70}\text{Mn}_9\text{Pd}_{21}$ as discussed in detail in Sec. 3.2.1, where this behaviour is analyzed in terms of resonant scattering of phonons by tunneling states, typically observed in amorphous solids [74, 75]. Experimental investigations probing tunneling states directly, e.g., ultrasound experiments studying the temperature variation of the sound velocity and power dependence of the acoustic-wave attenuation in decagonal $\text{Al}_{65}\text{Cu}_{20}\text{Co}_{15}$, as they have been undertaken in icosahedral Al-Mn-Pd [77], would be helpful to establish the origin of this T^2 -variation of λ_{ph}^q .

The occurrence of a plateau-type feature in the phonon thermal conductivity λ_{ph}^q of decagonal $\text{Al}_{65}\text{Cu}_{20}\text{Co}_{15}$ in the quasiperiodic plane (Fig. 3.24) is compatible with the

concept of Umklapp processes in condensed matter with quasiperiodic order [40]. It was pointed out in Sec. 3.1.2, that the rate of generalized Umklapp processes in quasicrystals should have a power-law dependence, in contrast to the exponential dependence in periodic crystals. This weaker temperature dependence of the phonon scattering rate due to Umklapp processes would make the maximum in the $\lambda_{\text{ph}}^{\text{q}}(T)$ curve much more shallow or even turn it into a plateau, very much as what is displayed in the inset of Fig. 3.24. As described in Secs. 3.2.2 and 3.3, this plateau-type feature in the phonon thermal conductivity curve is also observed in icosahedral Al-Mn-Pd [72, 102, 115], Al-Cu-Fe [138], and Al-Re-Pd [117] and seems to be a general observation for icosahedral quasicrystals.

3.4.2 Decagonal Al-Ni-Co

Periodic direction

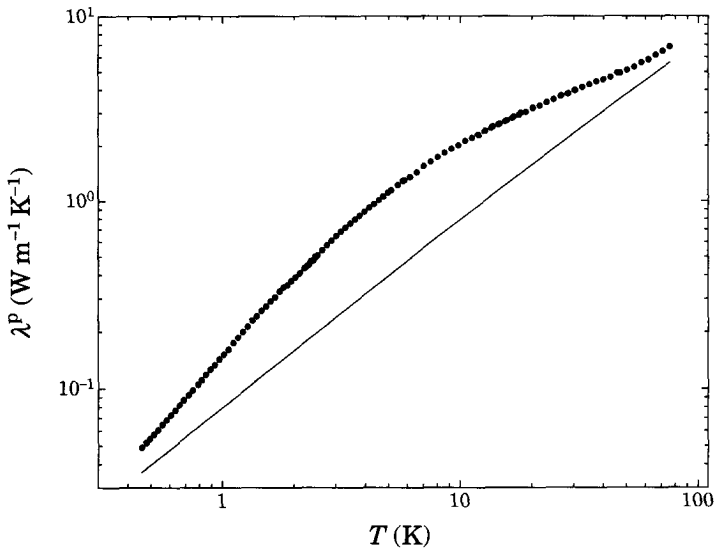


Figure 3.25: Temperature dependence of the thermal conductivity λ^P along the periodic direction of decagonal $\text{Al}_{71}\text{Ni}_{16}\text{Co}_{13}$ between 0.45 and 80 K. The solid line is an estimate of the electronic contribution λ_{el}^P , as explained in the text.

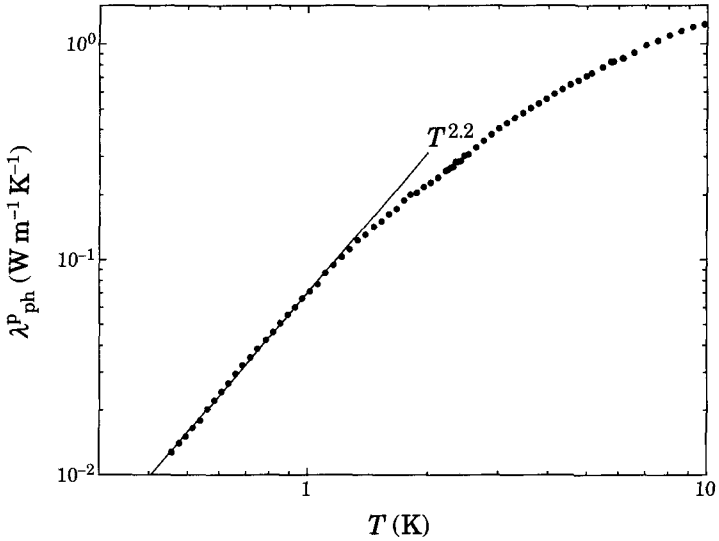


Figure 3.26: Phonon contribution $\lambda_{\text{ph}}^{\text{p}}$ along the periodic direction of decagonal $\text{Al}_{71}\text{Ni}_{16}\text{Co}_{13}$ as a function of temperature. The solid line indicates a power-law approximation $\lambda_{\text{ph}}^{\text{p}} \propto T^n$ between 0.45 and 1.2 K.

The thermal conductivity λ^{p} measured along the periodic direction of decagonal $\text{Al}_{71}\text{Ni}_{16}\text{Co}_{13}$ in the temperature range between 0.45 and 80 K presented on logarithmic scales in Fig. 3.25. An estimate of the electronic contribution $\lambda_{\text{el}}^{\text{p}}$ to λ^{p} may be obtained by assuming that $\lambda_{\text{ph}}(T)$ at high and low temperatures is dominated by $\lambda_{\text{el}}^{\text{p}}$ given by the law of Wiedemann and Franz, which is justified by comparison with the situation for Al-Cu-Co [129]. The result of this calculation is shown as the solid line in Fig. 3.25.

The lattice contribution $\lambda_{\text{ph}}^{\text{p}}$, obtained by subtracting $\lambda_{\text{el}}^{\text{p}}$ from the measured thermal conductivity λ^{p} , is shown in Fig. 3.28b. At 25 K, $\lambda_{\text{ph}}^{\text{p}}(T)$ passes over a maximum and decreases distinctly with further increasing T . This behaviour is reminiscent of that of periodic crystals, where $\lambda_{\text{ph}}(T)$ at intermediate temperatures (10–30 K) is characterized by a crossover from the regime of boundary-limited or phonon-electron scattering to the regime of Umklapp scattering. As elaborated in Sec. 3.4.1 such a maximum in $\lambda_{\text{ph}}^{\text{p}}(T)$ -curve is also revealed in decagonal $\text{Al}_{65}\text{Cu}_{20}\text{Co}_{15}$ and one is lead to conclude that a maximum of $\lambda_{\text{ph}}^{\text{p}}$ at intermediate temperatures is an intrinsic property of decagonal quasicrystals.

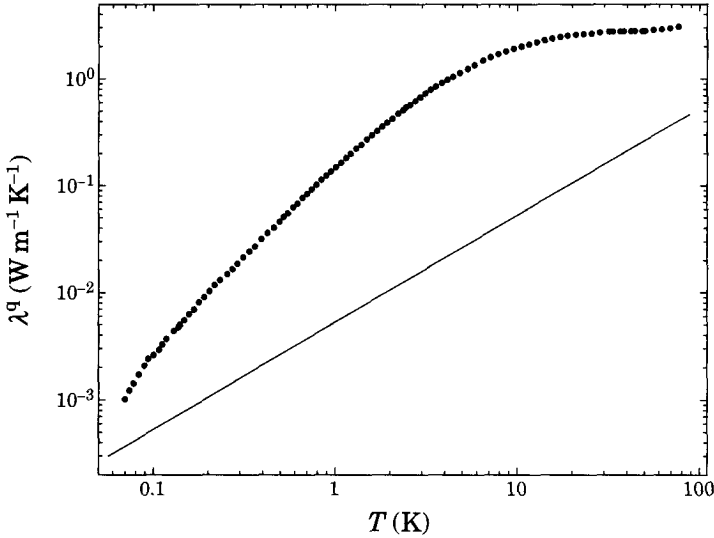


Figure 3.27: The total measured thermal conductivity λ^q of decagonal $\text{Al}_{71}\text{Ni}_{16}\text{Co}_{13}$ in a quasiperiodic direction between 0.06 and 80 K. The solid line is an estimate of the electronic contribution λ_{el}^q (see text).

Between 0.45 and 1.2 K, the phonon thermal conductivity is well described by $\lambda_{ph}^p \propto T^n$, where $n = 2.2 \pm 0.1$ (see solid line in Fig. 3.26). Following the arguments given in Sec. 3.4.1 for decagonal $\text{Al}_{65}\text{Cu}_{20}\text{Co}_{15}$, the relatively low resistivity $\rho^p(T)$ of this sample suggests that a substantial part of the phonon thermal resistance $(\lambda_{ph}^p)^{-1}$ of decagonal $\text{Al}_{71}\text{Ni}_{16}\text{Co}_{13}$ might be attributed to phonon-electron interactions.

Quasiperiodic direction

The thermal conductivity λ^q of $\text{Al}_{71}\text{Ni}_{16}\text{Co}_{13}$ along a direction in the quasiperiodic plane in the temperature range between 0.06 and 80 K is shown on double logarithmic scales in Fig. 3.27. The solid line is an estimate of the electronic contribution λ_{el}^q , which was calculated from electrical resistivity ρ^q data measured on this same sample and assuming the validity of the Wiedemann-Franz law.

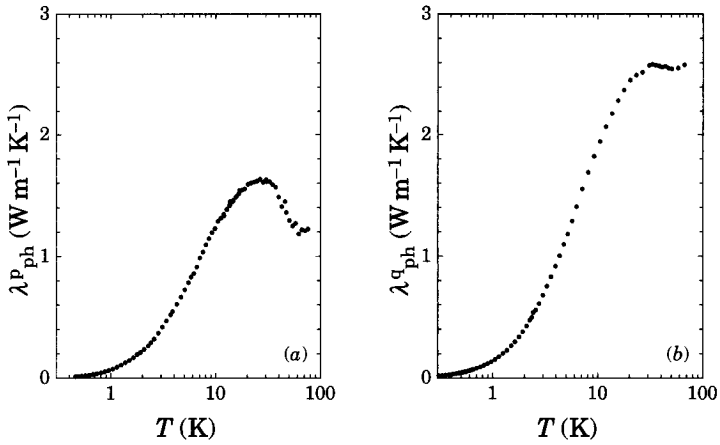


Figure 3.28: (a)–Phonon contribution λ_{ph}^p to the thermal conductivity of decagonal $Al_{71}Ni_{16}Co_{13}$ along the periodic direction. (b)–Phonon contribution λ_{ph}^q to the thermal conductivity along the quasiperiodic direction of decagonal $Al_{71}Ni_{16}Co_{13}$. Both figures have the same scales.

The lattice contribution $\lambda_{ph}^q(T)$, obtained by subtracting $\lambda_{el}^q(T)$ from the measured thermal conductivity $\lambda^q(T)$, is shown in Fig. 3.28b. It increases considerably with increasing T between 0.07 and 2 K. With further increasing T , the trend of $\lambda_{ph}^q(T)$ to saturate at 30 K is noted and from 30 to 80 K λ_{ph}^q is almost temperature independent. The overall temperature dependence of λ_{ph}^q of decagonal $Al_{71}Ni_{16}Co_{13}$ is very similar to the one of decagonal Al-Cu-Co presented before in Sec. 3.4.1, where the λ -plateau was ascribed to Umklapp processes in solids with quasiperiodic order [40].

In Fig. 3.28 the phonon contribution to the thermal conductivity λ_{ph} of decagonal $Al_{71}Ni_{16}Co_{13}$ along the periodic and a quasiperiodic direction is shown on the same scales. This figure is intended to emphasize the apparently different behaviour of the phonon thermal conductivity at intermediate temperatures along the periodic and quasiperiodic direction in decagonal quasicrystals and provides further evidence for the characteristically different phonon scattering rate in Umklapp processes in periodically and quasiperiodically ordered solids.

Surprisingly, the lattice thermal conductivity in decagonal Al-Ni-Co is higher along a direction in the quasiperiodic plane, than along the periodic direction. The inequality $\lambda_{\text{ph}}^{\text{q}} > \lambda_{\text{ph}}^{\text{p}}$ seems to be a general observation for decagonal quasicrystals [129] and is possibly related to strongly anisotropic phonon-electron scattering.

3.4.3 Conclusions

The investigations of the the thermal conductivity for single crystalline decagonal $\text{Al}_{65}\text{Cu}_{20}\text{Co}_{15}$ and $\text{Al}_{71}\text{Ni}_{16}\text{Co}_{13}$ along the periodic direction and a direction in the quasiperiodic plane revealed a very similar temperature characteristic in both the systems [119, 129].

The phonon thermal conductivity $\lambda_{\text{ph}}^{\text{q}}(T)$ along a direction in the quasiperiodic plane is distinctly different from that along the periodic direction $\lambda_{\text{ph}}^{\text{p}}(T)$. Between 30 and 70 K, $\lambda_{\text{ph}}^{\text{q}}(T)$ is weakly temperature dependent. This feature of the $\lambda_{\text{ph}}^{\text{p}}(T)$ curve was previously observed for icosahedral quasicrystals [72, 102, 115, 117, 119, 129, 138] and we attribute it to Umklapp scattering of phonons in quasicrystals [40]. The phonon thermal conductivity along the periodic direction $\lambda_{\text{ph}}^{\text{p}}(T)$ is characterized by a distinct maximum at 25 K, which can be attributed to a crossover between the Peierls regime of the usual Umklapp phonon scattering [65] and the regime of phonon-electron scattering. This $\lambda_{\text{ph}}^{\text{p}}(T)$ behaviour is reminiscent of $\lambda_{\text{ph}}(T)$ of periodic crystals. Thus, the transport of heat via lattice excitations along the decagonal axis and along a direction in the quasiperiodic plane resembles closely that of periodic crystals and icosahedral quasicrystals, respectively. Surprisingly, the lattice thermal conductivity in decagonal Al-Cu-Co and Al-Ni-Co is higher along a direction in the quasiperiodic plane, than along the periodic direction [119, 129].

4 Specific heat

4.1 Icosahedral Al-Re-Pd

The complete set of the specific heat $C_p(T)$ data of icosahedral $\text{Al}_{70}\text{Re}_{8.6}\text{Pd}_{21.4}$ measured in the temperature range between 0.065 and 19 K is shown in Fig. 4.1 on a double logarithmic plot. As a first observation it should be noted that below 0.4 K, the specific heat

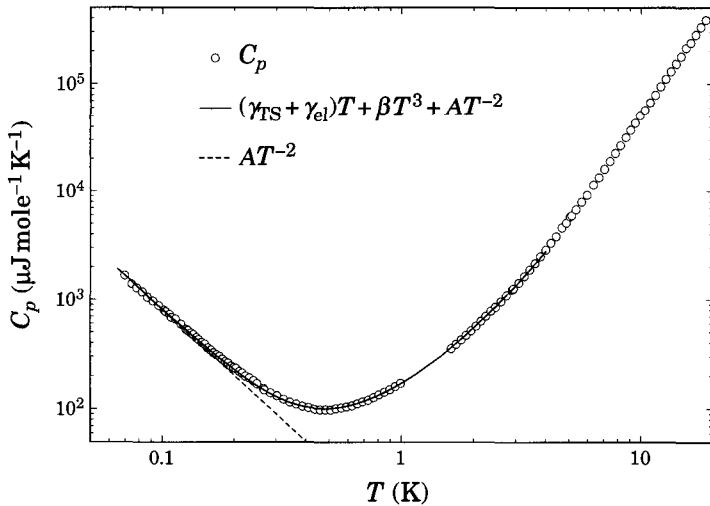


Figure 4.1: Specific heat $C_p(T)$ of icosahedral $\text{Al}_{70}\text{Re}_{8.6}\text{Pd}_{21.4}$ between 0.065 and 19 K. The solid line is the fit of Eq. 4.1 to the $C_p(T)$ data between 0.065 and 4 K.

$C_p(T)$ is increasing with decreasing temperature, indicating a large excess specific heat $C_{ex}(T)$. At the lowest temperatures of this experiment, $C_p(T)$ varies approximately as T^{-2} suggesting that $C_{ex}(T)$ is a nuclear hyperfine contribution $C_N = AT^{-2}$ representing the high-temperature tail of a Schottky-type anomaly with a maximum at a temperature considerably below the temperature range of this experiment. The thermal conductivity measurements presented in Sec. 3.3 indicate the presence of tunneling states in icosahedral Al-Re-Pd [117] and thus a linear contribution $\gamma_{TS}T$ to $C_p(T)$ is expected [74, 75] in addition to the electronic contribution $\gamma_{el}T$. In the further analysis of the specific heat $C_p(T)$ data it is assumed that the main contributions are from tunneling states, electronic, lattice and nuclear excitations, i.e.,

$$C_p = (\gamma_{TS} + \gamma_{el})T + \beta T^3 + AT^{-2} \quad (4.1)$$

A fit of Eq. 4.1 to the specific heat data between 0.065 and 4 K, shown in Fig. 4.1 as a solid line, yields $\gamma_{TS} + \gamma_{el} = 125 \pm 1 \mu\text{J mol}^{-1} \text{K}^{-2}$, $\beta = 36.0 \pm 0.4 \mu\text{J mol}^{-1} \text{K}^{-4}$ and $A = 8.23 \mu\text{J mol}^{-1} \text{K}$. It should be noted that the experimentally determined coefficient $\gamma_{TS} + \gamma_{el}$ of the linear term in the specific heat $C_p(T)$ of icosahedral $\text{Al}_{70}\text{Re}_{8.6}\text{Pd}_{21.4}$ is extremely small. It only amounts to approximately 1/10 of the coefficient γ_{el} of aluminium. It is difficult to evaluate the tunneling state contribution $\gamma_{TS}T$ that is compatible with the low-temperature λ_{ph} data (Sec 3.3) without additional assumptions on the spectral density $n_{TS}(\omega)$ of tunneling states. The value of the linear contribution $\gamma_{TS} + \gamma_{el}$ has to be considered as an upper limit of the electronic contribution γ_{el} . In the following, the different contributions to $C_p(T)$ are discussed separately.

Nuclear contribution to the low-temperature specific heat

The nuclear term C_N is most probably due to an interaction between the nuclear quadrupoles and the gradient of static electric fields induced by their neighbouring ions. The coefficient A of the nuclear specific heat C_N reads [139]

$$A = k_B N_A \sum_{i,k} \frac{\rho_i \nu_{ik} (2I_{ik} + 2)(2I_{ik} + 3)}{80 \cdot 2I_{ik}(2I_{ik} - 1)} \left(\frac{e^2 \bar{q} Q_{ik}}{k_B} \right)^2 \quad (4.2)$$

Here ρ_k is the concentration of the element i , ν_{ik} , I_{ik} and Q_{ik} are the natural abundance, the nuclear spin quantum number and the nuclear quadrupole moment of isotope k of the element i , respectively, and $e\bar{q}$ is the largest component of the electric-field-gradient tensor averaged over all sites [139]. In the case of Al-Re-Pd alloys there are four naturally occurring isotopes, i.e., ^{27}Al , ^{105}Pd , ^{185}Re and ^{187}Re , all with $I = 5/2$, which may contribute to C_N [140]. The nuclear quadrupole moments of both rhenium isotopes, i.e., ^{185}Re and ^{187}Re substantially exceed those of ^{27}Al and ^{105}Pd [140]. Because the electric quadrupole moment Q_{ik} enters Eq. 4.2 as Q_{ik}^2 it seems reasonable to consider only the contributions of ^{185}Re and ^{187}Re to $C_N(T)$. The value of A which follows from the specific-heat results is compatible with $\bar{q} = 2.31 \pm 0.01 \times 10^{15}$ esu. Surprisingly, this \bar{q} -value is comparable to the q -values of 1.65×10^{15} and 1.56×10^{15} esu for the ^{185}Re and ^{187}Re nuclei, respectively, in a hexagonal lattice of rhenium metal. They follow from the results of nuclear acoustic resonance experiments [141]. Similar \bar{q} -values of 1.67×10^{15} and 1.84×10^{15} esu have been deduced from nuclear specific heat results obtained on two different samples of rhenium metal in the normal state [142, 143]. Of course, one should be aware that this estimate concerning field gradients in Al-Re-Pd quasicrystals must be rather crude considering the structural properties of these materials. Nevertheless, it should be noted that a major part of rhenium atoms in Al-Re-Pd quasicrystals must occupy sites with a non-icosahedral local symmetry. This is because the splitting of the nuclear levels in Al-Re-Pd as revealed by the observation of the sizable nuclear hyperfine specific heat is possible only if the local symmetry is lower than cubic.

Linear contribution to the low-temperature specific heat

In the tunneling-states model [74, 75] the density of tunneling states is assumed to be frequency independent and limited to a certain frequency range. In this case excitations of tunneling states are expected to contribute a linear-in-temperature term $C_{\text{TS}} = \gamma_{\text{TS}}T$ to the total specific heat $C_p(T)$ [74, 75]. An approximately linear contribution to the low-temperature specific heat of the order of $50 T \mu\text{J mol}^{-1} \text{K}^{-1}$ has previously been reported for various amorphous insulators and superconducting metallic glasses [145]. For non-superconducting amorphous metals, $C_{\text{TS}}(T)$ cannot be separated in simple ways from the common electronic specific heat $\gamma_{\text{el}}T$, which also rises linearly with temperature. For

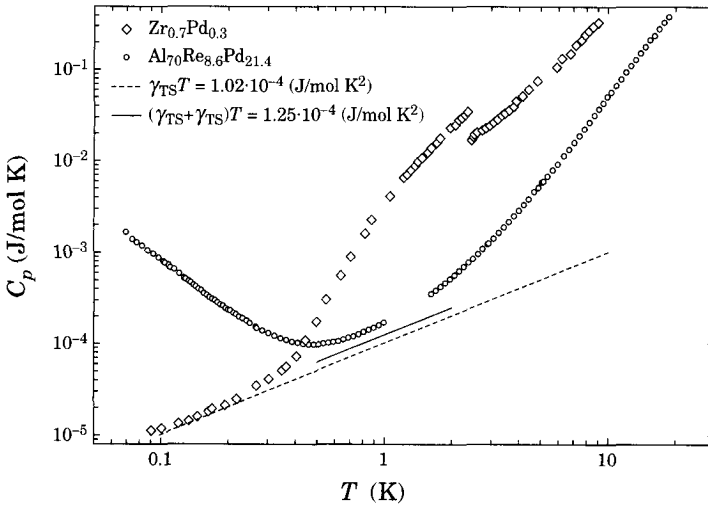


Figure 4.2: Specific heat $C_p(T)$ of icosahedral $\text{Al}_{70}\text{Re}_{8.6}\text{Pd}_{21.4}$ in comparison with $C_p(T)$ of the superconducting metallic glass $\text{Zr}_{0.7}\text{Pd}_{0.3}$ [144]. The solid line is the linear contribution $(\gamma_{\text{TS}} + \gamma_{\text{el}})T$ to C_p of $\text{Al}_{70}\text{Re}_{8.6}\text{Pd}_{21.4}$. In $\text{Zr}_{0.7}\text{Pd}_{0.3}$ the electronic contribution to the specific heat C_{el} vanishes exponentially below the superconducting transition at $T_c = 2.53$ K and a precise determination of the tunneling contribution $C_{\text{TS}} = \gamma_{\text{TS}}T$ is possible (broken line).

superconducting metallic glasses, however, the electronic specific heat vanishes exponentially with decreasing T below the critical temperature T_c , which allows a precise determination of C_{TS} from the low-temperature $C_p(T)$ data. This can be seen in Fig. 4.2, where the specific heat data of the superconducting metallic glass $\text{Zr}_{0.7}\text{Pd}_{0.3}$ with a tunneling state contribution $\gamma_{\text{TS}}T$ of $102 T \mu\text{J mol}^{-1} \text{K}^{-1}$ is shown [144]. The electrical-conductivity data of this sample of $\text{Al}_{70}\text{Re}_{8.6}\text{Pd}_{21.4}$ show that this material remains in the normal state down to 0.05 K at least (c.f. Sec. 5.2).

A value of the tunneling state contribution of the order of $50 T \mu\text{J mol}^{-1} \text{K}^{-1}$ corresponds to about 1/2 of the experimentally determined linear term $(\gamma_{\text{el}} + \gamma_{\text{TS}})T$ to the specific heat $C_p(T)$ of this sample, suggesting that caution is needed in interpreting low-temperature specific-heat data of Al-Re-Pd quasicrystals. In any case the density of electronic states at E_F must be rather small. In conventional metals the value of the electronic

DOS at the Fermi energy $n(E_F)$ can in principle be deduced from the Pauli paramagnetic susceptibility $\chi = \mu_B^2 n(E_F)$. However, icosahedral quasicrystals in the Al-Re-Pd system are diamagnetic with a susceptibility of the order of -4×10^{-7} emu/g and no correlation between the value of the magnetic susceptibility and the electrical conductivity is observed [111]. The diamagnetism of icosahedral quasicrystals [146] has been attributed to the many-pocketed Fermi surface, expected for a Hume-Rothery-type electronic stabilization mechanism of the quasicrystalline structure (See Secs 4.3.1 and 5.1). Making the assumption of a many pocketed Fermi surface, the effective mass of the carriers in a single pocket is anisotropic and for a low carrier concentration the sum of the diamagnetic contribution to the magnetic susceptibility of all the pockets can be larger than the Pauli paramagnetic contribution [146]. Thus, a direct evaluation of the electronic DOS at E_F from magnetic susceptibility data meets difficulties.

For icosahedral quasicrystals, the small electronic specific heat has tentatively been attributed to the presence of a pseudogap in the density of electronic states (DOS) at the Fermi energy E_F [35, 147]. Subsequent optical reflectivity measurements using the same samples gave further evidence supporting this conclusion [147, 148]. The presence of a pseudogap in the electronic DOS at E_F of icosahedral quasicrystals in the Al-Mn-Pd, Al-Re-Pd and Al-Cu-Fe alloy systems was also inferred from an analysis of the low-temperature high-resolution ultraviolet photoemission spectra [149]. Nuclear magnetic resonance experiments probing the spin-lattice relaxation rate T_1 in icosahedral quasicrystals indicate strong deviations at high temperatures from the usual Korringa-type behaviour $(T_1 T)^{-1} = \text{const.}$ observed in metals [150–152]. In icosahedral quasicrystals these deviations are commonly ascribed to the presence of a minimum in the electronic DOS [150–152]. Notable is, that the T_1 -data measured on different samples of icosahedral Al-Re-Pd [151–154] including those for which the electrical conductivity data is presented in Sec. 5 fall on one universal curve in a T_1^{-1} vs. T representation [154]. Indications for the presence of a parabolic minimum in the electronic DOS at E_F are also obtained from tunneling experiments [155]. Tunneling spectroscopy on bare and oxydized surfaces of in icosahedral Al-Cu-Fe and icosahedral Al-Re-Pd showed an approximately quadratic variation of the tunneling conductance $dI/dV \propto E^\alpha$ for $|E| < 50$ eV with α in the range 1.5 between 2 for different junctions.

It has been suggested that the minimum in the electronic DOS at E_F is the consequence of an Hume-Rothery type electronic stabilization mechanism of the quasicrystalline structure [156–158]. As suggested in Ref 158, the hypothesis of a Hume-Rothery type electronic stabilization mechanism has been the subject of a number of electronic bandstructure calculations of periodic approximants to quasicrystals over the recent years. Calculations of the electronic bandstructure for periodic approximants in the Al-Cu-Fe [159] and Al-Mn-Pd [160] systems indicated the existence of a well pronounced pseudo-gap at the Fermi energy E_F . In the Al-Mn-Pd system the calculated electronic DOS of a series of approximants indicated that the position of the pseudogap relative to E_F is influenced by changes in the chemical composition [160]. It was found that for higher order approximants the minimum in the electronic DOS is located closer to E_F [160], however, the depth of the pseudogap is almost independent of the order of the approximant [160]. In the same work the importance of the hybridization of the Al s and p states with the transition metal d-states in the formation of the pseudogap was pointed out as a result of a calculation of the electronic DOS of a series of clusters [160]. A calculation of the electronic bandstructure in periodic Al-based Hume-Rothery alloys lead to a similar conclusion [161]. The results of these bandstructure calculations gave evidence for the validity of a model assuming an enhanced formation of a pseudogap in the electronic DOS at E_F by the combination of the crossing of a d with an sp band at the pseudo Brillouin zone boundary [158].

Lattice contribution to the low-temperature specific heat

The phonon contribution $C_{\text{ph}}(T)$ obtained after subtracting off the nuclear C_N and the linear contribution $(\gamma_{\text{TS}} + \gamma_{\text{el}})T$ using the respective values as determined from the fit of Eq. 4.1 is plotted as C_{ph}/T^3 vs. T in Fig. 4.3 together with high temperature data measured on the same specimen as reported by Wälti *et al.* [57]. They pointed out that for temperatures below 3 K, C_{ph}/T^3 is approximately temperature independent, with $C_{\text{ph}}/T^3 = 3.6 \times 10^{-5} \text{ J mol}^{-1} \text{ K}^{-4}$ [57]. Above 3 K, C_{ph}/T^3 increases slowly with increasing temperature, passes over a broad maximum centered at approximately 25 K, indicating that at low frequencies the vibrational density of states $g(\omega)$ increases more strongly than the Debye DOS, i.e. $g \propto \omega^2$ [57]. An estimate of the Debye contribution C_D/T^3 of $\text{Al}_{70}\text{Re}_{8.6}\text{Pd}_{21.4}$ may be obtained from the renormalized average of the low-temperature

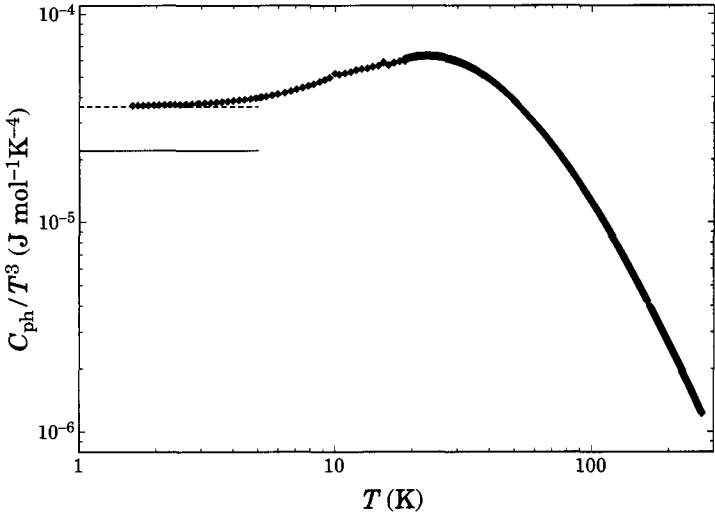


Figure 4.3: Lattice contribution to the specific heat $C_{ph}(T)$ of icosahedral $Al_{70}Re_{8.6}Pd_{21.4}$ plotted as C_{ph}/T^3 vs. T . The broken line depicts the results of the fit to Eq. 4.1, with $C_{ph}/T^3 = 3.6 \times 10^{-5} \text{ J mol}^{-1} \text{ K}^{-4}$. The horizontal solid line indicates the Debye specific heat $C_D/T^3 = 2.2 \times 10^{-5} \text{ J mol}^{-1} \text{ K}^{-4}$, calculated from estimates of the sound-velocities using Eq. 4.5. The figure is taken from Ref. 57.

sound velocity \bar{v} of icosahedral Al-Mn-Pd [99], as icosahedral Al-Re-Pd and Al-Mn-Pd quasicrystals have a similar structure [57]. A calculation of C_D/T^3 via Eq. 4.5 using the value of $\bar{v} = 3.7 \times 10^4 \text{ cm s}^{-1}$ yields $C_D/T^3 = 2.2 \times 10^{-5} \text{ J mol}^{-1} \text{ K}^{-4}$ [57] shown as the solid line in Fig. 4.3. This value of C_D/T^3 is substantially lower than the observed C_{ph}/T^3 contribution, suggesting a considerable excess specific heat C_{ex} in icosahedral $Al_{70}Re_{8.6}Pd_{21.4}$ also at high temperatures [57]. Such an excess cubic-in- T contribution C_{ex} to the specific heat was also noticed in icosahedral Al-Mn-Pd, for which it was ascribed to non-propagating lattice excitations [57].

In conclusion, the low-temperature specific-heat $C_p(T)$ variation of icosahedral $Al_{70}Re_{8.6}Pd_{21.4}$ is characterized by a large nuclear hyperfine contribution $C_N \propto T^{-2}$ due to the interaction of the quadrupole moments of the ^{185}Re and ^{187}Re nuclei with the gradient of electric fields induced by their neighbours, and a very small linear-in- T term. A comparison with glasses suggests that excitations of tunneling states may account for

approximately 1/2 of the coefficient of the linear term to the specific heat. The experimentally determined cubic-in- T term in the specific heat is distinctly higher than expected contribution from acoustic phonons, indicating a large excess specific heat C_{ex} [57].

4.2 Decagonal Al-Cu-Co

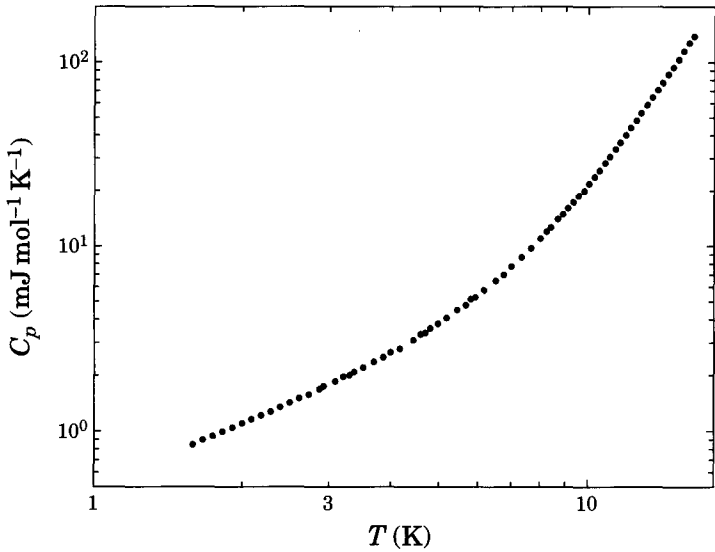


Figure 4.4: Specific heat $C_p(T)$ of decagonal $\text{Al}_{65}\text{Cu}_{20}\text{Co}_{15}$ between 1.5 and 17 K.

Figure 4.4 shows the complete set of the results of the specific heat $C_p(T)$ of decagonal $\text{Al}_{65}\text{Cu}_{20}\text{Co}_{15}$ measured in the temperature range between 1.5 and 17 K, plotted on logarithmic scales. The $C_p(T)$ data between 1.5 and 4.5 K, shown in Fig. 4.5 as $C_p(T)$ vs. T^2 , is well fitted by

$$C_p(T) = \gamma T + \beta T^3, \quad (4.3)$$

indicating that the main contributions are from the common electronic and lattice excitations at low temperatures. The results of the fit are $\gamma = 0.512 \text{ mJ mol}^{-1} \text{K}^{-2}$, and $\beta = 9.22 \text{ } \mu\text{J mol}^{-1} \text{K}^{-4}$. The coefficient γ of decagonal Al-Cu-Co cannot easily be compared with an estimate of a free-electron value of the electronic specific heat because the number of electrons, donated by the d-transition-element atoms to the conduction band, is not well defined. In any case, one should note a low value of the electronic specific heat, amounting to approximately one third of that of Aluminum, if all of the

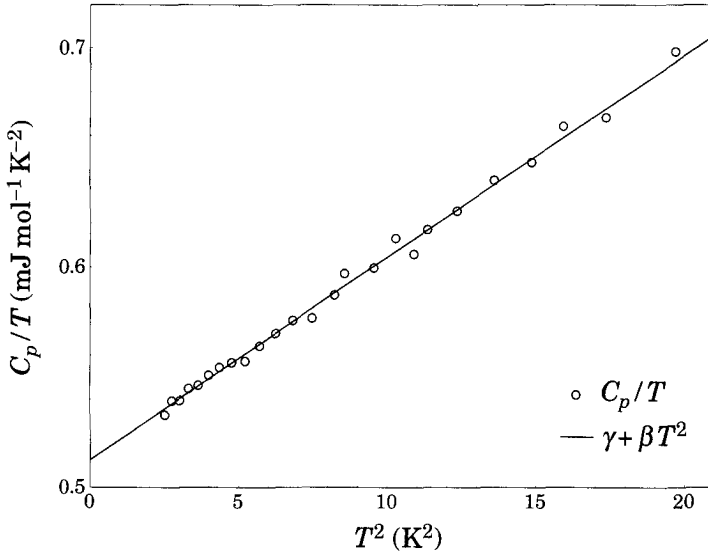


Figure 4.5: C_p/T vs. T^2 of decagonal $Al_{65}Cu_{20}Co_{15}$. The solid line represents the fit to Eq. 4.3.

γT term is ascribed to electronic degrees of freedom. This γ value is comparable to $\gamma = 0.41 \text{ mJ mol}^{-1} \text{ K}^{-2}$ previously reported for icosahedral $Al_{70}Mn_9Pd_{21}$ [35]. In accordance with subsequent optical reflectivity measurements using the same sample [148], this low value of the linear contribution to the specific heat was attributed to the presence of a pseudo-gap in the electronic density of states at the Fermi level E_F [35].

It has been claimed that a Hume-Rothery mechanism plays a dominant role in the stability of the icosahedral quasicrystals [156, 158]. As discussed in Sec 4.1, this is mainly because the existence of a pronounced pseudo-gap in the density of electronic states at E_F has experimentally been indicated for various icosahedral phases by a number of experiments [118, 162]. In contrast, it is controversial at present as to whether the same mechanism also leads to the stabilization of decagonal quasicrystals. Based on the results of Hall-effect measurements [163], it was claimed that the Hume-Rothery-type stabilization is essential. A band-structure calculation for a periodic approximant of a decagonal structure of Trambly de Laissardière and Fujiwara gave further support by confirming the

existence of a well pronounced pseudo-gap at the Fermi level for this particular case [164]. On the contrary, optical conductivity measurements [133] and low-resolution photoemission spectroscopy experiments [165] show no evidence for a pseudo-gap. The question of the presence of a pseudogap in the electronic DOS of decagonal quasicrystals will be addressed in greater detail in Sec. 4.3.1.

The value of the parameter β of the term proportional to T^3 in the specific heat is compatible with a Debye temperature Θ_D of 596 K, according to a survey of the current literature the highest of all the Θ_D values reported for thermodynamically stable quasicrystals [57].

In summary, the low linear-in- T contribution $\gamma T = 0.512 \text{ mJ mol}^{-1} \text{ K}^{-1}$ to the low-temperature specific heat $C_p(T)$ of decagonal $\text{Al}_{65}\text{Cu}_{20}\text{Co}_{15}$ suggests the existence of a pseudo-gap in the electronic density of states at the Fermi level. The cubic-in- T term to the specific heat is compatible with a Debye temperature Θ_D of 596 K, which is considerably higher than the Θ_D values previously reported for stable icosahedral quasicrystals.

4.3 Decagonal Al-Ni-Co

The complete set of the specific heat $C_p(T)$ data in the temperature range between 1.5 and 36 K for a single grain of decagonal $\text{Al}_{71}\text{Ni}_{16}\text{Co}_{13}$ is shown on a double logarithmic plot in Fig. 4.6. The same data in the form of C_p/T vs. T^2 , are plotted in Fig. 4.7. Between 1.5 and 3 K the temperature variation of $C_{\text{ph}}(T)$ can adequately be described by assuming that the main contributions are due to electronic and lattice excitations, i.e.

$$C_p(T) = \gamma T + \beta T^3 . \quad (4.4)$$

A fit to our specific-heat data $C_p(T)$ using Eq. 4.4, which is shown in Fig. 4.7 as the solid line, yields $\gamma = 0.629 \pm 0.003 \text{ mJ mol}^{-1} \text{ K}^{-2}$ and $\beta = 9.5 \pm 0.6 \mu\text{J mol}^{-1} \text{ K}^{-4}$, corresponding to a Debye temperature Θ_D of $589 \pm 12 \text{ K}$. For calculating Θ_D the experimentally determined density $\rho = 4.186 \text{ g cm}^{-3}$ was used [166]. It should be noted that the measured value of ρ for $\text{Al}_{71}\text{Ni}_{16}\text{Co}_{13}$ is distinctly lower than the averaged density of the constituent elemental metals.

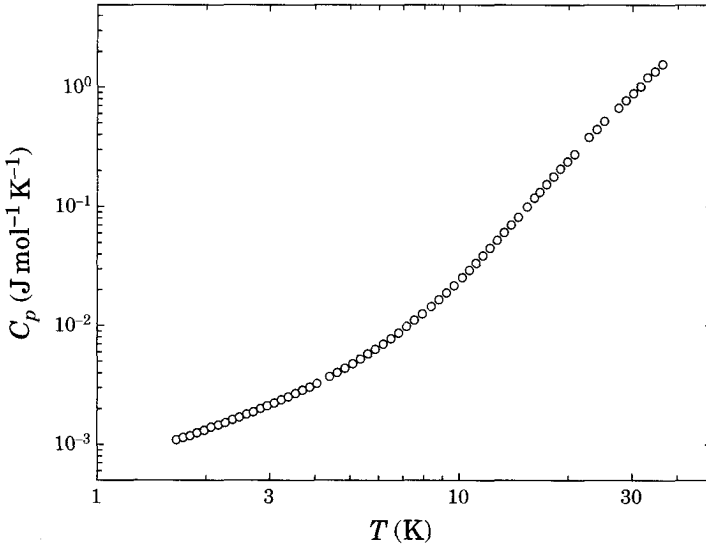


Figure 4.6: Specific heat $C_p(T)$ of decagonal $\text{Al}_{71}\text{Ni}_{16}\text{Co}_{13}$ between 1.5 and 36 K.

4.3.1 Electronic contribution

The value of the parameter γ reported here is close to analogous values reported previously for melt-spun $\text{Al}_{70}\text{Ni}_{30-x}\text{Co}_x$ ribbons, with $5 < x < 30$ [167]. This value of the electronic specific heat parameter γ is 2.5 times smaller than that of Aluminium but somewhat higher than the γ -values reported for highly ordered icosahedral Al-Mn-Pd and Al-Re-Pd quasicrystals with the face centered icosahedral structure, which fall into the range between 0.11 and 0.41 $\text{mJ mol}^{-1} \text{K}^{-2}$ [35, 147]. The low linear contribution to the specific heat in these materials is commonly associated with the presence of minimum in the electronic DOS at E_F , in line with the results a number of experiments probing the electronic DOS as pointed out in Sec. 4.1.

While abundant experimental evidence for the existence of a pronounced pseudogap in the density of electronic states at E_F has experimentally been obtained for various icosahedral phases [118, 162], suggesting that the Hume-Rothery mechanism plays an essential role in the stability of the icosahedrally ordered solids [156, 158], the presence of

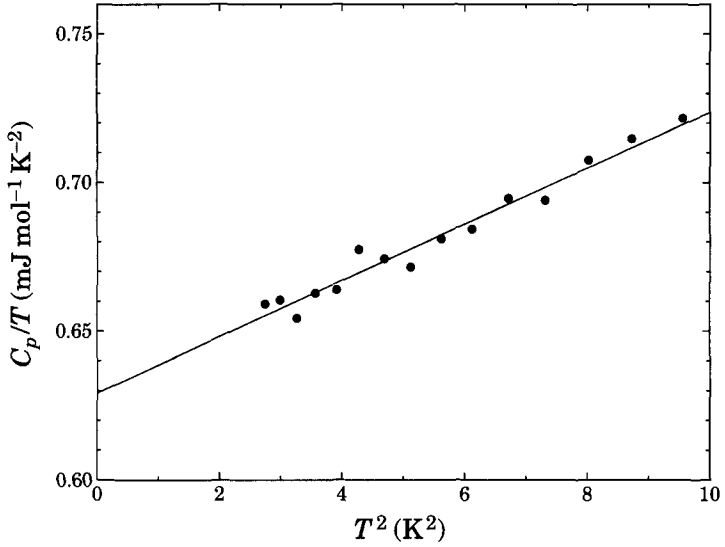


Figure 4.7: Specific heat of decagonal $\text{Al}_{71}\text{Ni}_{16}\text{Co}_{13}$ plotted as C_p/T vs. T^2 . The solid line is the fit to the data using Eq. 4.4 in the temperature range between 1.5 and 3 K.

a pseudogap at E_F in decagonal quasicrystals remains a controversial issue. The results of Hall-effect measurements reported in Ref. 163, seem to support the Hume-Rothery-type scenario. The low linear-in- T contribution to C_p of decagonal $\text{Al}_{65}\text{Cu}_{20}\text{Co}_{15}$ (See Sec. 4.2) and $\text{Al}_{71}\text{Ni}_{16}\text{Co}_{13}$ indicate a reduced DOS at E_F in decagonal quasicrystals. Based on the analysis of high-resolution photoemission experiments, the presence of a pseudogap in decagonal Al-Cu-Co and Al-Ni-Co was claimed by Stadnik and coworkers [168], in contrast to the earlier results of low-resolution experiments [165].

The absence of a pseudogap at E_F in the electronic density of states in decagonal $\text{Al}_{62}\text{Co}_{15}\text{Cu}_{20}\text{Si}_3$ and $\text{Al}_{65}\text{Co}_{17}\text{Cu}_{18}$ has been inferred from an analysis of the optical conductivity $\sigma_1(\omega)$, which indicated a higher density of free charge carriers n in these systems compared with the values of n observed in icosahedral quasicrystals [133]. Nevertheless, the results on $\sigma_1(\omega)$ in decagonal $\text{Al}_{71}\text{Ni}_{16}\text{Co}_{13}$ presented in Ref. 119 clearly show an absorption centered at approximately 1 eV for both directions (see Fig. 3.20b). Such an absorption is a general observation in the $\sigma_1(\omega)$ curves of icosahedral quasicrystals and is commonly associated with excitations across a pseudogap in the electronic excitation

spectrum [147, 148]. Such an absorption, although with less intensity, is also observed in the conductivity spectra decagonal $\text{Al}_{62}\text{Co}_{15}\text{Cu}_{20}\text{Si}_3$ and $\text{Al}_{65}\text{Co}_{17}\text{Cu}_{18}$ [133]. As argued in Ref. [119], the difference in the intensities of these absorptions between Al-Ni-Co and Al-Cu-Co most likely originates in the limited frequency range of the reflectivity data available for the Kramers-Kronig transformation for Al-Cu-Co [133]. Calculations of the electronic bandstructure of rational approximants to decagonal quasicrystals have raised some doubts as to whether the observed minimum in the electronic DOS of decagonal quasicrystals is due to an electronically driven stabilization of quasiperiodic structures [169, 170].

Recent band structure calculation using a model approximant $\text{Al}_{66}\text{Cu}_{30}\text{Co}_{14}$ of decagonal Al-Cu-Co showed the presence of a pseudogap with a width of ≈ 0.5 eV centered at an energy of ≈ 0.3 eV above E_F [164]. The overall energy dependence of the electronic DOS is, however, in poor agreement with the photoelectron spectra reported for a decagonal quasicrystal of a somewhat different chemical composition [168, 170]. In addition, it turned out that both the position and the depth of the pseudogap in the calculated electronic DOS of decagonal Al-Cu-Co strongly depend on the chemical decoration of the Cu/Co sites [169, 170]. For certain decorations of the Cu/Co sites, the minimum in the partial DOS of the Al s and p states near E_F is covered by the large contribution from the Co d states [170]. These observations have led to the conclusion that a pseudogap in the electronic DOS of decagonal Al-Cu-Co is the consequence of the hybridization between transition metal d states and Aluminum s and p states rather than the result of the interaction of the Fermi surface with the pseudo Brillouin zone [169, 170]. A similar conclusion regarding the origin of the pseudogap at E_F in decagonal quasicrystals has emerged from electronic band structure calculations for decagonal Al-Mn-Pd [171, 172]. Concluding this discussion, it should be noted that the results on the low temperature specific heat presented above indicate a small electronic DOS at E_F and are therefore consistent with the presence of a pseudogap in the electronic DOS at E_F .

4.3.2 Lattice contribution

This section will now be concentrating on the lattice contribution $C_{\text{ph}}(T)$ to the specific heat C_p of decagonal $\text{Al}_{71}\text{Ni}_{16}\text{Co}_{13}$. The specific heat data plotted in Fig. 4.7 as

C_p/T vs. T^2 falls on a straight line, indicating a Debye-type behaviour of $C_{ph}(T)$ for temperatures below 3 K. At low temperatures only the acoustic excitations contribute to $C_{ph}(T)$, which takes the form

$$C_D(T) = \frac{2\pi^2 k_B^4}{5\hbar^3 v_s^3} T^3 \quad , \quad (4.5)$$

where $1/v_s^3$ is the average of the inverse third power of the long-wavelength phase velocities $v_i(\mathbf{q})$ of the three acoustic modes [166]

$$\frac{1}{v_s^3} = \frac{1}{3} \sum_{i=1}^3 \int \frac{1}{v_i^3(\varphi, \theta)} \frac{d\varphi \sin\theta d\theta}{4\pi} \quad . \quad (4.6)$$

Here $v_i(\varphi, \theta)$ are the velocities of the sound waves propagating in a direction defined by the directional angles φ and θ . Decagonal quasicrystals are elastically isotropic in the quasiperiodic plane [166, 173] and therefore the sound velocities v_i depend only upon the angle θ between the propagation direction and the decagonal axis, i.e., the periodic direction. For decagonal quasicrystals, v_i are related to the elastic moduli C_{ij} and the angle θ in the same way [173] as for hexagonal crystals [174], i.e.,

$$\rho v_1^2 = c_{44} + \frac{1}{2}c \sin^2 \theta \quad (4.7)$$

$$\rho v_{2,3}^2 = c_{44} + \frac{1}{2} \{ a \sin^2 \theta + h \cos^2 \theta \pm [(a \sin^2 \theta + h \cos^2 \theta)^2 - 4(ah - d^2) \sin^2 \theta \cos^2 \theta]^{1/2} \}, \quad (4.8)$$

where ρ is the mass density and the parameters a , c , d and h are defined as follows:

$$a = c_{11} - c_{44} \quad (4.9)$$

$$c = c_{11} - c_{12} - 2c_{44} \quad (4.10)$$

$$d = c_{13} + c_{44} \quad (4.11)$$

$$h = c_{33} - c_{44} \quad . \quad (4.12)$$

From the low-temperature values of the elastic moduli c_{ij} obtained using resonant ultrasound spectroscopy [166] and the measured mass density ρ the average sound velocity v_s

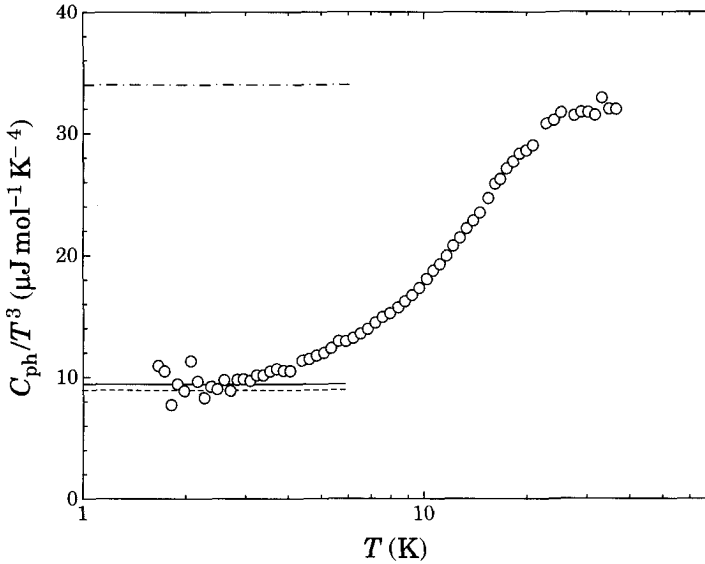


Figure 4.8: The lattice specific heat is plotted as C_{ph}/T^3 vs. T . The solid line shows the result of the fit to Eq. 4.4, with $C_{ph}/T^3 = 9.5 \mu\text{J mol}^{-1} \text{K}^{-4}$. The dashed line is the long-wavelength acoustic contribution to the specific heat $C_D/T^3 = 8.93 \mu\text{J mol}^{-1} \text{K}^{-4}$ (See text). The dash dotted line is an estimate of C_{ph}/T^3 calculated from the generalized density of vibrational states derived from neutron scattering experiments using Eq. 4.14.

is then deduced to be $(4.910 \pm 0.02) \times 10^3$ m/s. This value, inserted into Eq. 4.5, gives a low-temperature contribution to the specific heat of $C_D(T) = (8.93 \pm 0.11)T^3 \mu\text{J mol}^{-1} \text{K}^{-1}$, in fair agreement with the above mentioned experimental result

$\beta T^3 = (9.5 \pm 0.6)T^3 \mu\text{J mol}^{-1} \text{K}^{-1}$. This is quite different from the situation in icosahedral quasicrystals, for which a large excess cubic-in- T term in the low-temperature specific heat $C_p(T)$ has previously been observed in the Al-Mn-Pd and Al-Re-Pd systems [57].

The lattice specific heat $C_{ph}(T)$ obtained by subtracting off the linear contribution γT from the measured specific heat $C_p(T)$ is shown as a plot of C_{ph}/T^3 vs. T in Fig. 4.8. As noted above, the C_{ph}/T^3 ratio is temperature independent below 3 K. For temperatures higher than 3 K, the C_{ph}/T^3 ratio increases rapidly with increasing temperature above

the constant Debye limit, indicating that with increasing ω the vibrational DOS $g(\omega)$ increases stronger than the Debye approximation

$$g(\omega) = \frac{3}{2\pi^2 v_s^3} \omega^2 . \quad (4.13)$$

With further increasing temperature, C_{ph}/T^3 tends to saturate above 30 K at the level of $32 \mu\text{J mol}^{-1} \text{K}^{-4}$, approximately a factor of 3 higher than the ratio C_D/T^3 . At high temperatures $T > \Theta_D$ the lattice specific heat $C_{\text{ph}}(T)$ is expected to reach the constant Dulong and Petit limit and therefore C_{ph}/T^3 vs. T passes through a maximum at intermediate temperatures. This trend to saturation of the C_{ph}/T^3 vs. T curve simply indicates the proximity to this maximum.

In the harmonic approximation, the lattice specific heat $C_{\text{ph}}(T)$ depends on the DOS $g(\omega)$ as

$$C_{\text{ph}}(T) = \int_0^\infty g(\omega) \frac{\partial}{\partial T} \left(\frac{\hbar\omega}{\exp(\hbar\omega/k_B T) - 1} \right) d\omega . \quad (4.14)$$

The phonon DOS $g(\omega)$ cannot, strictly speaking, unambiguously be determined from the measured lattice specific heat $C_{\text{ph}}(T)$, as this requires solving an integral equation with an unstable kernel [175]. An analysis of the $C_{\text{ph}}(T)$ behaviour may nevertheless provide relevant information on $g(\omega)$, because the integral in Eq. 4.14 is especially sensitive to the variation of $g(\omega)$ close to $\omega \approx 2.3k_B T/\hbar$. The information on $g(\omega)$ obtained from the $C_{\text{ph}}(T)$ analysis is particularly accurate in the low-frequency limit, in which the contribution from high-frequency modes is exponentially small.

For monoatomic materials it is possible to evaluate the phonon DOS directly from inelastic neutron scattering experiments. However, for polyatomic materials containing elements with different neutron scattering cross-sections only a generalized density of vibrational states (GDVOS) can be obtained, which is a normalized sum of the partial phonon DOS, weighted with the Debye-Waller factor, the concentration, the scattering cross-section and the atomic mass of each element in the sample. In the Al-Ni-Co system the corresponding weights differ considerably due to the different scattering cross-sections of the elements [177], and the relation between the phonon DOS and the GDVOS may be

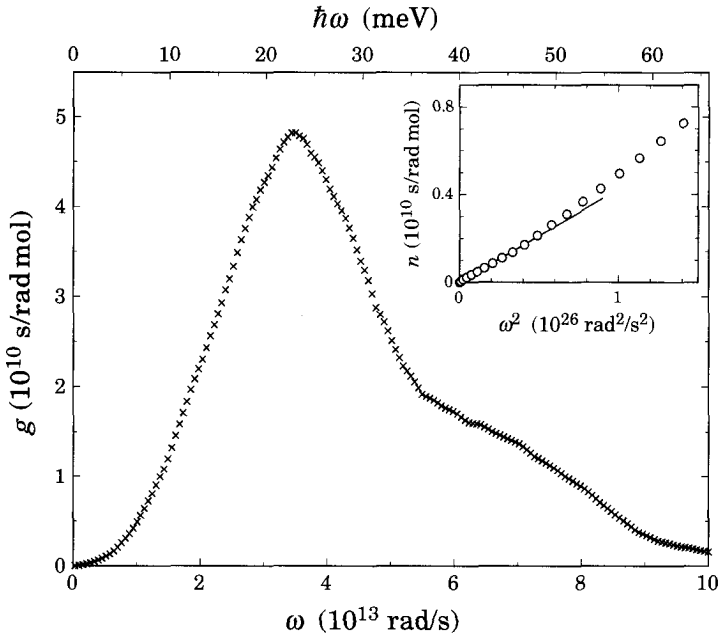


Figure 4.9: Generalized vibrational density of states $n(\omega)$ of decagonal Al-Ni-Co measured in an inelastic neutron scattering experiment with a time-of-flight spectrometer [176]. The inset shows $n(\omega)$ below 1.5×10^{12} rad/s plotted as n vs. ω^2 . The solid line is the fit as explained in the text.

ambiguous. The GDVOS of decagonal Al-Ni-Co measured in an inelastic neutron scattering experiment [176] with the time-of-flight technique is shown in Fig. 4.9. For frequencies ω below 7×10^{12} rad/s, $g(\omega)$ varies as $g = a\omega^2$, with $a = 4.23 \times 10^{-17}$ s³ rad⁻³ mol⁻¹ shown as the solid line in the inset of Fig. 4.9. Using Eq. 4.14, the corresponding ratio $C_{\text{ph}}/T^3 = 34 \mu\text{J mol}^{-1} \text{K}^{-4}$ can be calculated, indicated as the broken line in Fig. 4.8. However, this value is a factor of 3 larger than the long-wavelength acoustic contribution to the specific heat $C_D/T^3 = 8.93 \mu\text{J mol}^{-1} \text{K}^{-4}$. Such an incompatibility between the low frequency part of the GDVOS and low temperature values of $C_{\text{ph}}(T)$ was previously reported for icosahedral Al-Mn-Pd [57] (See Seq. 3.2.4) and could be related decreasing resolution of the time-of-flight technique for frequencies below 20 meV [57].

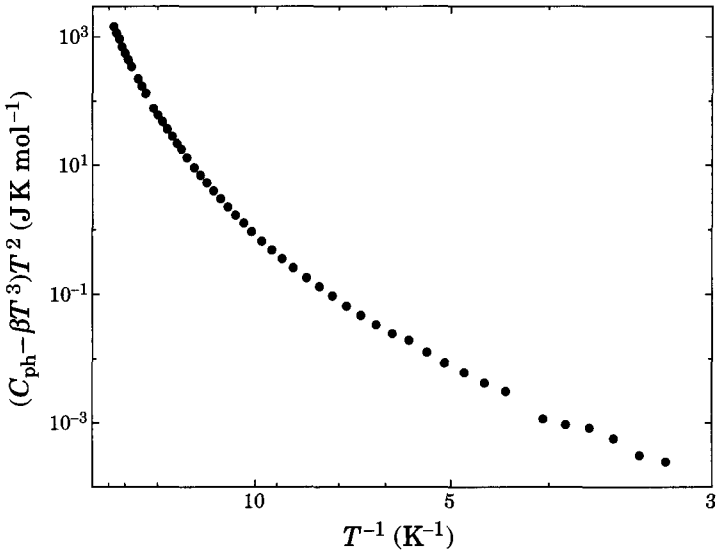


Figure 4.10: $(C_{\text{ph}} - \beta T^3)T^2$ vs. T^{-1} plotted on a semi-logarithmic scale.

The increase of $C_{\text{ph}}(T)$ with increasing temperature above the Debye limit may be related to either low lying optical modes or the dispersion of acoustical excitations. In decagonal $\text{Al}_{71}\text{Ni}_{16}\text{Co}_{13}$ the presence of an optical branch at the frequency $\omega = 1.9 \times 10^{13}$ rad/s may be inferred from the splitting of the $\omega(\mathbf{q})$ data for transverse excitations measured using inelastic neutron scattering along the $(1,1,-1,0)$ crystallographic direction [178]. Theoretical calculations of the vibrational DOS using the modified Burkov model [179] suggest the presence of an optical mode in the frequency range between 1.5×10^{13} and 2.4×10^{13} rad/s [176]. However, no optical mode in this frequency range was resolved in the generalized vibrational density of states (GDVOS) of quasicrystalline Al-Ni-Co as can be seen in Fig. 4.9 [176].

In Fig. 4.10 the difference between C_{ph} and βT^3 multiplied by T^2 is shown as function of the inverse temperature on a semi-logarithmic plot. The $(C_{\text{ph}} - \beta T^3)T^2$ data do not fall on a straight line indicating that a singular low-frequency optical branch can be ruled out as the origin of the observed $C_{\text{ph}} - \beta T^3$. This is because at temperatures $T \ll \hbar\omega_0/k_B$

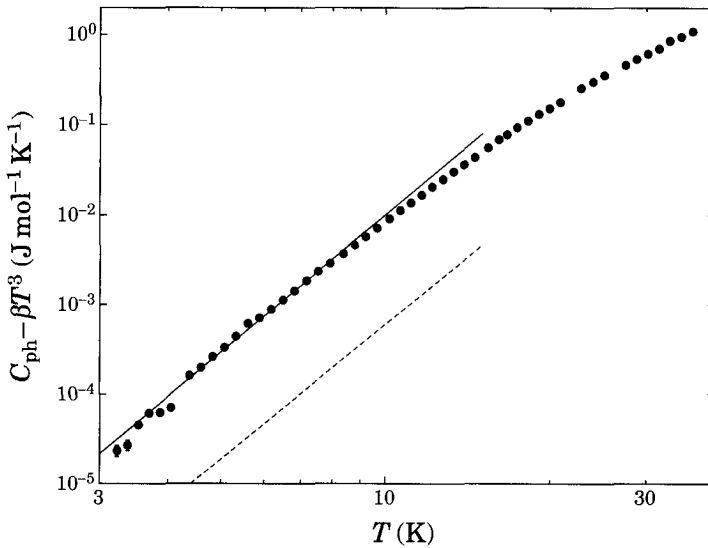


Figure 4.11: $C_{\text{ph}} - \beta T^3$ vs. T plotted on logarithmic scales. The solid line indicates a fit to a power law $C_{\text{ph}} - \beta T^3 \propto T^5$. The dashed line is an estimate of the T^5 contribution to $C_p(T)$ that is compatible with the experimentally determined values of the phonon dispersion relations $\omega(\mathbf{q})$ for decagonal Al-Ni-Co (see text).

a singular optical excitation with an energy $\hbar\omega_0$ is expected to contribute a term to the specific heat that increases exponentially with increasing temperature (Eq. 4.14). It should be noted that below 8 K $C_{\text{ph}} - \beta T^3$ displays rather a power-law behaviour, as can be seen on the double logarithmic plot of $C_{\text{ph}} - \beta T^3$ vs. T in Fig. 4.11. The solid line in Fig. 4.11 is compatible with $C_{\text{ph}} - \beta T^3 \propto T^n$ and $n = 5.1 \pm 0.1$. Approximating $C_{\text{ph}} - \beta T^3$ by δT^n with $n = 5$, a value of $\delta = 96 \pm 0.2 \text{ nJ mol}^{-1} \text{ K}^{-6}$ is obtained. A T^5 term in the lattice specific $C_{\text{ph}}(T)$ may have its origin in a ω^4 term in the vibrational density of states $g(\omega)$ indicating the dispersion of acoustic excitations.

Deviations of C_{ph} from a Debye-type behaviour due to phonon dispersion have been studied in the rocksalt-structure alkali halides [180, 181]. Theoretical calculations of the lattice dynamics and the specific heat in the rocksalt-structure alkali halide NaI with the “shell model” using experimentally determined values of the nearest-neighbours distances, compressibility and electric polarizability of the ions agreed satisfactorily with the

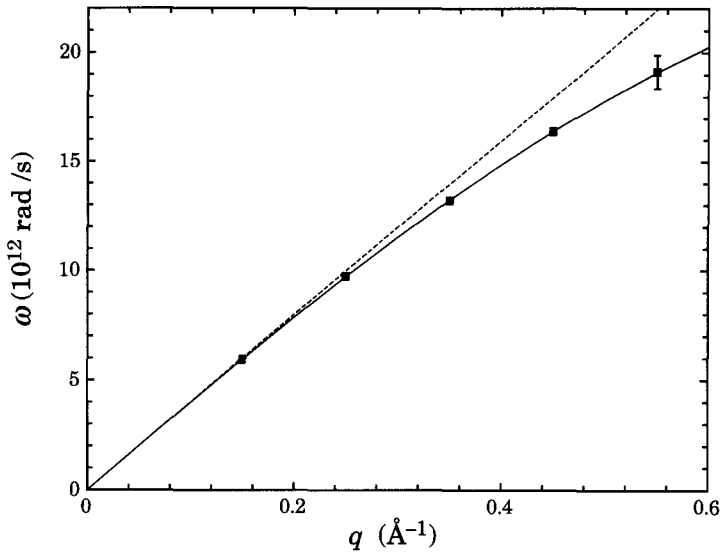


Figure 4.12: The squares show the phonon dispersion relation of the transverse acoustic excitations of decagonal Al-Ni-Co propagating parallel to the $(1,1,-1,0)$ crystallographic directions measured at 300 K [178] (see text). The solid line is a fit of the phonon dispersion to Eq. 4.15, and the dotted line is the resulting value of the sound velocity $v_l = 4060 \text{ m s}^{-1}$.

experimental results of the specific heat and of the phonon dispersion obtained in inelastic neutron scattering experiments [180]. In an other publication on the lattice dynamics in NaI and KBr the free parameters of similar model were fitted to the experimental results of elastic and dielectric constants and to the phonon dispersion relation along the symmetry directions [181]. Subsequently, the specific heat was calculated which was found to be in good agreement with the experimental results of C_{ph} in both systems [181]. The dispersion relation of acoustic excitations $\omega(q)$ can be expanded in a power series of the form

$$\omega_i(q) = v_i q + \alpha_i q^3 + O(q^5) \quad i = l, t_1, t_2 \quad (4.15)$$

direction	v_l (m/s)	α_l $\times 10^{-17}$ (m ³ /s)	v_t (m/s)	α_t $\times 10^{-17}$ (m ³ /s)
(0,0,0,0,2)	7490 ± 120	-5.8 ± 0.6	3990 ± 60	-1.7 ± 0.4
(1,1,-1,-1,0)	7900 ± 500	-8 ± 2	4060 ± 60	-1.3 ± 0.4

Table 4.1: Parameters of the fit of the phonon dispersion $\omega(\mathbf{q})$ -data of decagonal Al-Ni-Co in the range $|\mathbf{q}| < 0.55 \text{ \AA}$ using Eq. 4.15.

The phonon dispersion $\omega(\mathbf{q})$ in $\text{Al}_{71}\text{Ni}_{16}\text{Co}_{13}$ has been determined at 300 K by inelastic neutron scattering using a triple axis spectrometer [178]. Two transversal and two longitudinal modes were observed starting close to the Bragg peaks at (0,0,0,0,2) and (1,1,-1,-1,0) and propagating parallel to the (1,1,-1,-1,0) and (0,0,0,0,2), crystallographic directions, respectively [178]. The polarization vectors of these modes were lying in the plane defined by the (0,0,0,0,2) and (1,1,-1,-1,0) directions [178]. The parameters v_l and α_l of a fit of Eq. 4.15 to the $\omega(\mathbf{q})$ data in the wavevector range $|\mathbf{q}| < 0.55 \text{ \AA}$ are given in Table 4.1. We note, that the v_l determined from the fits to the $\omega(\mathbf{q})$ data are in good agreement with the sound velocities obtained from the measured low-temperature elastic stiffness constants c_{ij} [166]. The observed phonon dispersion was found to be isotropic within the experimental errors for $|\mathbf{q}| < 0.55 \text{ \AA}$. This is again in agreement with the results of the resonant ultrasound spectroscopy experiment [166] indicating that the variation of the sound velocities with the angle θ between the wave vector and the decagonal axis is 13 % at most. These experimental findings are quite in contrast to the results of a theoretical investigation of lattice excitations in decagonal Al-Mn, suggesting a strongly anisotropic dispersion for lattice excitations propagating in the quasiperiodic plane and along the periodic direction [182].

A crude estimate of $g_4(\omega)$ may be obtained assuming that the phonon dispersion in decagonal Al-Ni-Co is isotropic at low $|\mathbf{q}|$ and that the transverse acoustical branch is doubly degenerate. This assumption leads to the vibrational density of states $g_4(\omega)$ of the form

$$g_4(\omega) = -\frac{5}{2\pi^2} \left(\frac{\alpha_l}{v_l^6} + 2 \frac{\alpha_t}{v_t^6} \right) \omega^4. \quad (4.16)$$

Substituting this result into Eq. 4.14 gives

$$C_{\text{ex}}(T) = -\frac{40\pi^4 k_B^6}{21\hbar^5} \left(\frac{\alpha_l}{v_l^3} + 2 \frac{\alpha_t}{v_t^3} \right) T^5. \quad (4.17)$$

Using the values of v_l , v_t , α_l and α_t given in Table 4.1, leads to $C_{\text{ex}}/T^5 = 6 \text{ nJ mol}^{-1} \text{ K}^{-6}$. This value is 15 times smaller than the experimentally determined coefficient of the T^5 term to the specific heat $C_p(T)$. Thus the dispersion of acoustical excitations in decagonal Al-Ni-Co cannot account for the observed deviation from the Debye-type behaviour of the low-temperature lattice specific heat $C_{\text{ph}}(T)$. Given the small degree of polar elastic anisotropy in decagonal Al-Ni-Co as revealed by ultrasound resonant spectroscopy [166] and inelastic neutron scattering [178], it seems quite unlikely, that a stronger curvature of the phonon dispersion $\omega(\mathbf{q})$ along certain directions in the reciprocal space than that already measured is the cause of the observed deviation of $C_{\text{ph}}(T)$ from a Debye-type behaviour. But unless $\omega(\mathbf{q})$ has been measured along additional directions in reciprocal space this possibility cannot be ruled out completely. Another possible explanation of this discrepancy could be a distribution of non-propagating lattice excitations with a density $g(\omega) \propto \omega^4$, however unprecedented by a theoretical model.

4.3.3 Summary and Conclusion

Below 3 K, the specific heat of decagonal $\text{Al}_{71}\text{Ni}_{16}\text{Co}_{13}$ and $\text{Al}_{65}\text{Cu}_{20}\text{Co}_{15}$ can adequately be described as the sum of a linear- and a cubic-in- T term, i.e., assuming that $C_p(T)$ is due to electronic and lattice excitations. The coefficient γ of the linear term in the specific heat amounts to about one third of the γ -value of Aluminium indicating that the density of electronic states at E_F is reduced. The cubic-in- T term in $C_p(T)$ of $\text{Al}_{71}\text{Ni}_{16}\text{Co}_{13}$ agrees well with the contribution of the long wave length acoustic excitations calculated using low-temperature values of the elastic moduli c_{ij} obtained for this same sample [166]. We did not find any indications for an excess specific heat, contrary to what has previously been observed in icosahedral Al-Mn-Pd and Al-Re-Pd [57]. Above 3 K, the lattice specific heat $C_{\text{ph}} = C_p - \gamma T$ increases with increasing temperature more steeply than T^3 . The deviation $C_{\text{ph}} - \beta T^3$ between the experimentally determined lattice specific heat and the Debye-type expectations varies approximately as T^5 . A term in the lattice specific heat C_{ph} that varies as T^5 may originate from the dispersion of acoustic excitations. However,

the $\omega(\mathbf{q})$ data for decagonal Al-Ni-Co as determined from the results of inelastic neutron scattering experiments [178] cannot account for the magnitude of the T^5 -term in the specific heat.

5 Electrical conductivity of icosahedral Al-Re-Pd quasicrystals

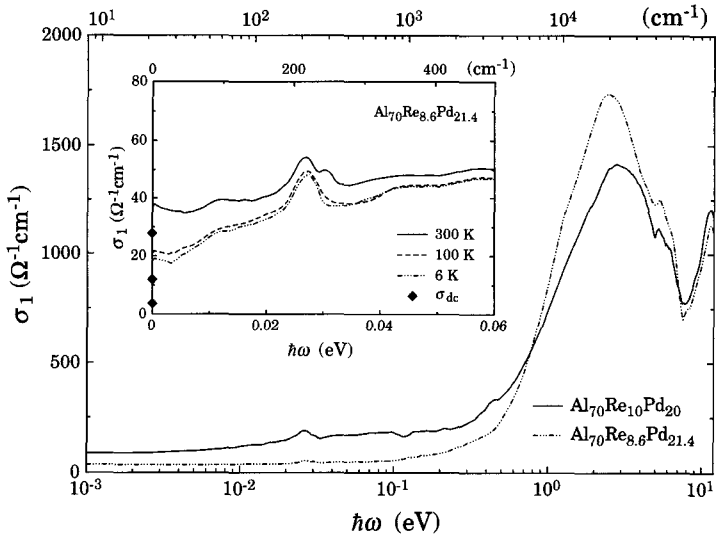


Figure 5.1: Room temperature optical conductivity $\sigma_1(\omega)$ of $\text{Al}_{70}\text{Re}_{10}\text{Pd}_{20}$ and $\text{Al}_{70}\text{Re}_{8.6}\text{Pd}_{21.4}$ for frequencies between 15 and 10^5cm^{-1} [147]. The inset displays $\sigma_1(\omega)$ in the FIR spectral range for $\text{Al}_{70}\text{Re}_{8.6}\text{Pd}_{21.4}$ at various temperatures [147].

Among thermodynamically stable quasicrystals, icosahedral Al-Re-Pd is a quasiperiodically structured material which often shows very low values of the electrical conductivity at low temperatures, comparable to those observed in heavily doped semiconductors [112, 113]. It seems possible to synthesize icosahedral Al-Re-Pd samples with different chemical composition and annealing procedures while maintaining about the same structural properties. The low-temperature values of the electrical conductivity of these alloys vary over three orders in magnitude [110, 111]. Therefore icosahedral quasicrystals in the Al-Re-Pd system may be considered as model substances for investigating electronic transport properties both at zero and non-zero frequency of quasi-periodically ordered solids with varying concentration of itinerant charge carriers. The optical conductivity $\sigma_1(\omega)$ of icosahedral $\text{Al}_{70}\text{Re}_{10}\text{Pd}_{20}$ and $\text{Al}_{70}\text{Re}_{8.6}\text{Pd}_{21.4}$ [147] is barely metallic. The most prominent feature in the charge dynamic spectrum is a large absorption in the visible spectral range, commonly associated with excitations across a pseudo gap in the density of electronic states as shown in Fig. 5.1. However, the change in composition from $\text{Al}_{70}\text{Re}_{10}\text{Pd}_{20}$ to $\text{Al}_{70}\text{Re}_{8.6}\text{Pd}_{21.4}$ does not lead to a sizable shift of the pseudogap absorption but to a redistribution of the total spectral weight between the effective “metallic”-like component at zero frequency and the non-zero frequency absorptions [147].

In Fig. 5.2 the electrical conductivity of both $\text{Al}_{70}\text{Re}_{10}\text{Pd}_{20}$ and $\text{Al}_{70}\text{Re}_{8.6}\text{Pd}_{21.4}$ measured in zero magnetic field H below room temperature is shown as a function of temperature. In both cases, the electrical conductivity σ first decreases with a constant slope $d\sigma/dT$ with decreasing temperature. The range of temperature for which $d\sigma/dT$ is approximately constant extends to 170 K for $\text{Al}_{70}\text{Re}_{10}\text{Pd}_{20}$ and 40 K for $\text{Al}_{70}\text{Re}_{8.6}\text{Pd}_{21.4}$ and the respective values are $0.2 \Omega^{-1}\text{cm}^{-1}\text{K}^{-1}$ and $0.09 \Omega^{-1}\text{cm}^{-1}\text{K}^{-1}$. The room temperature conductivities differ by a factor of 3 but the ratio of the limiting low temperature values of σ is approximately 18. In both cases, it is not a priori obvious what causes the enhanced reduction of σ at low temperatures. Distinctly different features of $\sigma(T)$ of the two alloys are also observed at very low temperatures and which will be presented and discussed separately in Sec. 5.1 and 5.2.

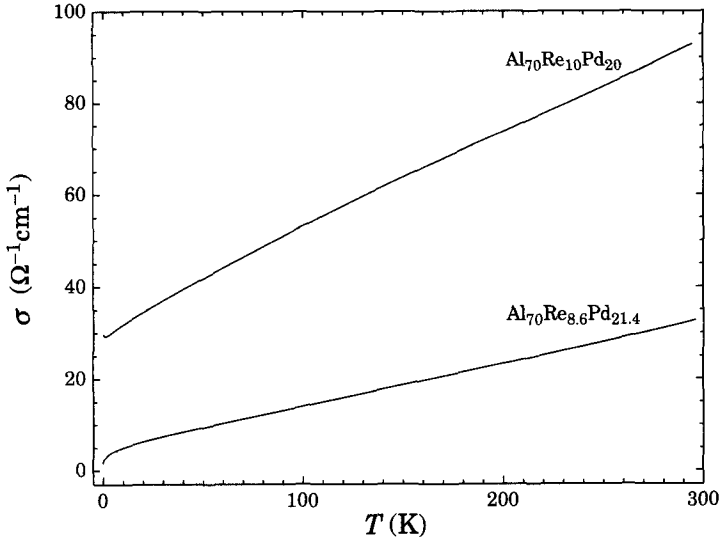


Figure 5.2: Electrical conductivity $\sigma(T)$ of $\text{Al}_{70}\text{Re}_{10}\text{Pd}_{20}$ and $\text{Al}_{70}\text{Re}_{8.6}\text{Pd}_{21.4}$ between 0.04 and 295 K.

5.1 $\text{Al}_{70}\text{Re}_{10}\text{Pd}_{20}$

In Fig. 5.3 a plot of σ vs. $T^{1/2}$ in different external magnetic fields for $\text{Al}_{70}\text{Re}_{10}\text{Pd}_{20}$ is shown. For $H = 0$ a minimum of $\sigma(T)$ is observed at approximately 1 K. Below 0.2 K, the electrical conductivity $\sigma(T, H = 0)$ varies as

$$\sigma(T) = \sigma_0 + aT^{\frac{1}{2}} \quad , \quad (5.1)$$

and an extrapolation of our $\sigma(T)$ data to $T = 0$, shown as the solid line in Fig. 5.3, yields the residual conductivity $\sigma_0 = 30 \text{ } \Omega^{-1}\text{cm}^{-1}$ and the slope $a = -1.02 \text{ } \Omega^{-1}\text{cm}^{-1}\text{K}^{-1/2}$. Upon application of an external magnetic field the negative slope of the $T^{1/2}$ variation at the lowest temperatures decreases in magnitude and changes sign at approximately 2 kOe (see inset). Below 0.2 K and in magnetic fields $H > 5$ kOe, the electrical conductivity $\sigma(T)$ varies still as $T^{1/2}$, but with a positive slope a . In this regime the observed magnetoconductivity $\Delta\sigma(H) = \sigma(H) - \sigma(0)$ is negative. In the inset of Fig. 5.3 the slope

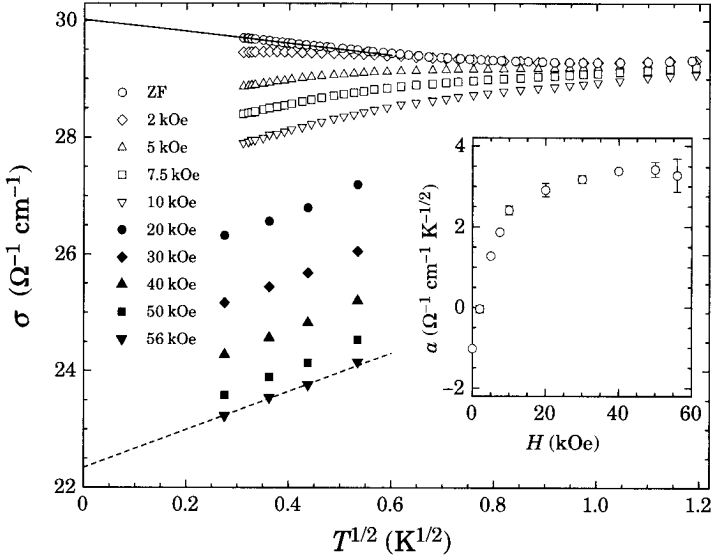


Figure 5.3: Electrical conductivity σ of icosahedral $\text{Al}_{70}\text{Re}_{10}\text{Pd}_{20}$ below 1 K in varying magnetic fields H plotted as a function of $T^{1/2}$. The lines represent the fits of Eq. 5.1 to the $\sigma(T)$ data between 0.1 and 0.2 K (see text). Inset: $d\sigma/d(T^{1/2})$ vs. H .

a resulting from the fits of Eq. 5.1 to the $\sigma(T)$ data taken in various magnetic fields H in the temperature range between 0.075 and 0.2 K, is plotted as a function of H . As mentioned above, a increases gradually with increasing H and changes sign at about 2 kOe. For magnetic fields exceeding 20 kOe, $a(H)$ tends to saturate, reaching a value of $3.27 \Omega^{-1} \text{ cm}^{-1} \text{ K}^{-1/2}$ at $H = 56$ kOe.

In the following these $\sigma(T, H)$ variations with respect to T and H are analyzed in terms of quantum-interference effects considering Coulomb interactions among itinerant electrons [183, 184]. It should be noted that quantum-interference contributions to the electrical conductivity should also include weak-localization terms [185]. The plots in Fig. 5.3 indicate that below 0.2 K $\sigma(T)$ is adequately described by Eq. 5.1, suggesting that the temperature dependence of σ is predominantly determined by a Coulomb-type interaction correction to the classical Boltzmann conductivity. Similar behavior of the

electrical conductivity at low temperatures has previously been observed for various icosahedral quasicrystals [69, 186–191].

In the case of a single isotropic band the Coulomb interaction corrections $\delta\sigma_I^{\text{ZF}}$ and $\delta\sigma_I^{\text{HF}}$ to the classical conductivity in zero magnetic field $H = 0$ and in the limit of high magnetic field $g\mu_B H \gg k_B T$, respectively, are [183]

$$\delta\sigma_I^{\text{ZF}}(T) = \frac{e^2}{4\pi^2\hbar} \frac{1.3}{\sqrt{2}} \left(\frac{4}{3} - \frac{3}{2}\tilde{F}_\sigma \right) \left(\frac{k_B T}{\hbar D} \right)^{\frac{1}{2}} \quad (5.2)$$

$$\delta\sigma_I^{\text{HF}}(T) = \frac{e^2}{4\pi^2\hbar} \frac{1.3}{\sqrt{2}} \left(\frac{4}{3} - \frac{1}{2}\tilde{F}_\sigma \right) \left(\frac{k_B T}{\hbar D} \right)^{\frac{1}{2}}. \quad (5.3)$$

Here \tilde{F}_σ is the Coulomb screening parameter and D is the electron diffusion constant [184]. Solving the system of Eqs. 5.2 and 5.3 for \tilde{F}_σ and D using the $d\sigma/d(T^{1/2})$ values obtained in the way described above yields $\tilde{F}_\sigma = 1.1$ and $D = 0.26 \text{ cm}^2 \text{ s}^{-1}$. It should be noted that \tilde{F}_σ values exceeding 0.92 are not really compatible with a first-order perturbation theory considering a single isotropic band [183], but values of \tilde{F}_σ exceeding 0.92 have previously been reported for heavily doped semiconductors [192, 193] and for icosahedral quasicrystals [188, 191]. In both cases a single isotropic band is not necessarily a good approximation. Also, the unusually high value of D for a material with $\sigma_0 = 30 \text{ } \Omega^{-1} \text{ cm}^{-1}$ is noteworthy, suggesting a very low density of electronic states at E_F [147].

In principle an independent evaluation of the electron diffusion constant D may be made using the Einstein relation for the electrical conductivity $\sigma_B = e^2 N(E_F) D$, where σ_B is the classical Boltzmann conductivity and $N(E_F)$ is the density of electronic states at the Fermi level. The latter quantity may be obtained from the coefficient γ_{el} of the electronic specific heat $\gamma_{\text{el}} T$. However, that the large residual conductivity ratio of Al₇₀Re_{8.6}Pd_{21.4} may lead to a considerable difference between the residual conductivity σ_0 and the Boltzmann conductivity σ_B at zero temperature and, consequently, to an uncertainty in the estimate of the electron diffusion constant D [147].

As discussed in Sec. 4.1, a reliable evaluation of $N(E_F)$ from the electronic contribution $\gamma_{\text{el}} T$ to the specific heat $C_p(T)$ Al-Re-Pd quasicrystals is obscured by the presence of tunneling states, which are also expected to contribute a linear term $\gamma_{\text{TS}} T$ to the

specific heat $C_p(T)$. Tunneling states in Al-Re-Pd are indicated by results of thermal-conductivity measurements [117, 194] indicated by the thermal conductivity results of Sec. 3.3. In metallic glasses the tunneling states contribution $\gamma_{TS}T$ is typically of the order of $50 T \mu\text{J mol}^{-1} \text{K}^{-1}$ [145]. This $\gamma_{TS}T$ value corresponds to approximately 1/3 of the linear contribution $\gamma T = 139 T \mu\text{J mol}^{-1} \text{K}^{-1}$ to $C_p(T)$ of this particular $\text{Al}_{70}\text{Re}_{10}\text{Pd}_{20}$ alloy [194]. Assuming that $\sigma_B = \sigma_0$ and that $\gamma_{\text{el}} = \frac{2}{3}\gamma$, yields $D = 0.071 \text{ cm}^2 \text{ s}^{-1}$, i.e., a factor of four smaller value than the D value obtained in the way described above. Inserting this value in Eq. 5.2 results in $\tilde{F}_\sigma = 0.98$ [147].

The Coulomb interaction corrections to the electrical conductivity, as given by Eqs. 5.2 and 5.3 have been obtained for the case of a single isotropic band. Burkov and co-workers [195–197] proposed a model for the band structure of quasicrystals based on the explicit assumption of nearly free electrons close to a Fermi surface. They have argued that for a Hume-Rothery-type electronic stabilization mechanism the interaction of the Bragg planes with the Fermi surface results in an almost complete collapse of the latter. Within this scenario, the only pieces of the Fermi surface to survive are pockets of electrons and holes determined by the ratio of the Fermi wave vector k_F and the reciprocal lattice vectors associated with the strongest structure factors. The generalization of Eq. 5.2 to a many-pocketed Fermi surface has previously been discussed in detail for heavily doped semiconductors [192, 193]. In the case of a Fermi surface that consists of n valleys identically oriented in reciprocal space and negligible intervalley scattering, the factor $3/2$ in front of \tilde{F}_σ in Eq. 5.2, which gives the zero-field correction to $\sigma(T)$ resulting from the interaction of a particle and a hole with total spin $j = 1$, needs to be replaced by $(2n - \frac{1}{2})$ [183]. For the case of strong intervalley scattering the quantum correction to the electrical conductivity $\sigma(T)$ is expected to have the same form as for a single isotropic band [183].

The anisotropy of a non-spherical Fermi surface is also expected to modify the quantum corrections, as it leads to anisotropic diffusion of electrons and holes. The electron-electron interaction effects result from particle diffusion, as a consequence they will possess the same anisotropy as the diffusion coefficient [183]. The spherical symmetry of the problem can be restored by deforming the frame associated with the main axes of the diffusion coefficient tensor ellipsoid. The diffusion coefficient D in Eqs. 5.2

and 5.3 has to be replaced by $D_a = (D_{\perp}^2 D_{\parallel})^{1/3}$. The correction to the electrical conductivity $\Delta\sigma$ should then be multiplied by the factor D_{ik}/D_a [183], where D_{ik} is the classical diffusion tensor. For example, the anisotropy of the magnetoconductivity between the periodic and the quasiperiodic direction in decagonal $\text{Al}_{65}\text{Cu}_{20}\text{Co}_{15}$ was analyzed in terms of weak-localization corrections that is consistent with an anisotropic diffusion tensor [198]. Experiments probing the variation of the magnetoconductivity $\Delta\sigma(H, x)$ with uniaxial strain x applied along a symmetry direction using single grain quasicrystals, as were done for Antimony doped Germanium [199], would be helpful to test the hypothesis of a many-pocketed Fermi surface.

5.2 $\text{Al}_{70}\text{Re}_{8.6}\text{Pd}_{21.4}$

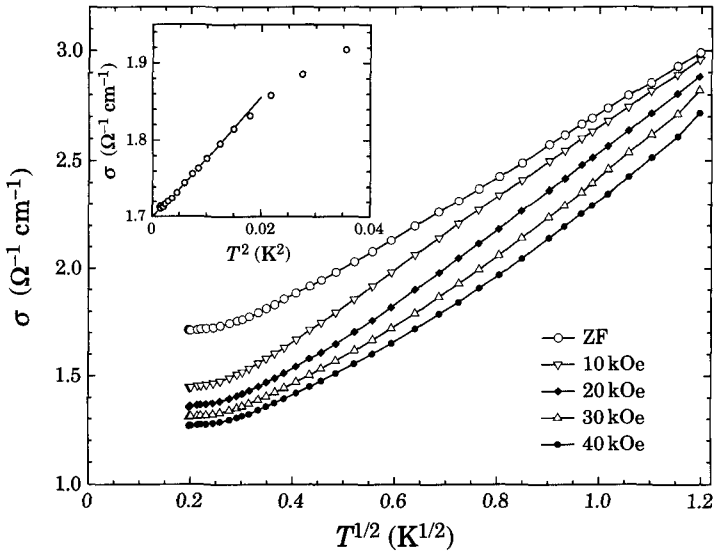


Figure 5.4: σ vs. $T^{1/2}$ of icosahedral $\text{Al}_{70}\text{Re}_{8.6}\text{Pd}_{21.4}$ below 1 K in varying magnetic fields H . The lines are to guide the eye. The inset shows the zero field conductivity σ plotted as a function of T^2 . The solid line is the fit to a power-law of Eq. 5.4.

In this section the temperature and the magnetic field dependencies of the electrical conductivity σ of $\text{Al}_{70}\text{Re}_{8.6}\text{Pd}_{21.4}$ are presented and compared with the results for

Al₇₀Re₁₀Pd₂₀ described above. The electrical conductivity $\sigma(T)$ of Al₇₀Re_{8.6}Pd_{21.4}, shown in Fig. 5.2, continues to decrease monotonically with decreasing temperature and below 0.1 K it saturates at the level of $\sigma_0 = 1.7 \Omega^{-1}\text{cm}^{-1}$. This type of $\sigma(T)$ behavior is distinctly different from that of Al₇₀Re₁₀Pd₂₀ (see Sec.5.1). In Fig. 5.4 the low-temperature electrical conductivity $\sigma(T)$ of Al₇₀Re₁₀Pd₂₀ is shown as a function of $T^{1/2}$ for $T < 1.5$ K and in applied magnetic fields up to 40 kOe. Between 0.04 and 1.5 K, the measured magnetoconductivity $\Delta\sigma = \sigma(H) - \sigma(0)$ is negative and fairly large. For $T = 0.04$ K and $H = 40$ kOe, e.g., $\Delta\sigma/\sigma = -0.3$, similar in magnitude as the analogous relative change of $\Delta\sigma/\sigma = -0.25$ for Al₇₀Re₁₀Pd₂₀. Below 0.1 K, $\sigma(T)$ approaches constant values for all applied magnetic fields up to 40 kOe, again in contrast to the $\sigma(T, H)$ behavior of Al₇₀Re₁₀Pd₂₀ described above. It should be noted that the trend towards saturation of $\sigma(T)$ of Al₇₀Re_{8.6}Pd_{21.4} at very low temperatures unambiguously implies a *metallic* ground state. On the other hand, the observed magnetic field and temperature dependent features of σ of this material cannot be described using the above mentioned calculations [184] considering quantum-interference effects including Coulomb interaction. A closer inspection of electrical conductivity data of Al₇₀Re_{8.6}Pd_{21.4} below 0.1 K reveals that for these temperature $\sigma(T)$ varies approximately as T^2 , as can be seen in the inset of Fig. 5.4, instead of a $T^{1/2}$ variation as observed in the case of Al₇₀Re₁₀Pd₂₀. Such an increase of the exponent of the power-law variation of $\sigma(T)$ has previously been observed for phosphorus doped silicon Si:P in the vicinity of the metal non-metal transition [193] and was also noted in cobalt doped FeSi [200].

In Si:P on the metallic side of the transition the electrical conductivity can be well described by a power-law

$$\sigma(T) = \sigma_0 + mT^\alpha \quad , \quad (5.4)$$

for temperatures below 0.1 K [193]. For Si:P samples with a ratio of the residual conductivity σ_0 and the minimum metallic conductivity σ_{\min} which is larger than $\sigma_0/\sigma_{\min} > 1$ the exponent is of the order of $\alpha \sim 0.5$. However, for $\sigma_0/\sigma_{\min} < 1$ an increase of the exponent to $\alpha \sim 2$ occurs, as can be seen in Fig 5.5 [193]. The minimum metallic conductivity σ_{\min} is defined as

$$\sigma_{\min} = C_3 \frac{e^2}{h l_{\min}} \approx 30 - 61 \Omega^{-1} \text{cm}^{-1} \quad , \quad (5.5)$$

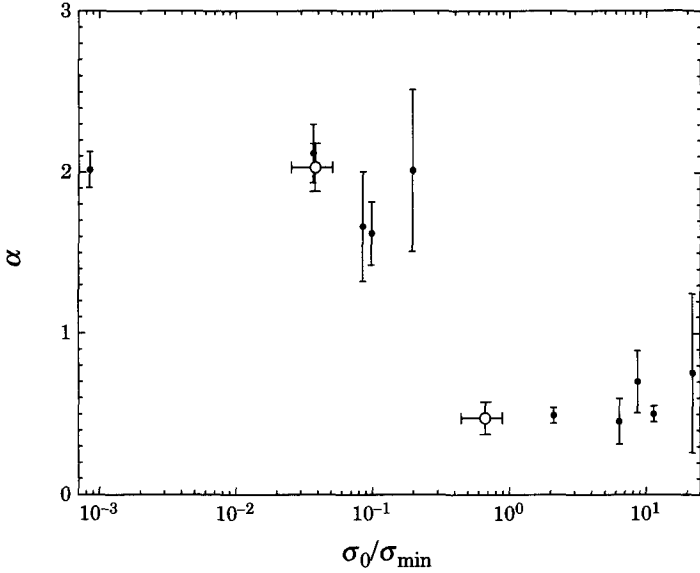


Figure 5.5: The open circles depict the power law exponent α vs. σ_0/σ_{\min} of icosahedral Al-Re-Pd. Here $\sigma_{\min} = 45 \Omega^{-1} \text{cm}^{-1}$ and $C_3 = 0.035$ were used for icosahedral Al-Re-Pd. In phosphorus-doped silicon Si:P on the metallic side of the metal non-metal transition α increases from approximately 0.5 to 2 around $\sigma_0/\sigma_{\min} \sim 1$ when the transition is approached (full circles) [193].

where l_{\min} is the shortest possible mean free path [201]. In the Anderson model of the metal non-metal transition with a half filled band, l_{\min} coincides with the lattice constant, while for the Mott transition in a doped uncompensated semiconductor, l_{\min} represents the mean separation between impurities [201], and C_3 lies in the range between 0.025 and 0.05 [202]. In icosahedral quasicrystals, the characteristic size of the structural motif, i.e. the diameter of an icosahedral cluster which is of the order of 20 \AA [203], may be considered as the natural choice for l_{\min} in the calculation of σ_{\min} . In Fig. 5.4, the power-law exponent obtained from a fit of Eq. 5.4 to the $\sigma(T)$ data of $\text{Al}_{70}\text{Re}_{10}\text{Pd}_{20}$ and $\text{Al}_{70}\text{Re}_{8.6}\text{Pd}_{21.4}$ is shown on the same graph together with the values obtained in Si:P [193]. The observed increase of α is an indication that the $\text{Al}_{70}\text{Re}_{8.6}\text{Pd}_{21.4}$ alloy is in the proximity of a metal non-metal transition, but nonetheless on the metallic side.

A metallic ground state of icosahedral Al-Re-Pd was also claimed in Ref. 204, in which the electrical conductivity of a series of $\text{Al}_{70.5}\text{Re}_{8.5}\text{Pd}_{21}$ alloys which were subject to different annealing procedures was measured. All samples in this study showed a trend to saturation of $\sigma(T)$ at a non-zero value between 0.05 and 0.3 K; even for the sample with a value of the residual conductivity σ_0 of $0.5 \Omega^{-1} \text{cm}^{-1}$, thus in agreement with the results presented here. The results presented in this work and those of Ref. 204 are very much in contrast with the claim of the occurrence of a metal to non-metal transition in manganese doped icosahedral Al-Re-Pd [205]. In Ref. 205, after the subtraction of an unspecified residual conductivity σ_0 , the electrical conductivity data of $\text{Al}_{70.5}\text{Re}_{8.5-x}\text{Mn}_x\text{Pd}_{21}$ in the temperature range between 0.45 and 10 K was claimed to show a temperature variation characteristic of Mott variable range hopping. However, the $\sigma(T)$ data of $\text{Al}_{70.5}\text{Re}_{8.5}\text{Pd}_{21}$ and $\text{Al}_{70.5}\text{Re}_{6.5}\text{Mn}_2\text{Pd}_{21}$ show an almost linear temperature dependence between 0.4 and 1 K; the lowest temperatures reached in the experiment of Ref. 205.

5.2.1 Summary

It should be noted that the electrical transport in low-conductivity icosahedral quasicrystals reveals distinct temperature dependencies in different ranges of temperature. The linear T variation of σ at higher temperatures is compatible with a scattering rate $\tau^{-1} \sim T^{-1}$, a rather unusual temperature dependence considering the magnitude of the electrical conductivity. The $T^{1/2}$ variations of the low-temperature electrical conductivity of icosahedral $\text{Al}_{70}\text{Re}_{10}\text{Pd}_{20}$ in zero and non-zero magnetic field implies that quantum-interference effects invoking the Coulomb interaction among itinerant electrons still occur at this level of conductivity in icosahedral quasicrystals. Because of the unknown details of the electronic structure of these quasicrystals the prefactors of the $T^{1/2}$ variation of σ may not be those given in Eq. 5.2 and 5.3. Nevertheless, the most simple analysis confirms that the density of electronic states at the Fermi energy is very low in these materials. The electrical conductivity $\sigma(T)$ of icosahedral $\text{Al}_{70}\text{Re}_{8.6}\text{Pd}_{21.4}$ saturates below 0.1 K in all applied magnetic fields up to 40 kOe, suggesting that for this material a different approach for describing the electronic transport at the lowest temperatures needs to be considered. Nevertheless, the relative reduction of $\sigma(T \rightarrow 0)$ by application of an external magnetic field is similar in magnitude in both cases. The comparison of our $\sigma(T, H)$ results for icosahedral $\text{Al}_{70}\text{Re}_{10}\text{Pd}_{20}$ and $\text{Al}_{70}\text{Re}_{8.6}\text{Pd}_{21.4}$ indicates that the breakdown of the

quantum-interference-type behavior in Al-Re-Pd quasicrystals occurs within the *metallic regime* of conductance, at a residual conductivity value in the range between 1.7 and $30 \Omega^{-1}\text{cm}^{-1}$.

Leer - Vide - Empty

6 Summary and Conclusions

In this work, low-temperature thermal conductivity $\lambda(T)$, specific heat $C_p(T)$ and magnetoconductivity $\sigma(T, H)$ data on quasicrystals are presented for decagonal and icosahedral phases.

Eigenstates in quasicrystals are not localized in momentum space and therefore always affected by an intrinsic decay rate of the structure [45] and this decay rate varies exponentially with the strength of the quasiperiodic potential [48]. However, for the case of phonons in the long wave length limit it is possible that a phonon scattering mechanism different from the intrinsic decay, like phonon-phonon scattering due to the lattice anharmonicity, may overcome the intrinsic decay rate and become the leading mechanism in limiting the phonon lifetime [40, 43]. In inelastic neutron scattering experiments, well defined phonon modes showing a linear dispersion relation have been observed, providing experimental evidence for this assumption. The particular structural properties of quasicrystals are thus expected to influence the transport and thermal properties related to propagating lattice excitations, for which thermal conductivity and specific heat measurements are powerful spectroscopic tools.

The thermal conductivity of a polygrained samples of icosahedral $\text{Al}_{70}\text{Mn}_9\text{Pd}_{21}$ and $\text{Al}_{70}\text{Re}_{8.6}\text{Pd}_{21.4}$ and a single grained sample of $\text{Al}_{70.5}\text{Mn}_{8.5}\text{Pd}_{21}$ was measured over varying temperatures between 0.065 and 320 K. The low electrical conductivity of icosahedral quasicrystals allows a precise determination of the lattice contribution $\lambda_{\text{ph}}(T)$ to the thermal conductivity, as $\lambda \gg \lambda_{\text{el}}$ over the the whole temperature range covered in these experiments. The lattice contribution to the thermal conductivity $\lambda_{\text{ph}}(T)$ in icosahedral Al-Mn-Pd and Al-Re-Pd, which are quasiperiodic in three dimensions, is characterized

at the lowest temperatures by a crossover between scattering of phonons on tunneling states and a regime where λ_{ph} is limited by a temperature independent mean free path. The λ_{ph} -data of $\text{Al}_{70}\text{Mn}_9\text{Pd}_{21}$ indicates that the Casimir regime [73] in which the thermal conductivity is dominantly limited by scattering on the boundary could be attained in high quality single grain icosahedral quasicrystals.

The presence of tunneling states in icosahedral quasicrystals is indicated by the approximate T^2 -variation of $\lambda_{\text{ph}}(T)$ in icosahedral Al-Mn-Pd and Al-Re-Pd and also by the logarithmic variation of the sound velocity of shear waves with temperature and the non-linear attenuation of shear waves [166]. In contrast to glasses, where the coefficient $\bar{P}\gamma^2/\rho\bar{v}$ of the density of tunneling states \bar{P} and the coupling to the phonons γ^2 as deduced from a fit of tunneling state contribution to the phonon thermal resistance is almost the same for a number of different metallic and insulating glasses [98], $\bar{P}\gamma^2$ shows a remarkable sample dependence in icosahedral quasicrystals, suggesting that tunneling states are most probably not intrinsic to quasicrystals. In the specific heat $C_p(T)$ of icosahedral quasicrystals an additional linear contribution $\gamma_{\text{TS}}T$ from the tunneling states beside the usual electronic contribution $\gamma_{\text{el}}T$ is expected [74, 75].

The most remarkable feature in the thermal conductivity of icosahedral Al-Mn-Pd is the observation of a shallow maximum at 20 K. This behaviour is reminiscent of that of periodic crystals, where $\lambda_{\text{ph}}(T)$ at intermediate temperatures (10–30 K) is characterized by a crossover from the regime of boundary-limited or phonon-electron scattering and to the regime of increasing Umklapp phonon scattering [65, 67]. Above the maximum, $\lambda_{\text{ph}}(T)$ of the single grained sample of icosahedral Al-Mn-Pd decreases with increasing temperature up to 85 K, implying a frequency and temperature dependent phonon mean free path. In periodic crystals this decrease of the phonon mean free path is ascribed to an increasing number of high frequency phonons available for Umklapp scattering [65]. In quasicrystals the momentum of vibrational excitations can be transferred to the quasilattice in inelastic scattering events by arbitrarily small portions, i.e., not limited in magnitude from below, thus leading to a power-law dependence of the phonon scattering rate [40], instead of an exponential dependence observed in periodic crystals [65]. With an increasing density of tunneling states, the maximum in the $\lambda_{\text{ph}}(T)$ -curve becomes less prominent and is shifted to higher temperatures, or can be even reduced to a plateau, very much as what is observed in the polygrained samples of icosahedral $\text{Al}_{70}\text{Mn}_9\text{Pd}_{21}$ and $\text{Al}_{70}\text{Re}_{8,6}\text{Pd}_{21,4}$.

Above 100 K, the value of $\lambda_{\text{ph}}(T)$ of icosahedral Al-Mn-Pd is close to the prediction of Einstein's model [105, 106], suggesting that the lattice vibrations in the THz frequency range are predominantly localized, and the energy transfer between them occurs via a strong coupling mechanism.

The overall temperature dependence of λ_{ph} of icosahedral Al-Mn-Pd can be fairly well reproduced by a kinetic model. In this model a frequency and temperatures dependent mean free path is used which accounts for all the different scattering mechanisms employing the phonon equivalent of Matthiessen's rule and a model density of vibrational states which is compatible with the measured specific heat $C_p(T)$ of icosahedral Al-Mn-Pd [57].

Decagonal quasicrystals share the structural properties of periodic crystals and quasicrystals, as they are periodic along the tenfold axis and quasiperiodic in the plane perpendicular to it. Investigations of the thermal conductivity $\lambda(T)$ of single grained $\text{Al}_{65}\text{Cu}_{20}\text{Co}_{15}$ and $\text{Al}_{71}\text{Ni}_{16}\text{Co}_{13}$ along the periodic direction and along a direction in the quasiperiodic plane between 0.65 and 110 K, revealed a very similar temperature characteristic in both the systems. The calculated electronic contribution $\lambda_{\text{e}}^{\text{p}}(T)$ to the thermal conductivity along the periodic direction is close to $\lambda^{\text{p}}(T)$ below 0.8 and above 80 K, suggesting that the Wiedemann Franz law is approximately valid and that the phonon contribution $\lambda_{\text{ph}}^{\text{p}}(T)$ can be determined fairly reliable. The electrical conductivity measured along a direction in the quasiperiodic plane is an order of magnitude smaller than along the periodic direction, thus allowing for an accurate determination the lattice contribution $\lambda_{\text{ph}}^{\text{q}}(T)$. The phonon thermal conductivity $\lambda_{\text{ph}}^{\text{q}}(T)$ along a direction in the quasiperiodic plane is distinctly different from that along the periodic direction $\lambda_{\text{ph}}^{\text{p}}(T)$. In the quasiperiodic plane, $\lambda_{\text{ph}}^{\text{q}}(T)$ changes only little with temperature above 30 K, as observed for icosahedral quasicrystals and in agreement with expectations for Umklapp scattering in quasicrystals. Along the periodic direction the phonon thermal conductivity displays a distinct maximum at approximately 25 K, characteristic for lattice thermal transport in periodic crystals. The transport of heat via lattice excitations along the decagonal axis and along a direction in the quasiperiodic plane thus resemble closely that of icosahedral quasicrystals and periodic crystals, respectively.

The specific heat of icosahedral $\text{Al}_{70}\text{Re}_{8.6}\text{Pd}_{21.4}$ was measured between 0.065 and 19 K. At the lowest temperatures, $C_p(T)$ of icosahedral $\text{Al}_{70}\text{Re}_{8.6}\text{Pd}_{21.4}$ is dominated by

a large nuclear hyperfine contribution $C_N \propto T^{-2}$ due to the interaction of the quadrupole moments of the ^{185}Re and ^{187}Re nuclei with the gradient q of electric fields induced by their neighbours. The \bar{q} -value found in icosahedral Al-Re-Pd is comparable to the q -values of the ^{185}Re and ^{187}Re nuclei, respectively, in a hexagonal lattice of rhenium metal, indicating that most of the Rhenium atoms must occupy sites with a non-icosahedral local symmetry. The small linear contribution γT to the specific heat implies a low density of electronic states at E_F . A comparison with glasses suggests that excitations of tunneling states may account for approximately 1/2 of the coefficient of the linear term to the specific heat. This low density of electronic states is thought to be the consequence of a Hume-Rothery-type electronic stabilization mechanism of quasicrystals [158]. Independent evidence for a pseudogap in the electronic DOS of icosahedral Al-Re-Pd is obtained from optical conductivity spectra [147], tunneling experiments [155] and spin-lattice relaxation time measurements by nuclear magnetic resonance [151]. The experimentally determined cubic-in- T term in the specific heat is distinctly higher than expected contribution from acoustic phonons, indicating a large excess specific heat C_{ex} [57].

Measurements of the specific heat in decagonal $\text{Al}_{71}\text{Ni}_{16}\text{Co}_{13}$ and $\text{Al}_{65}\text{Cu}_{20}\text{Co}_{15}$ were carried out between 1.5 and 36 K. Below 3 K, the specific heat in both systems can adequately be described as the sum of a linear- and a cubic-in- T term, i.e., assuming that $C_p(T)$ is due to electronic and lattice excitations. The coefficient γ of the linear term in the specific heat amounts to about one third of the γ -value of Aluminium indicating that the density of electronic states at E_F is reduced, consistent with the presence of pseudogap in the electronic DOS. The cubic-in- T contribution to the specific heat of decagonal $\text{Al}_{71}\text{Ni}_{16}\text{Co}_{13}$ is in good agreement with the Debye contribution calculated from the low temperature values of the sound velocity [166]. This finding is in contrast to the results in icosahedral Al-Mn-Pd and Al-Re-Pd, where an excess cubic-in- T contribution to $C_p(T)$ is found [57]. Above 3 K, the lattice specific heat $C_{\text{ph}} = C_p - \gamma T$ increases rapidly with increasing T and this additional contribution varies approximately as T^5 . While such variation may be ascribed to the dispersion of acoustic excitations, the magnitude of the T^5 term to $C_{\text{ph}}(T)$ is a few times larger than the calculated value that follows from measured phonon dispersion curves of decagonal Al-Ni-Co [178].

Magnetoconductivity measurements $\sigma(T, H)$ of icosahedral $\text{Al}_{70}\text{Re}_{10}\text{Pd}_{20}$ and $\text{Al}_{70}\text{Re}_{8.6}\text{Pd}_{21.4}$ covered the temperature range between 0.04 and 295 K and in magnetic fields up to 56 kOe. At high temperatures, the electrical conductivity of both $\text{Al}_{70}\text{Re}_{10}\text{Pd}_{20}$

and $\text{Al}_{70}\text{Re}_{8.6}\text{Pd}_{21.4}$ quasicrystals decreases linear with temperature. However, below 10 K distinctly different temperature characteristics of $\sigma(T)$ are observed for $\text{Al}_{70}\text{Re}_{10}\text{Pd}_{20}$ and $\text{Al}_{70}\text{Re}_{8.6}\text{Pd}_{21.4}$, with zero temperature conductivity values of 30 and $1.7 \Omega^{-1}\text{cm}^{-1}$, respectively. At the lowest temperatures, the electrical conductivity of $\text{Al}_{70}\text{Re}_{10}\text{Pd}_{20}$ in zero and non-zero magnetic field varies as $T^{1/2}$ implying that quantum-interference effects invoking the Coulomb interaction among itinerant electrons still occur at this level of conductivity in icosahedral quasicrystals. Because of the unknown details of the electronic structure of these quasicrystals [195] the prefactors of the $T^{1/2}$ variation of σ may differ theoretical values expected for a single spherical band [183]. The electrical conductivity $\sigma(T)$ of icosahedral $\text{Al}_{70}\text{Re}_{8.6}\text{Pd}_{21.4}$ saturates below 0.1 K in all applied magnetic fields up to 40 kOe. Below 0.1 K, $\sigma(T)$ of $\text{Al}_{70}\text{Re}_{8.6}\text{Pd}_{21.4}$ varies approximately as T^2 . Such an increase of the exponent of the power-law variation of $\sigma(T)$ has previously been observed for phosphorus doped silicon Si:P in the vicinity of the metal non-metal transition on the metallic side [193]. The low values of the electrical conductivity observed in icosahedral Al-Re-Pd can only be partially be attributed to the low electronic DOS at E_F . Both $\text{Al}_{70}\text{Re}_{10}\text{Pd}_{20}$ and $\text{Al}_{70}\text{Re}_{8.6}\text{Pd}_{21.4}$ show the same spin-lattice relaxation rates within the experimental resolution above 1.5 K, suggesting a similar energy dependence of the electronic DOS in the vicinity of E_F [151, 154]. Optical conductivity spectra taken on both materials are dominated by a large absorption in the visible spectral range centered at 2.6 – 2.9 eV [147]. The comparison between the optical conductivity of $\text{Al}_{70}\text{Re}_{10}\text{Pd}_{20}$ and $\text{Al}_{70}\text{Re}_{8.6}\text{Pd}_{21.4}$ indicates a redistribution of the spectral weight from the effective “metallic”-like component to the non-zero frequency absorptions [147].

Leer - Vide - Empty

Bibliography

- [1] D. Shechtman, I. Blech, D. Gratias, and J. W. Cahn, *Phys. Rev. Lett.* **53**, 1951 (1984).
- [2] P. M. de Wolff, *Acta Crystallogr. A* **30**, 777 (1974).
- [3] A. Janner and T. Janssen, *Phys. Rev. B* **33**, 2814 (1977).
- [4] P. A. Bancel, P. Heiney, P. W. Stephens, A. I. Goldman, and P. M. Horn, *Phys. Rev. Lett.* **54**, 2422 (1985).
- [5] V. Elser, *Phys. Rev. B* **32**, 4892 (1985).
- [6] P. A. Kalugin, A. Y. Kitaev, and L. S. Levitov, *Sov. Phys. JETP* **41**, 145 (1985).
- [7] P. Kramer and R. Neri, *Acta Crystallogr. A* **40**, 580 (1984).
- [8] M. Duneau and A. Katz, *Phys. Rev. Lett.* **54**, 2688 (1985).
- [9] P. Bak, *Phys. Rev. Lett.* **54**, 1517 (1985).
- [10] P. Bak, *Phys. Rev. B* **32**, 5764 (1985).
- [11] T. C. Lubensky, S. Ramaswamy, and J. Toner, *Phys. Rev. B* **1985**, 7444 (1985).
- [12] M. D. Ball and D. J. Lloyd, *Scripta Metall.* **19**, 1065 (1985).
- [13] F. Dénoyer, G. Heger, M. Lambert, J. M. Lang, and P. Sainfort, *J. Phys. (France)* **48**, 1357 (1987).
- [14] A. P. Tsai, A. Inoue, and T. Masumoto, *Jpn. J. Appl. Phys.* **26**, L1505 (1987).
- [15] A. P. Tsai, A. Inoue, and T. Masumoto, *Jpn. J. Appl. Phys.* **27**, L1587 (1987).
- [16] S. W. Kycia, A. I. Goldman, T. A. Lograsso, D. W. Delaney, D. Black, M. Sutton, E. Dufresne, R. Brüning, and B. Rodricks, *Phys. Rev. B* **48**, 3544 (1993).

- [17] A. P. Tsai, A. Inoue, Y. Yokoyama, and T. Masumoto, *JIM* **31**, 98 (1990).
- [18] A. P. Tsai, A. Inoue, Y. Yokoyama, and T. Masumoto, *Phil. Mag. Lett.* **61**, 9 (1990).
- [19] A. P. Tsai, A. Inoue, Y. Yokoyama, and T. Masumoto, *Phil. Mag. Lett.* **62**, 95 (1990).
- [20] C. Beeli, H.-U. Nissen, and J. Robadey, *Phil. Mag. Lett.* **63**, 85 (1991).
- [21] C. Beeli, Ph.D. thesis, ETH, Zürich, 1992.
- [22] M. Boudard, M. de Boissieu, C. Janot, J. M. Dubois, and C. Dong, *Phil. Mag. Lett.* **64**, 197 (1991).
- [23] M. Boudard, M. de Boissieu, C. Janot, G. Heger, C. Beeli, H.-U. Nissen, H. Vincent, R. Ibberson, M. Audier, and J. M. Dubois, *J. Phys.: Condens. Matter* **4**, 10149 (1992).
- [24] M. de Boissieu, P. Stephens, M. Boudard, C. Janot, D. L. Chapman, and M. Audier, *Phys. Rev. Lett.* **72**, 3538 (1994).
- [25] Z. Luo, S. Zhang, Y. Tang, and D. Zhao, *Scripta Metall.* **28**, 1513 (1993).
- [26] A. P. Tsai, A. Niikura, A. Inoue, and T. Masumoto, *Phil. Mag. Lett.* **70**, 169 (1994).
- [27] I. R. Fisher, K. O. Cheon, A. F. Panchula, K. Dennis, and P. C. Canfield (unpublished).
- [28] Z. Islam, I. R. Fisher, J. Zarestky, P. C. Canfield, C. Stassis, and A. I. Goldman, *Phys. Rev. B* **57**, 11047 (1998).
- [29] T. Ishimasa, H.-U. Nissen, and Y. Fukano, *Phys. Rev. Lett.* **55**, 511 (1985).
- [30] L. Bendersky, *Phys. Rev. Lett.* **55**, 1461 (1985).
- [31] N. Wang, N. Chen, and K. H. Kuo, *Phys. Rev. Lett.* **59**, 1010 (1987).
- [32] M. Saito, M. Tanaka, A. P. Tsai, A. Inoue, and T. Matsumoto, *Jap. J. Appl. Phys.* **31**, L109 (1992).
- [33] L. X. He, Y. K. Wu, and K. H. Kuo, *J. Mater. Sci. Lett.* **7**, 1284 (1987).
- [34] A. P. Tsai, A. Inoue, and T. Masumoto, *JIM* **30**, 463 (1989).
- [35] M. A. Chernikov, A. Bernasconi, C. Beeli, A. Schilling, and H. R. Ott, *Phys. Rev. B* **48**, 3058 (1993).
- [36] S. Ritsch, Ph.D. thesis, ETH, Zürich, 1996.
- [37] O. Marti, Master's thesis, ETH, Zürich, 1982.

- [38] H. F. Rudigier, Ph.D. thesis, ETH, Zürich, 1984.
- [39] A. Bernasconi, Ph.D. thesis, ETH, Zürich, 1991.
- [40] P. A. Kalugin, M. A. Chernikov, A. Bianchi, and H. R. Ott, *Phys. Rev. B* **53**, 14145 (1996).
- [41] J. M. Luck and D. Petritis, *J. Stat. Phys.* **42**, 289 (1986).
- [42] J. P. Lu, T. Odagaki, and J. L. Birman, *Phys. Rev. B* **33**, 4809 (1986).
- [43] S. E. Burkov, B. E. C. Koltenbah, and L. W. Bruch, *Phys. Rev. B* **53**, 14179 (1996).
- [44] M. Kohmoto, L. P. Kadanoff, and C. Tang, *Phys. Rev. Lett.* **50**, 1870 (1983).
- [45] P. A. Kalugin, A. Y. Kitaev, and L. S. Levitov, *Sov. Phys. JETP* **64**, 410 (1986).
- [46] J. P. Lu and J. L. Birman, *Phys. Rev. B* **36**, 4471 (1987).
- [47] B. Sutherland and M. Kohmoto, *Phys. Rev. B* **36**, 5877 (1987).
- [48] A. Y. Kitaev, *JETP Lett.* **48**, 298 (1988).
- [49] J. Hafner and M. Kražčí, *J. Phys.: Condens. Matter* **5**, 2489 (1993).
- [50] M. Windisch, J. Hafner, M. Kražčí, and M. Mihalkovič, *Phys. Rev. B* **49**, 8701 (1994).
- [51] G. Poussiguet, C. Benoit, M. de Boissieu, and R. Currat, *J. Phys.: Condens. Matter* **6**, 659 (1994).
- [52] J. Los, T. Janssen, and F. Gähler, *J. Phys. I (Paris)* **3**, 1431 (1993).
- [53] M. Quilichini and T. Janssen, *Rev. Mod. Phys.* **69**, 277 (1997).
- [54] M. Quilichini, G. Heger, B. Hennion, S. Lefebvre, and A. Quivy, *J. Phys. France* **51**, 1785 (1990).
- [55] A. I. Goldman, C. Stassis, M. de Boissieu, R. Currat, C. Janot, R. Bellissent, H. Moudden, and F. W. Gayle, *Phys. Rev. B* **45**, 10280 (1992).
- [56] M. de Boissieu, M. Boudard, R. Bellissent, M. Quilichini, B. Hennion, R. Currat, A. I. Goldman, and C. Janot, *J. Phys.: Cond. Matter* **5**, 4945 (1993).
- [57] Ch. Wälti, E. Felder, M. A. Chernikov, H. R. Ott, M. de Boissieu, and C. Janot, *Phys. Rev. B* **57**, 10504 (1997).
- [58] Y. Amazit, M. de Boissieu, and A. Zarembowitch, *Europhys. Lett.* **20**, 703 (1992).
- [59] F. W. Gayle, *J. Mater. Res.* **2**, 1 (1987).

- [60] M. Boudard, M. de Boissieu, A. I. Goldman, B. Hennion, R. Bellissent, M. Quilichini, R. Currat, and C. Janot, *Physica Scripta* **T57**, 84 (1995).
- [61] H. Patel and D. Sherrington, *Phys. Rev. B* **40**, 11185 (1989).
- [62] C. Benoit, G. Poussige, and A. Azougarh, *J. Phys.: Condens. Matter* **2**, 2519 (1990).
- [63] M. Boudard, M. de Boissieu, S. Kycia, A. I. Goldman, B. Hennion, R. Bellissent, M. Quilichini, R. Currat, and C. Janot, *J. Phys.: Condens. Matter* **7**, 7299 (1995).
- [64] J.-B. Suck, *J. Non-Cryst. Solids* **153&154**, 573 (1993).
- [65] R. Peierls, *Ann. Physik* **3**, 1055 (1929).
- [66] J. M. Ziman, *Electrons and Phonons* (Claredon Press, Oxford, 1960).
- [67] R. Berman, *Thermal Conduction in Solids* (Claredon Press, Oxford, 1976).
- [68] L. S. Levitov and J. Rhyner, *J. Phys. (France)* **49**, 1835 (1988).
- [69] M. A. Chernikov, A. Bernasconi, C. Beeli, and H. R. Ott, *Europhys. Lett.* **21**, 767 (1993).
- [70] R. C. Zeller and R. O. Pohl, *Phys. Rev. B* **4**, 2029 (1971).
- [71] R. Berman and J. F. C. Brock, *Proc. R. Soc.* **A289**, 66 (1965).
- [72] M. A. Chernikov, A. Bianchi, and H. R. Ott, *Phys. Rev. B* **51**, 153 (1995).
- [73] H. B. G. Casimir, *Physica* **5**, 495 (1938).
- [74] P. W. Anderson, B. I. Halperin, and C. M. Varma, *Philos. Mag.* **25**, 1 (1972).
- [75] W. A. Phillips, *J. Low Temp. Phys.* **7**, 351 (1972).
- [76] J. R. Matey and A. C. Anderson, *Phys. Rev. B* **17**, 5029 (1978).
- [77] N. Vernier, G. Bellessa, B. Perrin, A. Zarembowitch, and M. de Boissieu, *Europhys. Lett.* **22**, 187 (1993).
- [78] S. Hunkliger and W. Arnold, in *Ultrasonic properties of glasses at low temperatures*, Vol. 12 of *Physical Acoustics*, edited by W. P. Mason and R. N. Thurston (Academic Press, New York, 1976), pp. 155–212.
- [79] S. Hunkliger and A. K. Raychaudhuri, *Progress in Low Temperature Physics*, edited by D. F. Brewer (Elsevier, Amsterdam, 1986), Vol. 9.
- [80] L. Piché, R. Maynard, S. Hunkliger, and J. Jäckle, *Phys. Rev. Lett.* **32**, 1426 (1974).
- [81] G. Belessa and O. Bethoux, *Phys. Lett. A* **62**, 125 (1977).

- [82] P. Doussineau, A. Levelut, G. Belessa, and O. Bethoux, *J. Phys. Lett. (Paris)* **38**, 483 (1977).
- [83] N. O. Birge, B. Golding, W. H. Haemmerle, H. S. Chen, and J. M. Parsey, Jr., *Phys. Rev. B* **36**, 7685 (1987).
- [84] G. Coddens, *Int. J. Mod. Phys. B* **11**, 1679 (1997).
- [85] J. Dolinšek, B. Ambrosini, P. Vonlanthen, . M. A. C. J. L. Gavilano, and H. R. Ott, *Phys. Rev. Lett.* **81**, (1998).
- [86] S. Lyonnard, G. Coddens, Y. Calvayrac, and D. Gratias, *Phys. Rev. B* **53**, 3150 (1996).
- [87] G. Coddens, S. Lyonnard, and Y. Calvayrac, *Phys. Rev. Lett.* **78**, 4209 (1997).
- [88] D. Joseph, M. Baake, P. Kramer, and H. R. Trebin, *Europhys. Lett.* **27**, 452 (1994).
- [89] P. A. Kalugin and A. Katz, *Europhys. Lett.* **21**, 921 (1993).
- [90] R. Blüher, P. Scharwaechter, W. Frank, and H. Kronmüller, *Phys. Rev. Lett.* **80**, 1014 (1998).
- [91] B. S. Chandrasekhar, H. R. Ott, and H. Rudigier, *Solid State Commun* **42**, 419 (1982).
- [92] M. P. Zaitlin and A. C. Anderson, *Phys. Rev. B* **12**, 4475 (1975).
- [93] E. P. Roth and A. C. Anderson, *Journ. Appl. Phys.* **47**, 3644 (1976).
- [94] M. P. Zaitlin, L. M. Scherr, and A. C. Anderson, *Phys. Rev. B* **12**, 4487 (1975).
- [95] P. D. Thacher, *Phys. Rev.* **156**, 975 (1967).
- [96] W. Odoni, P. Fuchs, and H. R. Ott, *Phys. Rev. B* **28**, 1314 (1983).
- [97] R. Berman, E. L. Foster, and J. M. Ziman, *Proc. Roy. Soc. (London)* **231A**, 130 (1955).
- [98] J. J. Freeman and A. C. Anderson, *Phys. Rev. B* **34**, 5648 (1986).
- [99] Y. Amazit, M. Fischer, B. Perrin, A. Zarembowitch, and M. de Boissieu, *Europhys. Lett.* **25**, 441 (1994).
- [100] P. Sheng and M. Zhou, *Science* **253**, 539 (1991).
- [101] P. Sheng, M. Zhou, and Z.-Q. Zhang, *Phys. Rev. Lett.* **72**, 234 (1994).

- [102] S. Legault, B. Ellman, J. Ström-Olsen, and L. Taillefer, in *Proceedings of the 5th International Conference on Quasicrystals, Avignon, France, 22–26 May 1995*, edited by C. Janot and R. Mosseri (World Scientific, Singapore, 1995).
- [103] N. Tamura, M. Feuerbacher, M. Beyss, M. Wollgarten, and K. Urban (unpublished).
- [104] C. Kittel, *Phys. Rev.* **75**, 972 (1949).
- [105] A. Einstein, *Ann. Physik* **35**, 679 (1911).
- [106] D. G. Cahill and R. O. Pohl, *Solid State Comm.* **70**, 927 (1989).
- [107] M. A. Chernikov, K. Edagawa, E. Felder, A. D. Bianchi, Ch. Wälti, M. Kenzelmann, H. R. Ott, M. de Boissieu, C. Janot, M. Feuerbacher, N. Tamura, and K. Urban, in *Proceedings of the 6th International Conference on Quasicrystals, Tokyo, Japan, 26–30 May 1997*, edited by S. Takeuchi and T. Fujiwara (World Scientific, Singapore, 1998), pp. 451–458.
- [108] T. Janssen and M. Kohmoto, *Phys. Rev. B* **38**, 5811 (1988).
- [109] J. A. Ashraff and R. B. Stinchcombe, *Phys. Rev. B* **39**, 2670 (1989).
- [110] Y. Honda, K. Edagawa, A. Yoshioka, T. Hashimoto, and S. Takeuchi, *Jpn. J. Appl. Phys.* **33**, 4929 (1994).
- [111] H. Sawada, R. Tamura, K. Kimura, and H. Ino, in *Proceedings of the 6th International Conference on Quasicrystals, Tokyo, Japan, 26–30 May 1997*, edited by S. Takeuchi and T. Fujiwara (World Scientific, Singapore, 1998), pp. 451–458.
- [112] H. Akiyama, Y. Honda, T. Hashimoto, K. Edagawa, and S. Takeuchi, *Jpn. J. Appl. Phys.* **32**, L1003 (1993).
- [113] F. S. Pierce, S. J. Poon, and Q. Guo, *Science* **261**, 737 (1993).
- [114] U. Gubler, Master's thesis, ETH, Zürich, 1994.
- [115] S. Legault, B. Ellmann, J. Ström-Olsen, L. Taillefer, T. Lograsso, and D. Delaney, in *Proceedings of the 6th International Conference on Quasicrystals, Tokyo, Japan, 26–30 May 1997*, edited by S. Takeuchi and T. Fujiwara (World Scientific, Singapore, 1998), pp. 475–478, the electron-phonon interaction may lead to $\lambda_{\text{ph}} = AT^2$ [67]. However, for different samples of icosahedral Al-Mn-Pd no correlation is observed between the zero temperature value σ_0 of the electrical conductivity and the coefficient A of the power-law. The hypothesis of the electron-phonon interaction being predominantly responsible for the T^2 -variation can thus be discarded, at least for the icosahedral Al-Mn-Pd system.

- [116] R. Penrose, in *Introduction to the Mathematics of Quasicrystals*, edited by M. V. Jaric (Academic Press, Boston, 1989).
- [117] M. A. Chernikov, A. D. Bianchi, E. Felder, U. Gubler, and H. R. Ott, *Europhys. Lett.* **35**, 431 (1996).
- [118] K. Kimura and S. Takeuchi, in *Quasicrystals: The State of the Art*, edited by D. P. DiVincenzo and P. J. Steinhardt (World Scientific, Singapore, 1991).
- [119] A. D. Bianchi, F. Bommeli, E. Felder, M. Kenzelmann, M. A. Chernikov, L. Degiorgi, H. R. Ott, and K. Edagawa, *Phys. Rev. B* **58**, 3046 (1998).
- [120] B. Grushko, *Heterogeneous Chemistry Review* **1**, 255 (1994).
- [121] A. R. Kortan, F. A. Thiel, H. S. Chen, A. P. Tsai, A. Inoue, and T. Masumoto, *Phys. Rev. B* **40**, 9397 (1989).
- [122] B. Grushko and K. Urban, *Philos. Mag. B* **70**, 1063 (1994).
- [123] K. Edagawa, H. Tamaru, S. Yamaguchi, K. Suzuki, and S. Takeuchi, *Phys. Rev. B* **150**, 12413 (1994).
- [124] T. Gödecke, *Z. Metallkunde* **88**, 557 (1997).
- [125] T. Gödecke, M. Scheffer, R. Lück, S. Ritsch, and C. Beeli, *Z. Metallkunde* **88**, 687 (1997).
- [126] S. Lin, X. Wang, L. Lu, D. Zhang, L. X. He, and K. X. Kuo, *Phys. Rev. B* **41**, 9625 (1990).
- [127] T. Shibuya, T. Hashimoto, and S. Takeuchi, *J. Phys. Soc. Jap.* **59**, 1917 (1990).
- [128] L. Z. Dian, C. C. Shao, P. W. Yun, L. Lu, M. W. Xue, X. L. Ma, and K. H. Kuo, *Phys. Rev. Lett.* **66**, 2778 (1991).
- [129] K. Edagawa, M. A. Chernikov, A. D. Bianchi, E. Felder, U. Gubler, and H. R. Ott, *Phys. Rev. Lett.* **77**, 1071 (1996).
- [130] D. G. Naugle, W. D. Bruton, K. D. D. Rathnayaka, and A. R. Kortan, *J. Non-Cryst. Solids* **205-207**, 17 (1996).
- [131] A. D. Bianchi, E. Felder, M. Kenzelmann, M. A. Chernikov, H. R. Ott, and K. Edagawa, in *Proceedings of the 6th International Conference on Quasicrystals, Tokyo, Japan, 26–30 May 1997*, edited by S. Takeuchi and T. Fujiwara (World Scientific, Singapore, 1998), pp. 471–475.
- [132] M. Matsuka, M. Yoshizawa, K. Noto, Y. Yokoyama, and A. Inoue, in *Proceedings of the 6th International Conference on Quasicrystals, Tokyo, Japan, 26–30 May*

- 1997, edited by S. Takeuchi and T. Fujiwara (World Scientific, Singapore, 1998), pp. 479–482.
- [133] D. N. Basov, T. Timusk, F. Barakat, J. Greedan, and B. Grushko, *Phys. Rev. Lett.* **72**, 1937 (1994).
- [134] H. Fröhlich, *Elektronentheorie der Metalle* (Springer, Berlin, 1936).
- [135] P. G. Klemens, in *Kältephysik I*, Vol. XIV of *Handbuch der Physik*, edited by S. Flügge (Springer, Berlin, 1956), p. 198.
- [136] M. Garber, B. W. Scott, and F. J. Blatt, *Phys. Rev.* **130**, 2188 (1963).
- [137] M. C. Karamargin, C. A. Reynolds, F. P. Lipschultz, and P. G. Klemens, *Phys. Rev. B* **10**, 3624 (1972).
- [138] A. Perrot, J.-M. Dubois, M. Cassart, and J. P. Issi, in *Proceedings of the 5th International Conference on Quasicrystals, Avignon, France, 22–26 May 1995*, edited by C. Janot and R. Mosseri (World Scientific, Singapore, 1995), p. 588.
- [139] N. E. Phillips, *Crit. Rev. Solid State Sci.* **12**, 467 (1971).
- [140] *Bruker Almanac* (Bruker, , 1991).
- [141] J. Buttet and P. K. Baily, *Phys. Rev. Lett.* **24**, 1220 (1970).
- [142] S. D. Rockwood, E. H. Gregory, and D. L. Goodstein, *Phys. Rev. Lett.* **30**, 225 (1969).
- [143] D. R. Smith and P. H. Keesom, *Phys. Rev. B* **1**, 188 (1970).
- [144] J. E. Graebner, B. Golding, R. J. Schutz, F. S. L. Hsu, and H. S. Chen, *Phys. Rev. Lett.* **39**, 1480 (1977).
- [145] R. O. Pohl, in *Amorphous Solids: Low-Temperature Properties*, Vol. 24 of *Topics in Current Physics*, edited by W. A. Phillips (Springer, Berlin, 1981), p. 167.
- [146] F. Cyrot-Lackmann, *Solid State Comm.* **103**, 123 (1997).
- [147] A. D. Bianchi, F. Bommeli, M. A. Chernikov, U. Gubler, L. Degiorgi, and H. R. Ott, *Phys. Rev. B* **55**, 5730 (1997).
- [148] L. Degiorgi, M. A. Chernikov, C. Beeli, and H. R. Ott, *Solid State Comm.* **87**, 721 (1993).
- [149] Z. M. Stadnik, D. Purdie, M. Garnier, Y. Baer, A. P. Tsai, A. Inoue, K. Edagawa, and S. Takeuchi, *Phys. Rev. Lett.* **77**, 1777 (1996), in this work the photoelectron spectra that, strictly speaking, do not show the pseudogap at E_F directly, were

analyzed assuming that the electronic DOS can adequately be represented by a superposition of a pseudogap of Lorentzian shape centered at E_F and a linearly varying DOS in the vicinity of E_F . The background contribution was determined using a linear extrapolation of the data taken in the energy range between -1.2 and -0.7 eV. The data analysis yielded a width of the pseudogap between 0.22 and 0.36 eV with a relative reduction of the density of electronic states in the range from 28 to 61 %.

- [150] E. A. Hill, T. C. Chang, Y. Wu, S. J. Poon, F. S. Pierce, and Z. M. Stadnik, *Phys. Rev. B* **49**, 8615 (1994).
- [151] J. L. Gavilano, B. Ambrosini, P. Vonlanthen, M. A. Chernikov, and H. R. Ott, *Phys. Rev. Lett.* **79**, 3058 (1997).
- [152] V. Simonet, F. Hippert, C. Gignoux, and C. Berger, in *Proceedings of the 6th International Conference on Quasicrystals, Tokyo, Japan, 26–30 May 1997*, edited by S. Takeuchi and T. Fujiwara (World Scientific, Singapore, 1998), pp. 696–700.
- [153] X.-P. Tang, E. A. Hill, S. K. Wonnell, S. J. Poon, and Y. Wu, *Phys. Rev. Lett.* **79**, 1070 (1997).
- [154] J. L. Gavilano, B. Ambrosini, P. Vonlanthen, M. A. Chernikov, and H. R. Ott (unpublished).
- [155] D. N. Davydov, D. Mayou, C. Berger, C. Gignoux, A. Neumann, A. G. M. Jansen, and P. Wyder, *Phys. Rev. Lett.* **77**, 3173 (1996).
- [156] P. A. Bancel and P. A. Heiney, *Phys. Rev. B* **33**, 7917 (1986).
- [157] A. P. Smith and N. W. Ashcroft, *Phys. Rev. Letts.* **59**, 1365 (1987).
- [158] J. Friedel, *Helv. Phys. Acta* **61**, 538 (1988).
- [159] G. T. de Laissardière and T. Fujiwara, *Phys. Rev. B* **50**, 5999 (1994).
- [160] M. Krajčí, M. Windisch, J. Hafner, G. Kresse, and M. Mihalkovič, *Phys. Rev. B* **51**, 17355 (1995).
- [161] G. T. de Laissardière, D. N. Manh, L. Magaud, J. P. Julien, F. Cyrot-Lackmann, and D. Mayou, *Phys. Rev. B* **52**, 7920 (1995).
- [162] S. J. Poon, *Advances in Physics* **41**, 303 (1992), and references therein.
- [163] Y. Wang, D. Zhang, and L. G. Chen, *Phys. Rev. B* **48**, 10542 (1993).
- [164] G. T. de Laissardière and T. Fujiwara, *Phys. Rev. B* **50**, 9843 (1994).

- [165] Z. M. Stadnik, G. W. Zhang, A. P. Tsai, and A. Inoue, Phys. Lett. A **198**, 327 (1995).
- [166] M. A. Chernikov, H. R. Ott, A. Bianchi, A. Migliori, and T. W. Darling, Phys. Rev. Lett. **80**, 321 (1998).
- [167] U. Mizutani, T. Matsuda, Y. Itoh, K. Tanaka, H. Domae, T. Mizuno, S. Murasaki, Y. Miyoshi, K. Hashimoto, and Y. Yamada, J. Non-Cryst. Solids **156-158**, 882 (1993).
- [168] Z. M. Stadnik, D. Purdie, M. Garnier, Y. Baer, A. P. Tsai, A. Inoue, K. Edagawa, S. Takeuchi, and K. H. J. Buschow, Phys. Rev. B **55**, 10938 (1997), in this work the experimentally determined photoemission intensity in the energy range between -2.0 and -1.5 eV and from -2.2 to -1.8 eV, for Al-Cu-Co and Al-Ni-Co, respectively, was linearly extrapolated. An analysis of the photoemission spectra, assuming the DOS in the form of a Lorentzian pseudogap at E_F superimposed on a linear term, is consistent with a pseudogap that is wider, i.e., between 0.9 and 1.1 eV, but deeper (80-85 %) than in icosahedral quasicrystals [149]. We note, however, that similarly to what was reported for icosahedral phases [149], the as-measured photoelectron emission spectra do not display a pseudogap at the Fermi energy E_F .
- [169] R. F. Sabiryanov, S. K. Bose, and S. E. Burkov, J. Phys. Condens. Matter **7**, 5437 (1995).
- [170] M. Krajčič, J. Hafner, and M. Mihalkovič, Phys. Rev. B **56**, 3072 (1997).
- [171] M. Krajčič, J. Hafner, and M. Mihalkovič, Europhys. Lett. **34**, 207 (1996).
- [172] M. Krajčič, J. Hafner, and M. Mihalkovič, Phys. Rev. B **55**, 843 (1997).
- [173] W. Yang, C. Hu, D. H. Ding, and R. Wang, Phys. Rev. B **51**, 3906 (1995).
- [174] M. J. P. Musgrave, Proc. Roy. Soc. **A226**, 356 (1956).
- [175] I. M. Lifshitz, Zh. Eksp. Teor. Fiz. **26**, 551 (1954).
- [176] M. Mihalkovič, F. Dugain, and J.-B. Suck, J. Non. Cryst. Sol. **205-207**, 701 (1996).
- [177] V. F. Sears, Neutron News **3**, 26 (1992).
- [178] F. Dugain, M. de Boissieu, K. Hradil, K. Shibata, R. Currat, A. R. Kortan, A. P. Tsai, J.-B. Suck, and F. Frey, in *Aperiodic'97: International Conference on Aperiodic Crystals, Alpe d'Huez, France, 27-31 August, 1997*, edited by M. de Boissieu, R. Currat, and J.-L. Verger-Gaugry (World Scientific, Singapore, 1998).
- [179] C. L. Henley, J. Non. Cryst. Sol. **153-154**, 172 (1993).

- [180] A. M. Karo and J. R. Hardy, *Phys. Rev.* **129**, 2024 (1963).
- [181] R. A. Cowley, W. Cochran, B. N. Brockhouse, and A. D. B. Woods, *Phys. Rev.* **131**, 1030 (1963).
- [182] J. Hafner, M. Krajčí, and M. Mihalkovič, *Phys. Rev. Lett.* **76**, 2738 (1996).
- [183] B. L. Altshuler and A. G. Aronov, in *Electron-Electron Interactions in Disordered Systems*, Vol. 10 of *Modern Problems in condensed matter sciences*, edited by V. M. Agranovich and A. A. Maradudin (North Holland, Amsterdam, 1985), p. 690.
- [184] P. A. Lee and T. V. Ramakrishnan, *Rev. Mod. Phys.* **57**, 287 (1985).
- [185] L. P. Gor'kov, A. I. Larkin, and D. E. Khmel'nitskii, *JETP Lett.* **30**, 228 (1979).
- [186] B. D. Biggs, S. J. Poon, and N. R. Munirathnam, *Phys. Rev. Lett.* **65**, 2700 (1990).
- [187] T. Klein, H. Rakoto, C. Berger, and F. Cyrot-Lackmann, *Phys. Rev. B* **45**, 2046 (1992).
- [188] A. Sahnoune, J. O. Ström-Olson, and A. Zaluska, *Phys. Rev. B* **46**, 10629 (1992).
- [189] C. Berger, T. Grenet, P. Linquist, J. C. Grieco, G. Fourcodot, and F. Cyrot-Lackman, *Solid State Commun.* **87**, 977 (1993).
- [190] G. Haberkern, G. Fritsch, and J. Schilling, *Z. Phys. B* **92**, 383 (1993).
- [191] P. Lindqvist, P. Lanco, C. Berger, A. G. M. Jansen, and F. Cyrot-Lackmann, *Phys. Rev. B* **51**, 4796 (1995).
- [192] G. A. Thomas, A. Kawabata, Y. Ootuka, S. Katsumoto, S. Kobayashi, and W. Sasaki, *Phys. Rev. B* **26**, 2113 (1982).
- [193] T. F. Rosenbaum, R. F. Milligan, M. A. Paalanen, G. A. Thomas, R. N. Bhatt, and W. Lin, *Phys. Rev. B* **27**, 7509 (1983).
- [194] E. Felder, A. D. Bianchi, M. A. Chernikov, and H. R. Ott (unpublished).
- [195] S. E. Burkov, T. Timusk, and N. W. Ashcroft, *J. Phys.: Condens. Matter* **4**, 9447 (1992).
- [196] S. E. Burkov, A. A. Varlamov, and D. V. Livanov, *JETP Lett.* **62**, 361 (1995).
- [197] S. E. Burkov, A. A. Varlamov, and D. V. Livanov, *Phys. Rev. B* **53**, 11504 (1996).
- [198] Q. Guo and S. J. Poon, *Phys. Rev. B* **54**, 6046 (1996).
- [199] A. N. Ionov and I. S. Shlimak, *JETP Lett.* **35**, 196 (1982).

- [200] M. A. Chernikov, L. Degiorgi, E. Felder, S. Paschen, A. D. Bianchi, H. R. Ott, J. Sarrao, D. Mandrus, and Z. Fisk, *Phys. Rev. B* **56**, 1366 (1997).
- [201] B. I. Shklovskii and A. L. Efros, *Electronic properties of doped semiconductors*, Vol. 45 of *Solid-State Sciences* (Springer, Berlin, 1984), p. 388.
- [202] N. F. Mott, *Phil. Mag.* **B 44**, 265 (1981).
- [203] C. Janot, *Phys. Rev. B* **53**, 181 (1996).
- [204] M. Ahlgren, C. Gignoux, M. Rodmar, C. Berger, and O. Rapp, *Phys. Rev. B* **55**, R11915 (1997).
- [205] Q. Guo and S. J. Poon, *Phys. Rev. B* **54**, 12793 (1996).

Dank

Zuallererst möchte ich Professor Hans-Rudolf Ott danken, dass er es mir ermöglicht hat eine Doktorarbeit auf dem faszinierenden Gebiet der Quasikristalle zu machen. Sein wissenschaftlicher Stil und seine Art Resultate darzustellen haben mich stark beeinflusst. Zu tiefem Dank verpflichtet bin ich auch Dr. Michael Chernikov, der mir nicht nur bei den täglichen Problemen im Labor zur Seite stand und die Proben hergestellt hat. Sein Rat war oft von unschätzbarem Wert.

Erich Felder verdient speziellen Dank für die Messungen der spezifischen Wärme an meinen Proben. Erwähnen möchte ich auch Dr. Stefan Ritsch, der sich immer Zeit nahm mit dem Elektronenmikroskop einen kritischen Blick auf meine Proben zu werfen, und Dr. Hansjörg Schwer, der mir die Tricks und Kniffe beim Röntgen verraten hat. Peter Wägli verdanke ich die Untersuchung der Oberflächen meiner Proben mit dem Rasterelektronenmikroskop. Professor Pavel Kalugin war eine wertvolle Hilfe bei der Erklärung der Wärmeleitfähigkeitsdaten. Dr. Leonardo Degiorgi und Dr. Frank Bommeli danke ich für die Messungen der optischen Leitfähigkeit. Dr. Andreas Amman hat unzählige Male Pannenhilfe bei LaTeX Problemen geleistet und mir das Style File dieser Doktorarbeit zur Verfügung gestellt.

Dr. Keiichi Edagawa, Ueli Gubler, Michel Kenzelmann und Herbert Müller möchte ich für die gute Zusammenarbeit während ihrer Zeit in unserem Labor danken. Nicht zu vergessen sind Marisa Van der Mark für alle die administrativen Hürden, die sie aus dem Weg geräumt hat und natürlich Hans Ulrich Thomas, die gute Seele unserer Gruppe bei technischen Probleme aller Natur. Immer hatte Dr. René Monnier ein offenes Ohr für meine Probleme mit der Physik.

All meinen Kollegen in der Gruppe, Benno Ambrosini, Dr. David Brawner, Dr. Silke Bühler-Paschen, Dr. Jorge Gavilano, Konrad Gianni, Dr. Michael Hunt, Dr. Jürg Hunziker, Dr. Olivier Jeandupeux, Dmitry Pushin, Dr. Patrick Vonlanthen, Christoph Wälti, Dr. Andreas Schilling, Stefan Siegrist und Dr. Rong Ying Jin, möchte ich für das herzliche Arbeitsklima danken und für all die wissenschaftlichen und weniger wissenschaftlichen Diskussionen während meiner Zeit auf dem Höggerberg.

Zum Schluss möchte ich meinen Eltern danken für all die Jahre der grossen Unterstützung während meines Studiums und meiner Doktorarbeit. Alexandra danke ich für ihre Liebe und Geduld die sie mir gewährte, auch wenn es nicht immer einfach war.

Diese Arbeit wurde ermöglicht durch die finanzielle Unterstützung des Schweizerischen Nationalfonds zur Förderung der Wissenschaften und der ETH Zürich.

Curriculum vitae

Personal Details

Name : Bianchi, Andrea Daniele
Date of Birth : 11 August, 1968, Olten, Switzerland
Citizen of : Switzerland

Education

1974–1980 Primarschule Olten
1980–1982 Bezirksschule Olten
1983–1987 Kantonsschule Olten, C Matura
1987–1993 M.S. in Physics, Swiss Federal Institute of Technology, Zurich

Publications

1. A. D. Bianchi, F. Bommeli, E. Felder, M. Kenzelmann, M. A. Chernikov, L. Degiorgi, H. R. Ott, and K. Edagawa “Low-temperature thermal and optical properties of single grained decagonal Al-Ni-Co quasicrystals”, *Phys. Rev. B.* **58**, 3046 (1998).
2. M. A. Chernikov, H. R. Ott, A. Bianchi, A. Migliori, and T. W. Darling, “Elastic moduli of a single quasicrystal of decagonal Al-Ni-Co: evidence for transverse elastic isotropy”, *Phys. Rev. Lett.* **80**, 321 (1998).

3. A. D. Bianchi, E. Felder, M. Kenzelmann, M. A. Chernikov, H. R. Ott, and K. Edagawa, "Low-temperature thermodynamic and thermal-transport properties of decagonal Al-Ni-Co", in *Proceedings of the 6th International Conference on Quasicrystals*, Tokyo, Japan, 26–30 May 1997, edited by S. Takeuchi and T. Fujiwara (World Scientific, Singapore, 1997).
4. M. A. Chernikov, K. Edagawa, E. Felder, A. D. Bianchi, Ch. Wältli, M. Kenzelmann, H. R. Ott, M. de Boissieu, C. Janot, M. Feuerbacher, N. Tamura, and K. Urban, "Low-temperature lattice excitations and dynamics of quasicrystals from specific heat and thermal conductivity", in *Proceedings of the 6th International Conference on Quasicrystals*, Tokyo, Japan, 26–30 May 1997, edited by S. Takeuchi and T. Fujiwara (World Scientific, Singapore, 1997).
5. M. A. Chernikov, L. Degiorgi, E. Felder, S. Paschen, A. D. Bianchi, H. R. Ott, J. L. Sarrao, D. Mandrus, and Z. Fisk, "Low-temperature transport, optical, magnetic and thermodynamic properties of $\text{Fe}_{1-x}\text{Co}_x\text{Si}$ ", *Phys. Rev. B* **56**, 1366 (1997).
6. A. D. Bianchi, F. Bommeli, M. A. Chernikov, U. Gubler, L. Degiorgi, and H. R. Ott, "Electrical conductivity, magneto- and optical conductivity of quasicrystals in the Al-Re-Pd system", *Phys. Rev. B* **55**, 5730 (1997).
7. M. A. Chernikov, E. Felder, S. Paschen, A. D. Bianchi, H. R. Ott, J. L. Sarrao, D. Mandrus, and Z. Fisk, "Low-temperature magnetic and thermodynamic properties of $\text{Fe}_{1-x}\text{Co}_x\text{Si}$ ", *Physica B* **230-232**, 790 (1997).
8. M. A. Chernikov, A. Bianchi, E. Felder, U. Gubler and H. R. Ott, "Low-temperature thermal properties of icosahedral Al-Re-Pd", *Europhys. Lett.* **35**, 431 (1996).
9. K. Edagawa, M. A. Chernikov, A. D. Bianchi, E. Felder, U. Gubler and H. R. Ott, "Low-temperature thermodynamic and thermal-transport properties of decagonal $\text{Al}_{65}\text{Cu}_{20}\text{Co}_{15}$ ", *Phys. Rev. Lett.* **77**, 1071 (1996).
10. P. A. Kalugin, M. A. Chernikov, A. D. Bianchi and H. R. Ott, "Structural scattering of phonons in quasicrystals", *Phys. Rev. B* **53**, 14145, (1996).
11. P. A. Kalugin, M. A. Chernikov, A. D. Bianchi, and H. R. Ott, "Structural scattering of phonons in quasicrystals", *Czech. J. Phys.* **46**, Suppl. 5, 2707 (1996).

12. M. A. Chernikov, A. D. Bianchi, E. Felder, U. Gubler, and H. R. Ott, "Low-temperature thermodynamic and thermal-transport properties of icosahedral Al-Re-Pd", *Czech. J. Phys.* **46**, Suppl. 5, 2551 (1996).
13. A. D. Bianchi, M. A. Chernikov, K. Edagawa, E. Felder, U. Gubler, and H. R. Ott, "Low-temperature thermal properties of decagonal Al₆₅Cu₂₀Co₁₅", *Czech. J. Phys.* **46**, Suppl. 5, 2705 (1996).
14. A. D. Bianchi, M. A. Chernikov, E. Felder, S. Ritsch, and H. R. Ott, "Low-temperature electrical transport in icosahedral Al-Re-Pd", *Czech. J. Phys.* **46**, Suppl. 5, 2553 (1996).
15. K. Edagawa, M. A. Chernikov, A. D. Bianchi, E. Felder, U. Gubler, and H. R. Ott, "Low-temperature specific heat and anisotropy of the thermal conductivity of decagonal Al₆₅Cu₂₀Co₁₅", in *Workshop on Aperiodic Structures. Extended Abstracts*, Krakow, Poland, 1–5 June 1996.
16. M. A. Chernikov, A. D. Bianchi, H. Müller, and H. R. Ott, "Low-temperature thermal transport in icosahedral Al₇₀Mn₉Pd₂₁", in *Proceedings of the 5th International Conference on Quasicrystals*, Avignon, France, 22–26 May 1995, edited by C. Janot and R. Mosseri (World Scientific, Singapore, 1995), p. 569.
17. A. D. Bianchi, E. Felder, A. Schilling, M. A. Chernikov, F. Hulliger, and H. R. Ott, "Low-temperature thermal properties of CePd₂In", *Z. Phys. B* **99**, 69 (1995).
18. M. A. Chernikov, A. Bianchi, and H. R. Ott, "Low-temperature thermal conductivity of icosahedral Al₇₀Mn₉Pd₂₁", *Phys. Rev. B* **51**, 153 (1995).